Epidermal Loop Antennas

by

Haitham Abu Damis

A thesis submitted in partial fulfillment of the requirements for the degree of

Master of Science
in
Communications

Department of Electrical and Computer Engineering
University of Alberta

Abstract

The Quadruple Loop (QL) antenna was designed and investigated to deliver a robust body-worn antenna for bio-medical applications. The QL antenna is a very thin single-layer groundless structure which allows for the installation of neighboring electronics and sensors on biomedical device. The initial research objective was achieved after measurement results confirmed the superior performance of the QL antenna to the standard square loop. This was evident in gain and bandwidth improvement after the inclusion of the four circular patches to the original loop. In the second research stage, different fabrication tools and materials were used to make a number of QL antennas. The different antennas were intended to operate as GSM-900, GSM-1800, and BLE epidermal antennas. Radiation pattern measurements were conducted to compare their results with their simulation counterparts. Later, data communication tests showed that the acquired BER readings could qualify the BLE and GSM-900 antennas to work as part of 4-QAM wireless links. Moreover, a stretchable QL epidermal antenna made of novel silver ink had its measured results agree with simulations. Besides these hands-on endeavors, numerical analysis was used to explain the low values of gain of epidermal antennas. This is added to finding an equivalent and more efficient mathematical model of biological tissues which make up the human arm. The equivalent model was tested in software and has the practical potential to be realized in physical phantom making.

Preface

The Quadruple Loop antenna is an original design made by the author of this thesis. In addition, this thesis presents theoretical and measurement efforts which are usually avoided in the research of body-worn antennas due to the inconvenience and difficulties associated with performing them.

Parts of the first section of Chapter 4 was published in ANTEM 2016 under the title: "Flexible Printed Square Loop Antennas for Wearable Applications". Some parts of Chapter 3 and the later parts of Chapter 4 will be included in a future journal publication. This journal publication is currently in-progress and is to be submitted before the end of April, 2017. All content related to the fabrication, simulations, and measurements of the stretchable QL antenna was included as part of another submitted journal paper. This journal paper was co-authored by Dr. Hyun-Joong and his Chemical and Materials Engineering (CME) team who were behind the making of the novel silver ink as well as the fabrication of some of the antennas presented in this thesis.

Acknowledgments

Firstly, I would like to thank Dr. Pedram Mousavi for his kindness and patience which were very much needed during the writing of this thesis. In par with my supervisor, I also extend my thanks and appreciation to Dr. Rashid Mirzavand. It cannot be overstressed how valuable and great the positive impact Dr. Rashid had on this endeavor.

Finally, I would like to thank Dr. Hyun-Joong and his students for their contribution in the fabrication of several QL antennas. In addition, they were able to formulate a novel silver ink which was used in making the stretchable QL antennas presented in this thesis.

Table of Contents

List of Figures

List of Tables

Chapter One: Introduction to Body-worn Antennas

In general, body-worn antennas refer to those antennas which are worn on the body as part of a garment or any other wearable item such as a wristband. However, the thesis extends this definition to include all antennas which are supposed to function in close proximity to the body as well as those which are implanted within it. The term "close proximity", refers to those antennas which are either adhered or "tattooed" to skin, in addition to antennas with body-separation distances equivalent to what regular clothing would have (10 - 30) mm. Antennas whose skin separation is 1mm or less have to have an acceptable degree of conformity, such is the case with epidermal antennas (electronic tattoos). The level of antenna-body conformity, antenna profile and size are all determined by the application and frequency band of operation. A distinction between the three categories of body-worn antennas (wearable, epidermal, and implanted) is necessary to define before indulging in any further discussion about body-worn antennas. Nonetheless, one should keep in mind that all three categories of antennas share the feature of operating in close proximity to biological tissue.

1.1 Body-worn Antennas

Now, wired "body-worn" devices have been in existence for decades, but in recent times, the term almost always pertains to its wireless counterpart. The focus on wireless technology is due to the obvious practical reasons that radio frequency communications bring. Since this thesis is concerned with body-worn antennas in particular, let us provide some due terminology and definitions.

The term "wearable antennas", refers to those antennas which are usually integrated into clothing or otherwise worn on top of garment [1]. These antennas always have a separation gap between themselves and the body, and this gap is usually the largest to be present in any of the three antenna categories mentioned. Conductive textiles are usually used to fabricate the radiating elements for wearable antennas while low-permittivity fabrics are used as dielectric substrates [2]. The reason behind the considerable gap between skin and a wearable antenna is due to the intrinsic body-clothe separation present with regular clothing.

Epidermal antennas, as their name pertains, are placed in extreme proximity to the skin, hence the name "epidermal". These antennas could be integrated with intricate "tattoo" electronics [3] [4]. Accordingly, the body-antenna separation gap is usually less than 1 mm and it is taken up by a dielectric substrate. These substrates are desired to be stretchable, flexible, and sticky. If the antenna structure covers a substantial area of the skin, the substrate would be expected to be breathable. Given these features, epidermal antennas are mostly applied in sensing and biomedical applications where skin hydration levels and vital sign readings are to be transmitted wirelessly.

Implanted antennas take the concept of body-worn antennas a step further. These antennas are installed as part of electronic devices which are invasively implanted just under the skin or deeper within the body [5]. Such devices are mainly used in medical applications and, ironically, their very concept and design pose intricate challenges for these devices to be biocompatible and medically safe.

1.2 Wireless Communications

Before looking at examples of the different types of body-worn antennas, it would be appropriate to mention the few existing and emerging technology terms, which would have these devices ubiquitous to their foundation. The Internet of Things (IoT), Wireless Sensor Networks (WSN's), and Body Area Networks (BAN's) would be the forefront clients of body-worn technology. In this context, it would be appropriate to introduce the three general communication schemes of body-worn antennas:

1- In-body communications: take place between at least one node inside the body and at least one other node on or some distance away from the body.

2- On-body communications (Figure 1): take place between different nodes all placed on the external surface of the body.

Both of in-body and on-body schemes can be part of a BAN where sensor nodes implanted under the skin could communicate with other nodes worn externally such as an epidermal tattoo or a flexible Kapton-based antenna.

3- Off-body communications (Figure 2): take place between at least one node on the body and at least one node located some distance away. This scheme is necessary to establish a full WSN, with a wireless access point or other external nodes on one side forming a link with one or more body-worn devices.

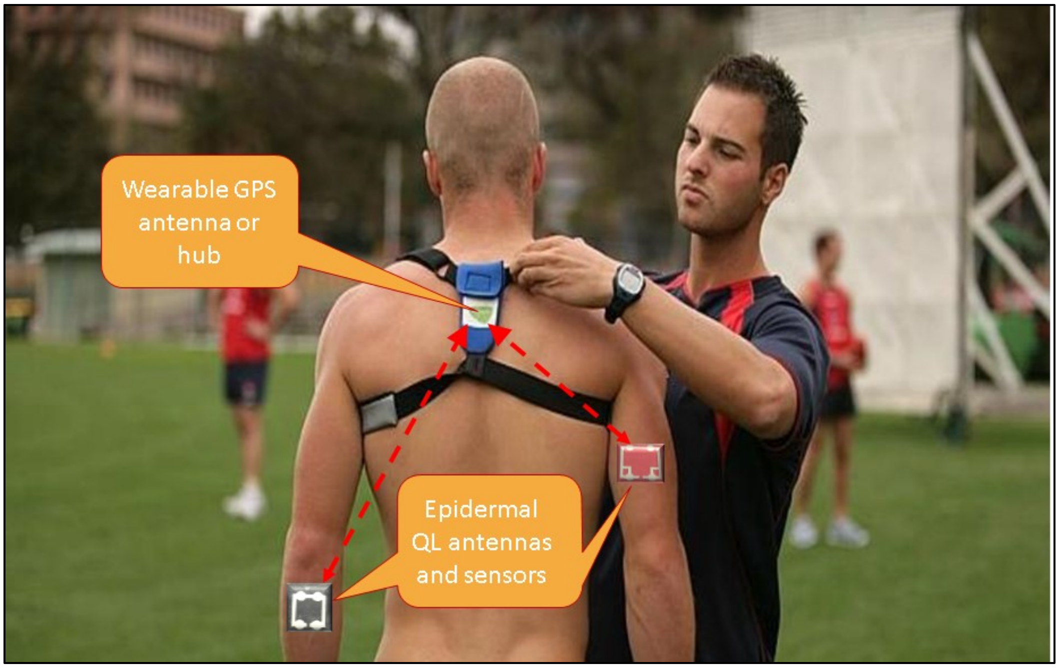

Figure 1. On-body communications (original image from [6]).

1.3 Frequency Bands

Given the above discussion, a wide range of body-worn technology applications exist which seek to serve different purposes. To this end, some licensed and unlicensed frequency bands have been exploited as seen below:

a. ISM: (2.4–2.5) GHz

The Federal Communications Commission (FCC) announced the assignment of industrial, scientific, and medical (ISM) bands in 1947 [5]. These unlicensed bands have almost no regulatory protection; as a result, they are very noisy and crowded. Nonetheless, unlicensed bands will always attract research and vendor attention, and this is especially true for the region of (2.4- 2.5) GHz. Bluetooth Smart, also known as Bluetooth low energy (BLE), is an initiative that sought to implement Bluetooth technology to body-worn devices and others where fast data rates and low transmit powers are required. Besides BLE, Zigbee also employs radio communications in the unlicensed band of (2.4- 2.5) GHz [7]. The networks using these technology standards usually come in the form of WSN's for medical or security applications.

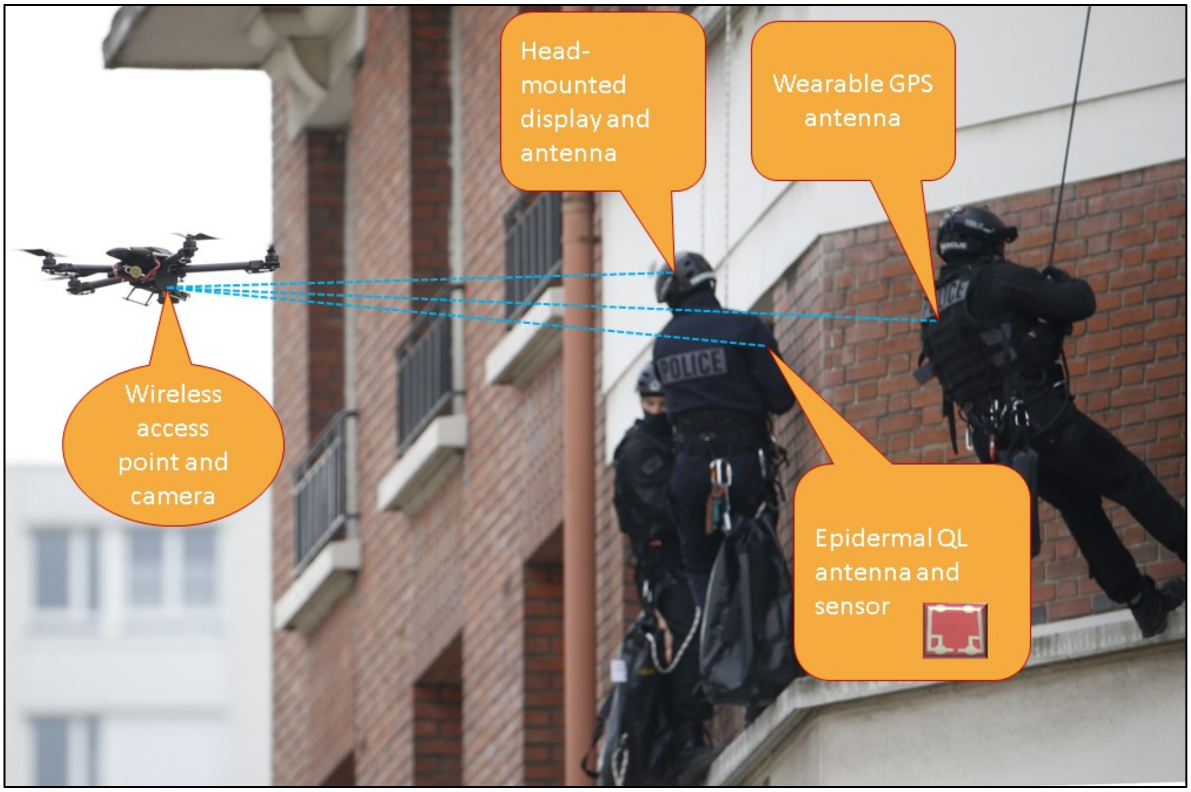

Figure 2. Off-body communications (original image from [8]).

b. MICS

The Federal communications council (FCC) did not spare any effort in allotting exclusive portions of the spectrum for medical applications. Moreover, the FCC gave special attention to implantable medical devices by assigning the 402–405 Medical Implant Communications Service (MICS) band in late 1999 [9] [10]. This band was later extended to encompass all frequencies between 401-406 MHz and was renamed the Medical Device Radio Communication Service (MedRadio) in March 2009 [11] [10]. Features such as high-data-rate transmission, miniaturized antenna designs and acceptable human body losses at these frequencies make MedRadio technology a better alternative to inductively linked devices [12].

c. RFID

Perhaps, RFID applications (868-928) MHz are at the forefront of body-worn technology employment [13] [14]. From a glance at the available literature, the majority of body-worn antenna research effort was directed into this field. Body-worn RFID devices have been used in hospital environments for patient identification and monitoring. Commercial wristband RFID tags as well as garment antennas can also be used for this purpose. As of now, wristband antennas are the more feasible solution, but textile antennas will eventually become practical. On the other hand, implanted tags are also used for animal and human patient monitoring [15]. This type of RFID tags has a reduced risk of being lost in addition to being invisible to uncooperative patients.

d. UWB

Back in 2002, The FCC authorized the unlicensed use of UWB in the frequency range of 3.1 to 10.6 GHz [1]. This came after proponents of UWB technology convinced the Federal Communication commission (FCC) that low power emissions in this band would not interfere with other narrow frequency band devices. Hence, the commission issued its 2002 ruling with certain communication link and radiated power restrictions [16]. Since then, UWB communications have been gaining increased and renewed interest.

1.4 Highlights of Body-worn Technology

Wireless sensors and monitoring systems are seeing aggressive integration into the world of WBANs and WSNs for use in healthcare (Telemedicine), industrial monitoring, and security. This is accompanied by hopes to make such networks become part of a near-future Smart Grid [17]. Nonetheless, current commercially available products such as Fitbit's "Surge" [18], TomTom's "Adventurer" [19], and "Spark 3" [20] are popular examples of multi-functional wearable devices used as body fitness sensors and vital sign tracking. These three particular instances also feature GPS functionality.

In 2013, Google Glass was released. Besides its use for personal entertainment, it was utilized in very interesting ways in different professional spheres. For instance, the device can provide convenient access to vital signs readings for surgeons in operation rooms. Spanish surgeon Dr. Pedro Guillén performed and streamed a surgical operation, via Google Glass, allowing experts at Stanford University (USA) to consult live and viewers around the world to watch the procedure in real time on the internet [21]. Yet another Google initiative is "Project Jacquard" which promises to integrate a range of interaction schemes into clothing to communicate with mobile phones and other electronic devices [22].

1.5 Structure, Topology, and Fabrication

A good body-worn antenna should have a satisfying level of performance in addition to being fit and comfortable to wear. The use of thick or rigid materials in its making is better avoided; it is preferable to make the antenna structure as flexible as possible. The size of the antenna and its intended placement on the body impose further design considerations. In order to be truly wearable, the antenna must have a low yet conformable profile. Depending on location, if the antenna is to cover an appreciable area of skin, it has to be breathable. The antenna must also exhibit an acceptable level of physical robustness. In other words, it has to be able to tolerate exposure to varying temperatures, moisture, and be resistant to wash and wear. Nonetheless, ensuring good performance of the antenna as part of a communication link should not be put second to meeting the previously mentioned criteria. Hence, the usual benchmarks of antenna robustness such as, efficiency and radiation properties are also kept in mind.

Even though body-worn antennas can be made flexible, discrete, and integrated into clothing, inclusion of the accompanying radio components for the overall structure poses some challenges. Detailed discussion of this matter is not the focus of this thesis, but it would be appropriate to mention a few common solutions to the problem of feeding current to wearable and epidermal antennas. The most direct one, would be to include a wired connection between the antenna and the radio circuitry. As such, small batteries could be used. In the domain of wireless sensor networks and motes, energy-harvesting means could be used to power up sensing-devices.

A common power-harvesting scheme would be that of powering passive RFID tags through an inductive link with a reader. However, this concept should be modified to fit the system at hand and its bandwidth of operation. More recently, printed electronics fabricated from very thin and flexible devices are being exploited as low power devices. It is worthwhile to note that printing technology was used in this research; more on this will follow in Chapter 3.

❖ Types of antennas

There is a variety of different antenna topologies that can be used for body-worn applications, and they could be categorized into two main groups based on the number of layers included in the design of the antenna. Single-layer antennas refer to those which are composed of only one layer on which the radiating element rests upon. Multi-layer antennas consist of at least two layers, a radiating element and a ground structure. Some antennas consist of three layers or more if frequency selective structures such as EBG's or AMC's were to be included.

❖ Materials and fabrication

Since there is a wide range of applications where body-worn antennas could be used, there is also a corresponding variety of substrates and fabrication methods suitable for any given application. Paper-based substrates, stretchable and flexible polymers, in addition to conductive textiles and inks are among some of those materials. Cutting printers, drilling and specialized sewing machines in addition to 3D printers and ink depositors are a few of the tools commonly used to fabricate such antennas.

1.6 The Research Project

The goal of the project was to come up with a telemetry device capable of sensing and communicating body signs wirelessly at ISM (2.4-2.5) GHz frequencies. A concept art of the goal device could be seen in Figure 3. The primary sensing components included body-hydration, glucose, and blood pressure sensors. Such body signs can be reliably sensed only if the sensors were to be placed extremely close to skin surface. This meant that the device had to be very thin, groundless and flexible. All of which are features of epidermal antennas.

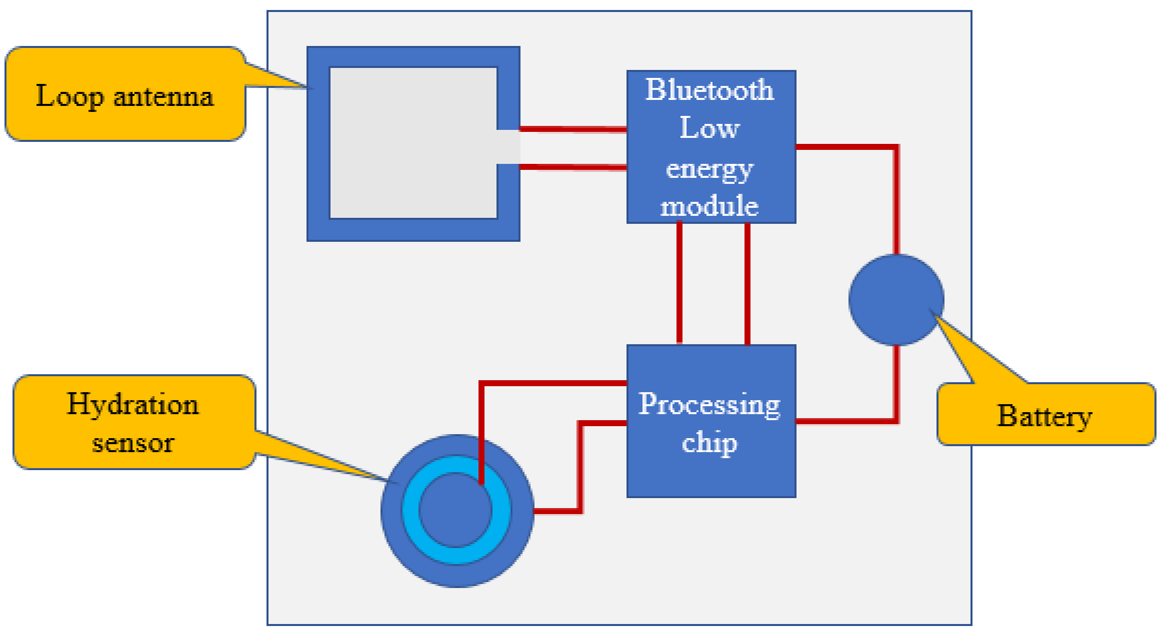

Figure 3. Project concept.

This project was also a great chance to explore the electromagnetics of body-antenna interaction. Hence, plans for measuring overall antenna performance parameters such as radiation patterns, efficiency and communications capability were made. In addition, investigating different modeling methodologies proper for this antenna-tissue interaction had to be part of the research. Given these considerations, the antenna team set two primary research objectives:

1- Delivering a very thin single-layer antenna capable of robust communications at ISM frequencies.
2- Exploring alternative frequency bands for optimal radiation and communications performance.

Work immediately began on comparing different single-layer topologies for epidermal applications. Dipoles, loops, and coplanar monopoles, all of which do not employ a bottom ground layer, were studied and reviewed. Realizing that the epidermal device should be small, the antenna shape had to allow neighboring electronics and sensors enough room to be installed. In addition, minimal conductor area is preferred to minimize heat absorption by the skin and underlying tissue. Thus, a loop antenna was chosen as a promising candidate. However, any antenna placed very close to the body without any ground structure is subject to significant detuning, gain and radiation efficiency degradation. In order to minimize these shortcomings, the antenna team modified loop geometry and created the Quadruple Loop (QL) antenna. The first objective was achieved after simulations, fabrication and measurement tests confirmed the superior performance of the QL antenna to the standard square loop antenna.

The next step was to understand the electromagnetics of epidermal antennas. This involved studies and measurements of the radiation patterns of three QL epidermal antennas, each designed to operate at a different frequency band. Link budget analysis was also carried out to gauge the transmitted and received power-levels between epidermal and probe-antennas. In addition, two of the designed antennas had their performance tested in actual data communications schemes. The results of these tests instilled confidence in the ability of very thin single-layer antennas to operate satisfactorily in a wireless link.

The previous stages proved the working concept of the QL epidermal antennas and gave insight into the electromagnetics of body-worn antennas. The final stage was to employ stretchable and printed-electronics technology in the fabrication and testing of similar QL antennas. This step came upon after the chemical and materials engineering team created a novel (at the time) silver ink which was used to print the radiating elements of the stretchable QL antennas. Hence, all of the work done until this stage made it possible to layout an effective plan for future projects that would without a doubt benefit from the effort presented in this thesis.

❖ Organization of the thesis

Foundational background about human biology, antenna topology and fabrication techniques are introduced in Chapter 2. A comprehensive literature review covering a range of different body-worn antennas and their respective simulation and measurement methods is also included in the chapter.

Project antennas, simulations and modeling approaches are addressed in Chapter 3. Based on the information presented in the second chapter, the design concept and the fabrication of different QL antennas are reported. Added to this, are the different HFSS simulation models used to help predict the performance of the antennas. The software models seek to approximate the make-up a human arm with four major tissue layers: skin, fat, muscle, and bone. The layered models are of different shapes and geometries as a result of the linear learning curve of the project and its cyclic progression. One of the main modeling milestones presented in the chapter is the single-layer arm HFSS model. Instead of including four tissue layers, with each having its own very different frequency-dependent dielectric parameters, the single-layer arm is a simulation time-saving alternative which uses processing resources more efficiently.

Chapter 4 presents the core measurement results and tests involving several QL antennas introduced in the third chapter. Besides reflection coefficient and radiation pattern measurements, data communication tests were also performed to prove the ability of the antennas to communicate in any 4-QAM wireless link. Then, the measured and simulated performance results of a stretchable QL antenna are presented. Finally, we base the motivation for future endeavors on side-projects which were commenced during the timeline of the project and were inspired by the design of the QL antenna.

Chapter Two: Special Interest Topics for Body-worn Antennas

This chapter presents the special topics of interest to body-worn antenna design. Background information on the electrical properties of biological tissue will be presented at first. Then, we will look at a review of software solutions and physical models used to study the performance of body-worn antennas. This is accompanied by a discussion on different computational electromagnetics techniques used in full-wave simulation software. Later, we will be looking at an extensive literature review of the different shapes and types of body-worn antennas. Added to this, are the materials and techniques used in their fabrication.

2.1 Physical and Electrical Features of the Human Body

Basically, if you were to consider the external geometry of the human body, it would appear symmetric when looked at from a far. This perspective would change if you were to draw a median-line through the center of the human body, hence dividing it into two equal halves -a left side and a right side. Form this view, surface irregularities and abrupt vectors of topology would be apparent. On an even smaller scale, say a microscopic one, the geometry of the body appears to be extremely unpredictable. The outermost layer of the human body, its external surface, includes areas of varying degrees of skin roughness, hair density, sweat pores, curves, and bumps. Yet, the internal composition of the human body is even more complex. It is made up of several underlying layers of heterogeneous and homogenous matter. Body fluids and internal organs as well as various other bio-matter of the body which make up the systems vital for human vitality are forced to interact with each other as efficiently as possible in a very compact and dense manner. Given the diversity of the functions of the numerous biological tissues found in the body, the constituents of these tissues are also as diverse and numerous. Hence, if the chemistry of each biological tissue is different, the electrical and dielectric properties of each will be correspondingly different.

2.1.1 Electrical features of biological tissue

An understanding of the fundamental chemistry of human tissues could help us characterize their electric and dielectric properties. Some of the basic constituents of bio-matter are organic molecules (carbon), water, and electrolytes. Water has a very high relative permittivity (80 at 20 C) [23], and it makes up about two thirds of the human body in both, weight and volume. This knowledge is extremely relevant to the realization that the dielectric properties of blood reflect the abundance of its water content. Compared to all other tissue in the body [24], blood has the highest relative permittivity and loss tangent. As such, we could refer to the levels of water-content present in body tissue to categorize bio-matter into three broad categories:

1. High water-content tissue: high loss and relative permittivity; soft tissue (e.g. muscle) and bodily fluids (e.g. blood).
2. Moderate water content: medium relative permittivity; bony tissue.
3. Low water-content tissue: low loss tangent and relative permittivity; fatty tissue.

Table I lists the dielectric parameters for the tissues of interest in this thesis.

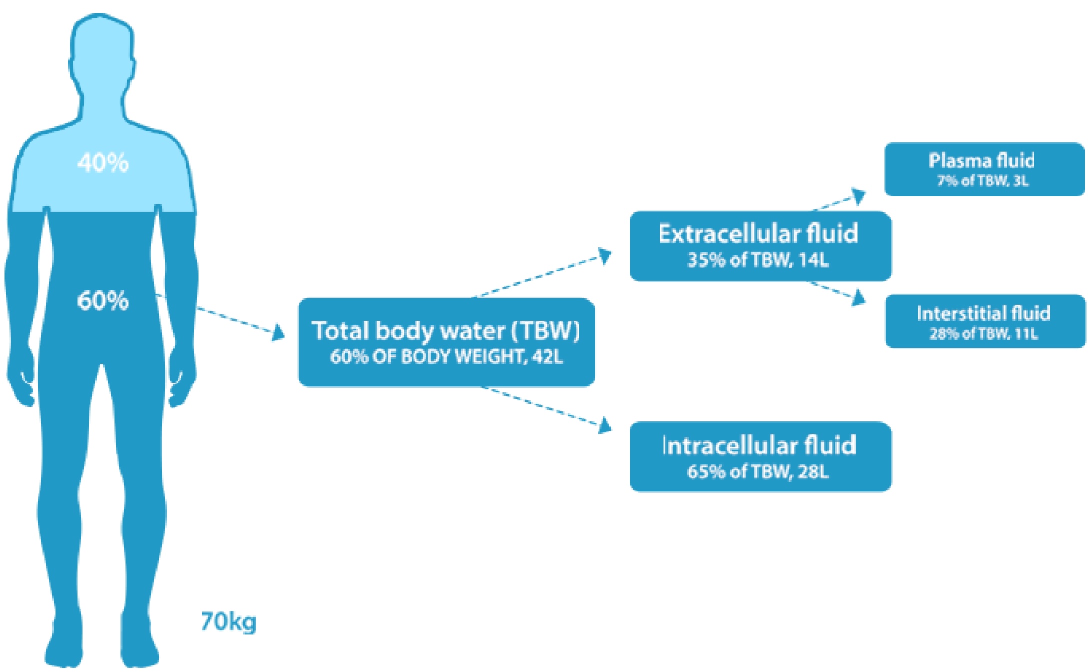

Figure 4. Water percentages in humans [25].

2.2 The Human Body as an Antenna Platform

It is important to note that the dielectric parameters of bio-matter are frequency dependent. This frequency-parameter relationship manifests to varying degrees according to the chemical constituents of a given tissue. And since water molecules constitute a significant portion of the body, using water-content levels as a reference to classify body tissue proves to be a very practical tool in predicting how any type of body-worn antennas would perform. Of course, knowledge of the dielectric properties of body-tissue is necessary within the limits of the antenna's area of operation or immediate vicinity. This is especially true for frequencies of antenna operation in the microwave region and above. At such frequencies, penetration depths of human tissues won't allow electromagnetic waves to reach bio-matter located more than ~ 50 mm away from a wearable or an epidermal antenna. For instance, a skin-hydration sensor tag antenna should be mainly interested in the properties of skin and any other tissues close to skin (e.g. fat and muscle). This means, that electromagnetic effects of internal organs, for instance, on antenna performance are irrelevant at such higher frequencies. Other considerations related to the area of operation or vicinity of a body-worn antenna include:

- Type of antenna application.
- The size and topology of the antenna.
- Radio components and receive/transmit power regulations.

Perhaps, the human body is one of the most challenging environments to employ as an antenna platform. As previously mentioned, it is an irregular surface with varying degrees of smoothness and curvature along its length and breadth. In addition, most body matter have significantly high relative permittivities. This forces much of the radiated electromagnetic fields into bio-tissue, hence degrading overall antenna performance. The location and dynamics of internal organs and bodily fluids further add to the complexity of predicting electromagnetic interaction between radiated waves and the body. On another note, it is important to keep in mind that the characterized or measured performance of any body-worn antenna could vary among different individuals; particularly among people of different age groups, body mass, muscle and fat indices.

Table I. Dielectric parameters of arm tissues (values presented here are rounded, but exact values taken from [23] were used. in the research).

Tissue	Frequency (GHz)	Relative permittivity	Loss tangent
Skin	0.9	41.40	0.42
	1.8	38.87	0.30
	2.45	38.00	0.28
Fat	0.9	5.46	0.19
	1.8	5.349	0.15
	2.45	5.280	0.15
Muscle	0.9	55.03	0.34
	1.8	53.55	0.25
	2.45	52.73	0.24
Bone	0.9	12.45	0.23
	1.8	11.78	0.23
	2.45	11.38	0.25

2.2.1 Biological tissue modeling for body-worn antennas

There could be several different graphical and mathematical ways to model the interaction of electromagnetic waves with biological matter. Each approach might include features that are otherwise not readily available in another. Whichever modeling approach is taken for electromagnetics analysis, the complex chemical and geometrical organization of bio-matter (within a human body) cannot be replicated exactly. In this section, we will be looking at different approaches to modeling body parts and biological tissue. To start, these approaches could be categorized into three distinct categories:

a) Physical
b) Analytical
c) Software

On paper, only approximate mathematical means which limit the number of bio-tissue and layers found in an actual body part (torso, arm, thigh) can be used. Such is the case present in [26], where a finite number of bio-layers were modeled as homogenous dielectric slabs. Regardless of such simplicity in modeling, a lot of useful conclusions can be drawn from a careful examination of scattering phenomena imposed by the dielectric layers found in the slab model. It is also important to realize that these simplifications can be particularly useful for application-specific or location-specific placements of the antenna under study. For instance, a wearable antenna operating in the 100 MHz FM region would be considerably large. Also, at a 100 MHz, penetration depths of many tissues are still larger than the thickness of the average human torso. Hence, a maximum of two infinitely long dielectric slabs with a thickness equal to that of an average human torso can be used for scattering analysis.

For simulations, software “full-body” phantoms referred to as "voxel phantoms" of varying levels of resolution and complexity are usually used to study the performance and effects of antenna radiation on the human body. Three such models could be seen in Figure 5. Acquiring this type of software tools can be costly and some forms of them might not be possible to alter or manipulate. Thus, simpler custom-made models are usually used [27] [28]. Single or multiple cylindrical and rectangular layers, representing different homogenous tissues, can be used to model different parts of the human body. This is one of the modeling scenarios implemented in the research project of this thesis.

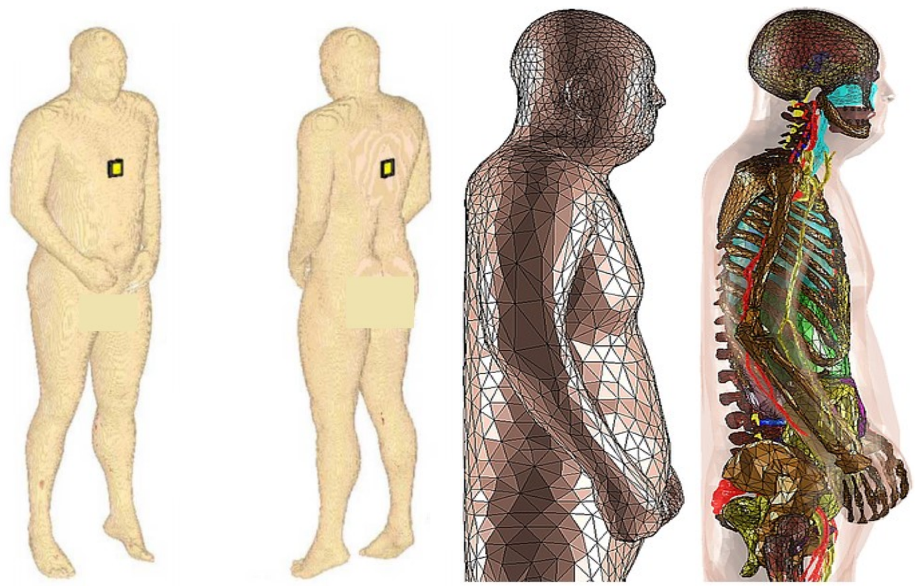

(a) (b)

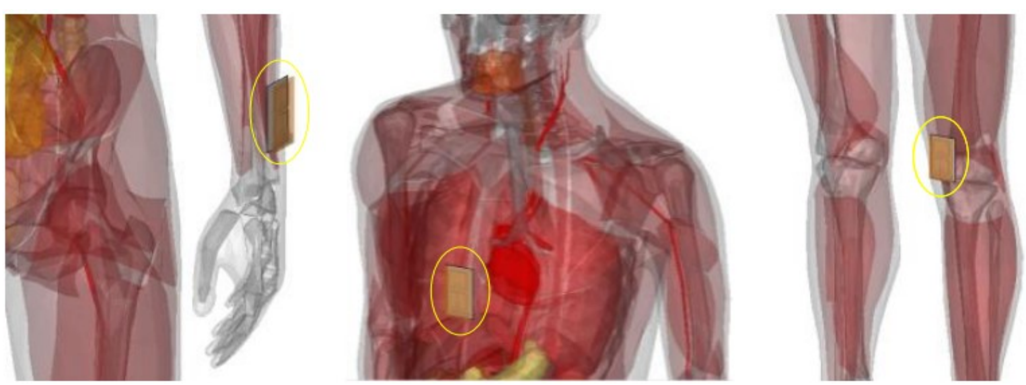

(c)

Figure 5. (a) CST “Hugo” model [29], (b) commercial body model used in HFSS [30], (c) ANSYS HFSS full body model [31].

Real life tests and measurements can be made with the help of physical phantoms or animal parts. However, a real human volunteer would be the most realistic test subject of all. The first alternative might consist of liquids or rigid jelly-like matter that has values of permittivity and loss tangent equivalent to those of real bio-tissue, Figure 6(a). The complexity and number of layers present in the physical phantom could vary. Dead animals, on the other hand, are also commonly used for body-worn antenna tests. In particular, implanted antenna research groups frequently employ dead pigs in their measurements [32] [5]. It is worth noting that it is uncommon to find actual human volunteers to act as measurement tests subjects instead of the previously mentioned alternatives.

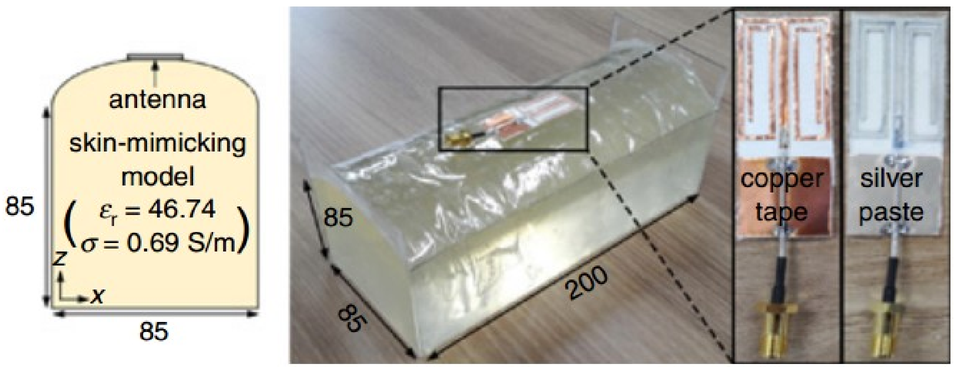

(a)

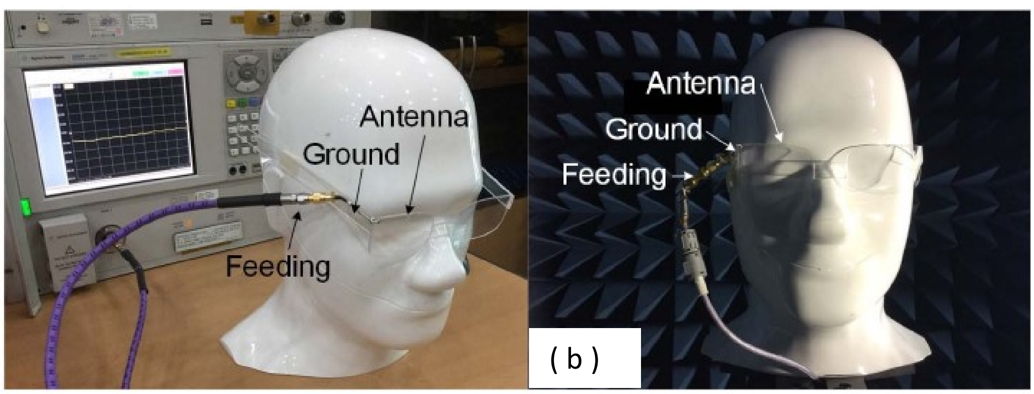

Figure 6. (a)Jelly-like slab dielectric phantom [33], (b) Human head phantom [34].

2.2.2 Software modeling

It goes without saying that the analysis of the performance of any body-worn antenna has to be done with the effects of the human body in mind. Literature reviews and simulations are the first steps that are taken into the design of any body-worn antenna. Therefore, it is of critical importance to create a wholesome or a partial human body simulation model that meets certain criteria. Some of those criteria include accuracy in shape and composition modeling, as well as accurate definitions of electrical and dielectric parameters of biological tissue. With this in mind, we need to address several issues in relation to human body modeling.

The ideal human body simulation model is one that encompasses all of the infinite states the body could be in, as well as all of the biological constituents it would have. This, however, and for all practical purposes, is impossible to realize. Therefore, approximations of the client's body have to be made. Hence, let us categorize modeling approximations into three categories:

1) Geometrical: shape and size approximations of the client's body.
2) Biological: consistency and composition of body matter.
3) Electrical/Dielectric: values of relative permittivity, magnetic permeability, loss tangent, and conductivity.

Based on what was discussed so far, let us delve into some practical rigor within the modeling process. We need to determine the body part which is subject to the attachment of the body-worn antenna (e.g. arm, leg, or chest) as well as any other immediately close body parts. This is where the geometry of the model comes into play, as well as the exact placement of the antenna. In this regards, performance of the antenna is first affected by the body part or tissue that is closest to it. In other words, performance parameters such as reflection coefficient (S_{11}), radiation patterns and gain are mostly determined by this part. Secondly, other layers of tissue still close to the antenna and its vicinity could affect the performance to varying degrees. It would be ideal to simulate the antenna on a whole-body model to take into account all such variables.

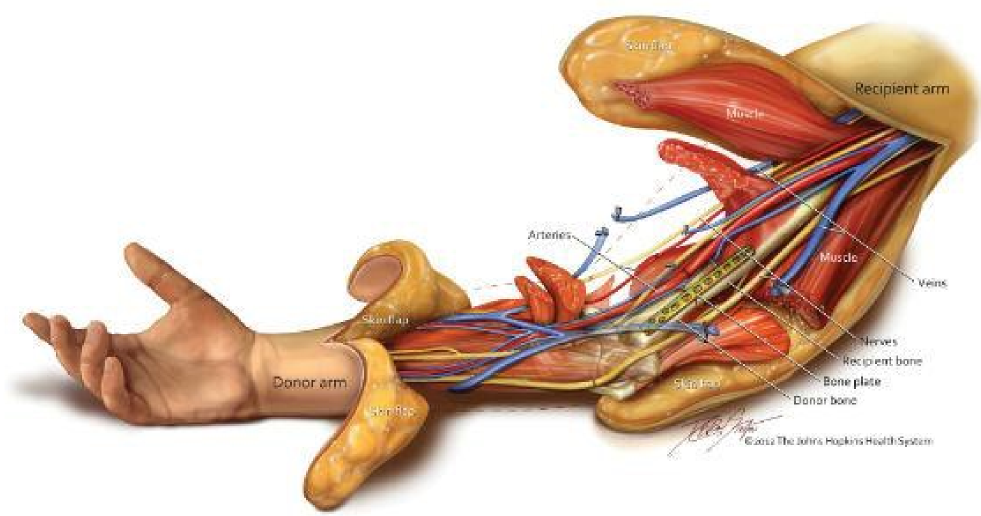

Figure 7. The many layers of bio-tissue in a human arm (original image from [35]).

Then, we would have to determine the biological constituents and layers of the body part. This is where biological and electrical modeling approximations come into play. There is a tremendous amount of major and other minor layers that make up any human body part. In a human arm we would find: skin (dermis epidermis), fat, blood vessels and arteries, nerves, muscles, bodily fluids, and bone (cortical, cancellous). All of those take up different shapes and forms. For practical reasons, the ability to accommodate bodily fluids as well as other minute and active bio matter into the body model is very limited due to their dynamic nature. Hence, it is acceptable to include bio matter with the greatest effect on antenna performance.

- **Available software**

In this section and the one following, we will take a brief look at three commercially available simulation software solutions and the methods they use in their computations.

a) XFdtd: This product, developed by Remcom Inc., uses the straightforward "Finite Difference Time Domain" (FDTD) technique. Although not as popular as the other CEM software, the FDTD method employed is very efficient in providing accurate results of field penetration into biological tissues. FDTD is usually labeled as the preferred method for performing electromagnetic computations that involve biological effects from wireless devices [36]; more on the FDTD technique is to follow in this section.

b) CST Microwave Studio: is based on the finite integration technique (FIT). It also allows the user to choose between solving in the time domain or in the frequency domain. CST has become a real competitor for HFSS, as it is gaining increased popularity in the last few years.

c) HFSS: being one of the first tools in the market, in addition to its practicality and ease of use, HFFS is one of the most popular CEM simulation tool used in the industry. The purpose of HFSS is to extract parasitic parameters (S, Y, Z), visualize 3D electromagnetic fields (near and far-field), and generate SPICE models, all based on a 3D FEM solution of the electromagnetic topology under consideration [37].

- **Computational Electromagnetics (CEM) methods**

a) The Finite Element Method (FEM): is a frequency domain method which uses Maxwell's equations in their differential form. The volume meshing technique employs tetrahedral cells to accurately mesh arbitrary shaped objects whose electrical/dielectric properties may vary with neighboring cells. The core unknown quantity in FEM analysis is usually an electric or magnetic field quantity. The field is approximated over each tetrahedral cell as a sum of known expansion functions with unknown coefficients. Hence, a sparse matrix is formulated to determine the expansion function coefficients [38]. FEM is appropriate to the modelling of electrically large and inhomogeneous dielectric objects [39].

b) The Finite Difference Time Domain (FDTD): is, just like FEM, a true 3D field solver which can be used to analyze arbitrary shaped 3D structures. FDTD algorithms solve Maxwell's equations in a fully explicit way, without the use of matrices. The volume meshing approach employs voxels (Yee cells) to accurately mesh the computational space [39]. Unlike FEM however, it is a time domain method. Since FDTD solves Maxwell's equations in the time domain, a time stepping algorithm is used which updates the field values across the mesh cell time-step by time-step. This means that the electromagnetic waves are explicitly followed as they propagate through a given material [38]. One of the significant benefits over FEM is its problem scaling advantage; which is a direct result for not requiring a matrix solve.

c) Finite Integration Technique (FIT): This technique is a time-domain method which employs the integral form of Maxwell's equations. FIT first describes Maxwell's equations on a grid space. FIT discretizes simulation objects in a similar manner to the FDTD method. However, the FIT transforms Maxwell's equations, in their integral form, to a linear system of equations. This technique treats boundaries between dissimilar media in a more accurate manner. FIT has the advantage of using Integral quantities. These quantities are more stable to calculate for a large grid or many time steps [39].

The authors of [40], used CST to simulate the performance of an FM wearable dipole. The same paper used an animated human voxel model in combination with XFDTD to analyze the effects of body dynamics on channel characterization of wearable antennas. In another instance, CST was used in [2] to simulate the performance of an embroidered wearable spiral antenna. The authors of [41] used another FDTD-based simulator, SEMCAD, to optimize their designed wearable antennas to operate in close proximity to a numerical representation of a physical tissue phantom of their design. On the other hand, a software HFSS phantom was employed to simulate and optimize an EBG antenna for wearable performance in [31]. Two more published research papers which made use of HFSS in their simulations are [33] [34].

The features of both competing full-wave simulators (CST and HFSS) were exploited in [42] where two different software phantoms were used for each simulator. The paper presents a circularly polarized (CP) integrated filtering antenna for wearable biotelemetry in the 2.4 GHz ISM band. The HFSS human model was obtained from [28] to test a summary of antenna performance criteria while the HUGO human body model [43] was incorporated into the CST microwave studio (MWS) software package to perform SAR calculations.

As for real-life physical modeling of human tissues, the authors of [27] realized gain measurements for their RFID tag by attaching it onto a liquid phantom resembling the human body. The phantom recipe consists of a mixture of water, sugar, and salt [44]. HFSS was employed in [33] where the authors also employed a skin-mimicking model inspired by [45] to conduct their antenna measurements. On another note, [15] proposed an implanted RFID antenna where simulation results in CST were compared to measurement results obtained with the use of a physical 3-layer (skin, fat, muscle) liquid phantom. The recipe the authors used was inspired by [45] and [46]. Link power efficiency between an implanted and an external antenna was measured in [32]. The measurement was conducted after placing an implanted loop inside a post-mortem pig's head, and also inside a human-head-equivalent liquid phantom. The pig's head used in the experiments was cut into two-halves, and the brain was removed from its skull. the implanted loop was then inserted in the skull after filling it with Satimo's Head Liquid phantom [47]. Table II lists a range of body-worn antenna software and physical measurement tools reported in the literature.

Table II. Literature examples of software and physical modeling of biological matter.

Paper	Simulations	Physical test subject	Application/ Frequency band
[27]	• FEKO (method of moment)	• Liquid Phantom	RFID
[34]	• HFSS	• Human head phantom	ISM (2.4-2.5) GHz
[40]	• XFdtd, CST	• Real Human	FM/ unspecified others
[40]	• SEMCOM (FDTD-based)	• Customized • Head-phantom	ISM 2.45GHz
[2]	• CST	• Real Human • Human Torso phantom	UHF broad-band
[31]	• FEM using HFSS • Unspecified FDTD solver	• Free space	ISM(2.4-2.5) GHz
[48]	• Unspecified	• Human Torso Phantom	WBAN/PAN
[32]	• HFSS	• Dead pig • Satimo's Head Liquid phantom	RFID
[42]	• CST, HFSS	• Real human	Biotelemetry/ ISM (2.4-2.5) GHz
[15]	• CST	• Liquid phantom recipe	RFID implanted
[49]	• FDTD solver (unspecified software package)	• None	MICS implanted

2.2.3 Radiation Efficiency and Specific Absorption Rate

- **Specific Absorption Rate (SAR)**

SAR characterizes the rate of absorption of electromagnetic energy by human tissues and is averaged over a sample volume. It is a crucial factor to evaluate for any antenna intended to operate in close proximity to the human body, and it is defined as follows:

$$\mathrm{SAR} = \frac{\sigma \,.\, E^2}{\rho} \qquad \text{Dot product form [50]} \qquad (1)$$

$$\mathrm{SAR} = \int_V \frac{\sigma(r)\,|E(r)|^2}{\rho(r)}\,dr \qquad \text{Integral form [17]} \qquad (2)$$

The FCC regulates SAR limits of body-absorbed radiation in accordance with IEEE C95.1-2005 [47] as noted in [48] and [31]. The international standard values of SAR in the U.S and Europe are 1.6 W/g averaged over 1 g of a sample volume and 2.0 W/g averaged over 10 g of the sample, respectively.

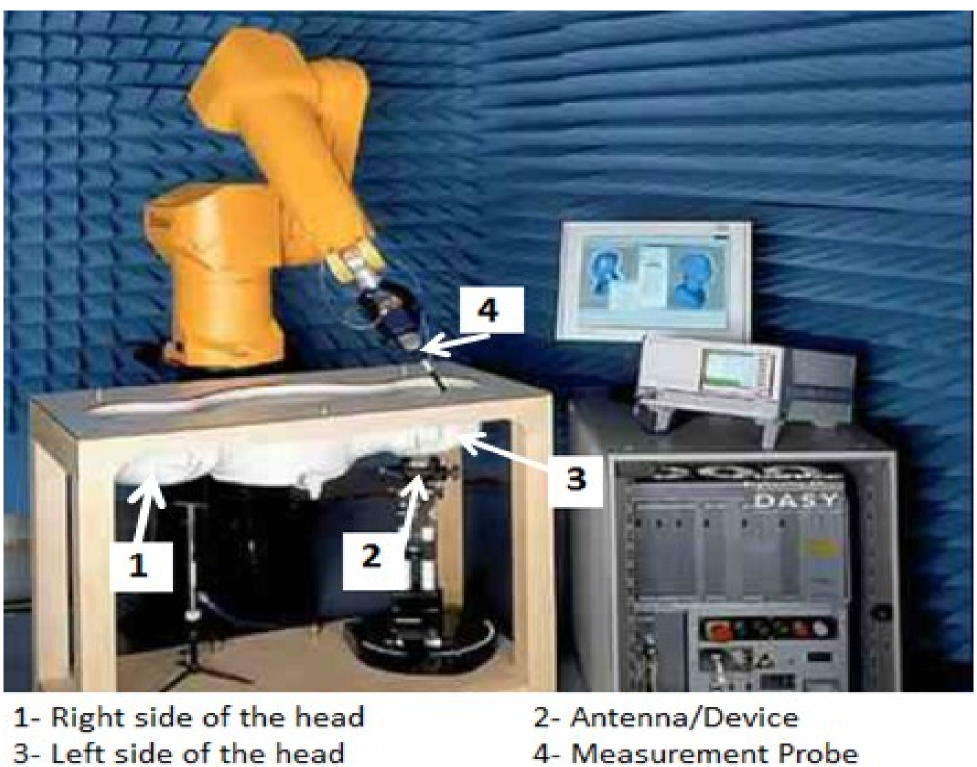

Figure 8. DASY-4 SAR measurement system [51].

The DASY-4 system created by SPEAG could be seen Figure 8. The DASY-4/52/6 series are a family of dosimetric assessment systems used to test SAR and near-field parameters for compliance with government regulations. As could be seen, there is a hollow head-phantom tub where liquids which replicate body tissue dielectric parameters are poured. The measuring probe is driven by a robot into the phantom containing the frequency-dependent liquids. The device or antenna under test is placed directly under one side of the phantom (left-head or right- head side) and is made to transmit at maximum power continuously. The averaging mechanism found in the SAR equation is performed by moving the probe through the head regions. The SAR must be measured on both the left and right side of the head-phantom. [52] and [53] provide full details on the exact measurement procedure with the DASY system.

In [54] the measurement set-up used for SAR characterization of UHF wearable antennas included three commercially available tools: a DASY-52 NEO set-up, a TX90L robot, and a liquid phantom (HBBL300-2700V4). In another instant [51], a DASY-4 was used to evaluate the SAR of topologically different textile antennas at 2.45 GHz, 5.2 GHz, and 5.8 GHz.

- **Radiation Efficiency**

Radiation efficiency is a measure of the power radiated by an antenna as electromagnetic waves in relation to the power fed to antenna terminals. Ideally, it is desired that an antenna would transform all of the power fed to its terminals into radiating electromagnetic energy which then propagates into the far-field. However, several natural factors, such as impedance mismatches between an antenna and its feeding network cause power losses. In body-worn antennas, the very lossy nature of human body tissues draws in electromagnetic energy (in the form of the reactive and radiating near-fields) into itself [12]. This phenomenon greatly reduces radiation efficiency. The magnitude of this degradation is dependent on body-antenna separation, antenna topology, and frequency of operation.

2.3 Body-worn Antenna Structures and Topology

The design of body-worn antennas should satisfy certain requirements that are otherwise not necessarily required of conventional antennas. As discussed in Chapter 2, the human body poses many challenges to the design of efficient and reliable antennas when it is used as an antenna platform. This is due to the high relative permittivities and loss tangents associated with biological tissue. Significant detuning and radiation loss could be incurred if the antenna structure was not designed to address these effects. Overcoming these challenges should still ensure the safety and comfort of the antenna’s client. The size of the antenna, its shape and associated fabrication materials are largely application-dependent. However, the client’s preferences should also be considered in the design procedure to ensure user satisfaction.

Technically, the type of body-worn application dictates the operational bandwidth of the antenna. This in turn influences its size, shape and profile level. Hence, depending on the antenna structure there is a range of different antenna structures that can be used for body-worn applications. Before addressing the details of fabrication and topology, it is necessary to state the following distinctive features of the three types of body-worn antennas:

- Implanted antennas have to be made of biocompatible materials, be extremely miniaturized, and ensure minimal SAR levels.
- Epidermal antennas are supposed to be extremely thin, if the surface area it covers is large, the antenna structure has to be breathable. Flexibility and stretchability are typical features of epidermal antennas. Also, they are usually preferred to have very low profiles and be conformable to skin surface.
- Wearable antennas are usually either integrated into clothing or made from conductive textiles and fabrics. They have the largest body-antenna separation gap. Wearable antennas might also be integrated into accessories, such as bracelets or glasses. Such kinds of antennas have the largest size profile of all body-worn antennas.

Some applications do not impose stringent size profile requirements. For instance, wearable GPS antennas integrated in the clothing of military or firefighting personnel do not have to be low profile. Moreover, some antennas have to be three-dimensional. This is evident in implantable applications [5] [32] as well as in other multi-purpose devices [34].

In addition, the application type also dictates the desired detuning-immunity and sensitivity of the antenna. For antennas where bandwidth detuning is not an issue, the antenna structures can be single-layer, with only one radiating element resting on the top of a thin substrate. Other antenna applications which demand reliable and efficient wireless communications require EM waves to be strongly decoupled from the body. This could be achieved by building multi-layer antenna structures, which normally include at least a ground layer besides the radiating layer.

Before delving into any further discussion about antenna topology, the terms "single-layer" and "multi-layer" mentioned in the paragraphs above need to be explained. Hence, we will now formally introduce the following two distinct categories of body-worn antenna structures:

1- Mono-layer/Single-layer antennas: are composed of only one layer on which the radiating element rests upon.

2- Multi-layer antennas: consist of at least two layers, a radiating element and a ground plane. Other multi-layer antennas might include an EBG layer or yet multiple radiating elements with each radiator resting on a separate individual layer.

The decision to choose between a multi-layer antenna and a single-layer antenna should be made upon understanding the nature of the application and its performance requirements. Multilayer antennas utilizing a ground plane shield the radiating elements from the effects of the human body. Hence, robust antenna operation is almost guaranteed regardless of small body-antenna separations. This could allow for higher transmission power if needed, as SAR values are considerably lower compared to single layer antennas. For overall optimal antenna radiation performance, a multi-layer antenna would be the favorable option.

To overcome body-worn antenna performance degradation, electromagnetic band-gap structures (EBGs) and Artificial Magnetic Conductor (AMC) structures could be used to isolate the antenna from the ambient biological environment [12]. These metasurface-enabled wearable antennas always take the form of multi-layer antennas. Although there is a distinction between EBG structures and AMC ones, they both allow wearable antennas to demonstrate stable performance when placed close to the human body in body-worn communication devices. This naturally leads to reduced body-absorbed radiation and SAR values.

On the other hand, single layer antennas can be especially favorable for a number of factors. For one, single-layer antennas are generally more flexible and deformable. Multi-layer antennas are more rigid given the inherent increased thickness and ground plane presence in them. Thus, applications that require flexibility and antenna conformability to body surface do not favor multi-layer antennas.

On another note, it is also easier to fabricate stretchable antennas which consist of only one layer of conductive material (single-layer). These are all features of special importance to epidermal applications. Without the presence of a ground structure to decouple a body-worn antenna from biological tissues, the radiating element will become inherently miniaturized due their high relative permittivities. Thus, lower frequency applications (less than 1 GHz) could make use of the size advantage single-layer antennas have. This is coupled to their ease of fabrication as multi-layer antennas require more accurate and precise alignment of constituent layers [55].

For applications where maximum radiation efficiency is required with minimal detuning and robust operation, multilayer antennas would make the better option. Nonetheless, human skin can act as a constructive reflector if an adequate gap is present between itself and a single-layer antenna [26] [56] .

2.3.1 Single-layer Antennas

There are two broad categories a single-layer antenna can be selected from:

a. Wire loops and dipoles
b. Slot and Coplanar antennas;

The first category of single-layer antennas requires minimal conductor area. This allows for more room and less electromagnetic coupling so that other electronic components could be placed within the vicinity of the antenna's plane. On the other hand, the second category of antennas is generally more robust with better body-antenna separation detuning immunity. Literature examples of both types will be presented later in a following section.

- **Loop antennas:**

There are two distinct loop antenna designs:

1- The small (magnetic) loop antenna: with a total length much smaller than one wavelength (< 0.1 λ) [57].

2- The large (resonant) loop antenna: with a total length of around one wavelength and longer [57].

Electrically small loop antennas have a complex input impedance with high reactance. This makes them unsuitable for transmitting applications [12]. The radiation pattern and resistance of small loop antennas are both independent of loop shape (circular, square) and depend only on the area of the loop itself. The constant phase and current amplitudes around the loop cause the radiation pattern to have a maximum in the plane of the loop and a null along the axis normal to the loop, Figure 23.

In contrast, large loops have current amplitude and phase variations along their lengths. This causes their impedance and radiation pattern to depend on loop size, and to a very small extent, loop shape [58]. This could be seen in Figure 24.

A resonant loop antenna would be the better option for transmit/receive applications. This is due to the fact that electrically large loop antennas have higher radiation efficiency and smaller input impedance compared to small loops. They are also better suited for data transmission in particular given that small loops retain highly inductive input impedance. The resonant loop antenna can be regarded as a folded dipole which has been reformed into a loop. In free space, maximum radiation is found parallel to the plane of small loop antennas (Figure 9); this is in contrast to the radiation pattern of large loop antennas where the maximum is normal to the plane of the antenna (Figure 10).

(a) (b)

Figure 9. (a) Radiation pattern of a small loop antenna, and (b) its current distribution.

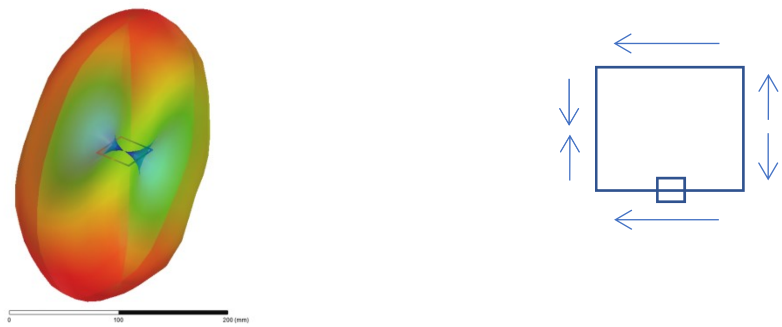

(a) (b)

Figure 10. (a) Radiation pattern of a large loop antenna, and (b) its current distribution.

Usually, large loops are used for applications at higher frequencies as their physical size decreases. This is added is added to the miniaturization provided with antenna placement close to high relative permittivity tissues. Hence, using electrically large loop antennas, around one wavelength long, would not pose a problem in relation to antenna size.

Although circular loop antennas are more comprehensively studied and analyzed in the literature, the square loop antenna was chosen due to the simplicity associated with its design, simulation, and fabrication. Nonetheless, measurements confirmed that electrically large loops have qualitatively similar electrical performance regardless of loop shape [58]. When it comes to body-worn antenna implementation, a practical design is a better design. All of the project's presented antennas were chosen to be approximately 1λ (one wavelength) long with each side equal to 0.25λ.

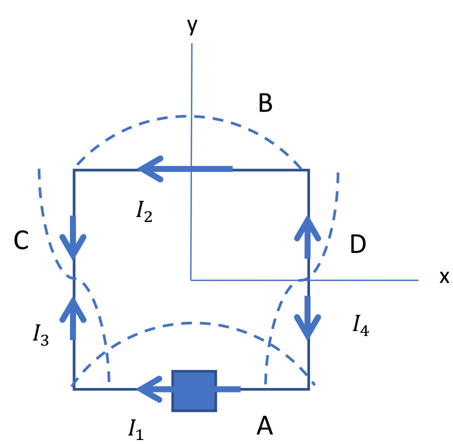

Figure 11. Current distribution on a large loop antenna.

Current distribution on each side of the loop:

$$I_1 = I_2 = -\mathbf{x} I_o \cos(\beta \dot{x}), \qquad |\,\dot{x}\,| \le \frac{\lambda}{8} \tag{3}$$

$$I_4 = -I_3 = -\mathbf{y} I_o \sin(\beta \dot{y}), \qquad |\,\dot{y}\,| \le \frac{\lambda}{8} \tag{4}$$

As can be seen in Figure 11, current distributions on the feed side (A) as well as that on the opposite side (B) are similar to those of half-wave dipoles. Current maxima occur at the center of each of these sides while minima occur on the opposing adjacent sides (C) and (D). The opposing currents I_3 and I_4 cancel each other, hence not contributing to radiation. The 0.25λ separation between (A) and (B), establishes a virtual array configuration consisting of both sides (A) and (B) with constructive interference enforcing their radiation every 0.5π (90 degrees) intervals.

2.4 Materials and Fabrication

Since there is a wide range of applications where wearable antennas could be used, there should also be a corresponding variety of substrates and fabrication methods suitable for a given application.

Body-worn antennas are distinguished by a high level of compactness, flexibility and durability. Certain added requirements of body-worn antennas, especially implanted and epidermal antennas, require that the materials used should be biocompatible and compliant with health and safety regulations [1]. If an application requires cloth integration, conductive textiles might be adopted for antenna fabrication. Special materials such as conductive ink and or adhesive copper foil might be needed to fabricate low-profile and stretchable antennas [55].

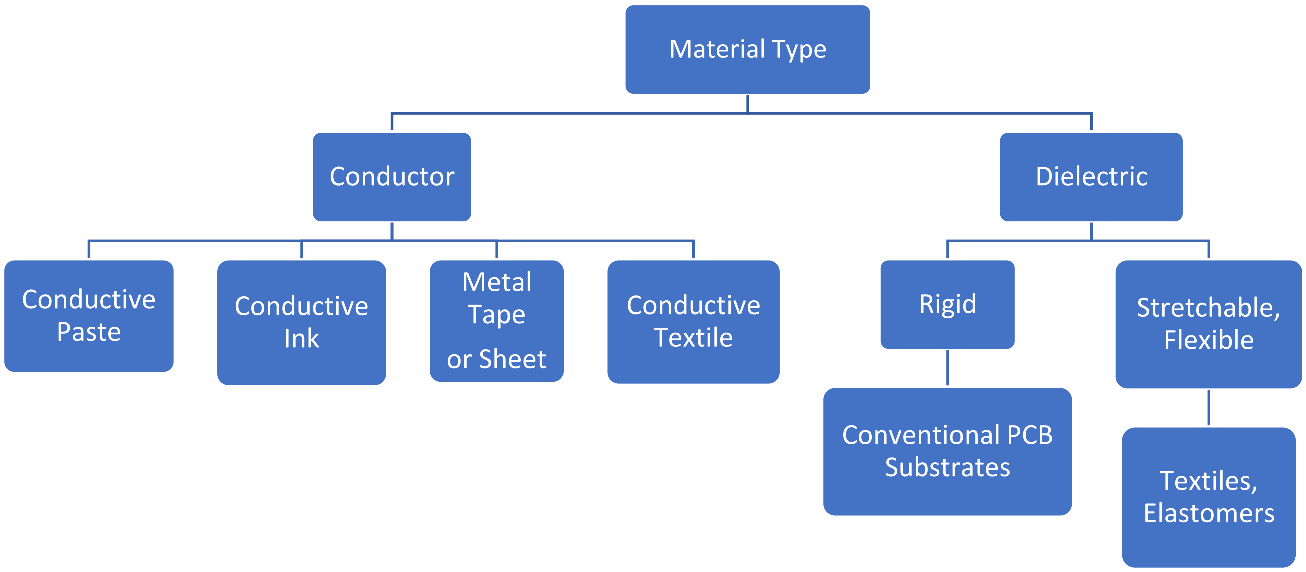

Figure 12. Materials used for body-worn antenna fabrication.

As can be seen in Figure 26, there is a wide range of materials to choose from for body-worn antennas. However, appropriate choices should be made which best serve the body-worn application of interest. There is also a corresponding variety of fabrication techniques available, some of which are:

- Sewing and embroidery: This is the preferred option for making wearable textile/fabric antennas instead of the direct adhesion of E-textiles over cloth fabric. Hence, the electrical properties of the fabric would not be altered by the inclusion of any adhesive material [1].
- Paste or ink printing: This popular technique can be done using silver and gold nanoparticles-based conductive inks. Inkjet-printers could be utilized for the purpose of depositing ink droplets (few picoliters in volume) at a very high resolution [55]. The quality of printing mainly depends on the viscosity of the ink or paste, as well as on the properties of the surface of the substrate upon which deposition will be done.
- Cutting printers: These machines could be used to cut flexible metal sheets and substrates to be later adhered with each other. Such fabrication tools are very practical and cost effective for research and proof-of-concept testing of body-worn antennas.

No matter what kind of materials are to be used, the electrical properties of the uncharacterized materials must be obtained, such as conductivity, loss tangent, and permittivity.

Antenna topology and shape can be chosen after fully understanding application requirements. Then, software simulations and other analysis means can be used for design optimization. Only then, the choice of materials and fabrication methodology can be decided upon.

2.5 Literature Examples

2.5.1 Multi-layer antennas

Based on what was discussed about different antenna topologies and fabrication methods, it would be appropriate now to examine related examples from the literature. By the end of section 2.5, Table III lists a range of multi-layer and other single-layer body-worn antennas including their applications and fabrication methods reported in the literature. Selected designs and others not included in the table are also discussed in this review section. In [28], three similar multi-layer antennas are studied for performance at 2.4 GHz. The antennas are composed of fabric substrates sandwiched between radiating elements on one side and ground planes on the other. Figure 13 shows a multi-layer patch antenna presented in [59]. Silver paste was used for the making of the radiating element and the ground plane. The fabric substrate is composed of polyester (66.2%) and cotton (33.8%). In another instance, an antenna consisting of two complementary radiating elements (loop and a dipole) is presented in [60]. The authors intended to use the complementary nature of the reactances of dipoles and loops to minimize near-filed stored energy in the body.

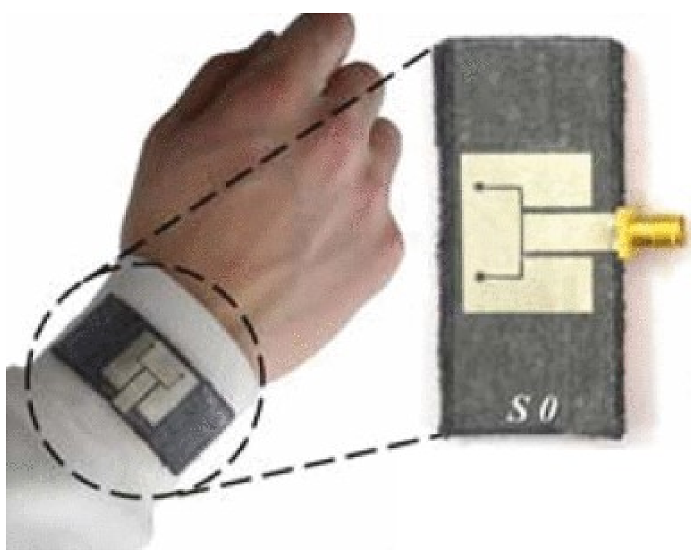

Figure 13. Silver ink multi-layer antenna [59].

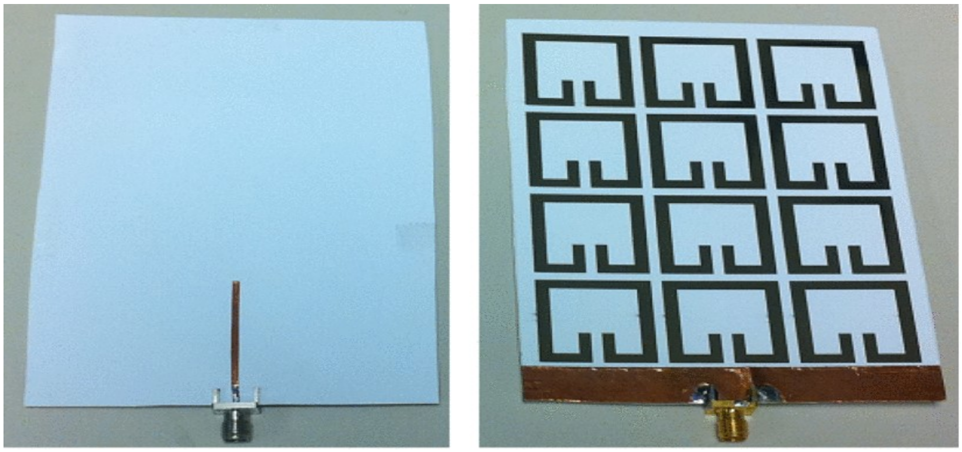
Figure 14. EBG backed monopole antenna [48].

In [61] the authors investigate antenna performance besides various fabrication techniques of textile multi-layer patch antennas, such as : copper mesh/foil and conductive spray . As for EBG multi-layer antennas, the authors of [62] presented the design, analysis, and performance of a bicep-mounted flexible EBG inverted-L for 1.85 GHz applications. Also, a microstrip monopole antenna backed with an inkjet-printed EBG array is presented in [48], see Figure 14. The improvements incurred in utilizing these special structures for antenna performance are studied in [63]. The authors also presented a slot antenna with two different-sized AMC ground planes for 2.8 GHz wearable applications.

Another EBG inspired wearable antenna in [31] was fabricated on a semi-flexible RT/duroid 5880 substrate. Detailed analysis and measurements are presented for various cases when the antenna is subjected to structural deformation and human body loading, and in all cases the EBG-backed monopole antenna retains its high performance. The antenna was fabricated on an LPKF ProtoMat H 100 milling machine. The EBG array does not only isolate the antenna from the human body resulting in very low SAR, but also enhances radiation efficiency and gain. In [64], a dual-band CPW-fed wearable antenna in combination with an AMC surface for 2.45 GHz and 5.8 GHz applications is presented.

2.5.2 Single-layer antennas

A folded dipole besides number of other single-layer RFID slot antennas for wearable applications are studied in [14]. In [27] a temperature sensing RFID tag is presented where the antenna is an inductively fed single-layer loop antenna. Tuning capability for the same antenna was previously featured in [65] where body temperature was directly measured by an EM4325 microchip, Figure 15(a). However, the power transfer-coefficient tuning "whiskers" of [65] were not presented in their more recent publication [27]. Nonetheless, they were able to demonstrate how epidermal antennas can be significantly sensitive to placement conditions.

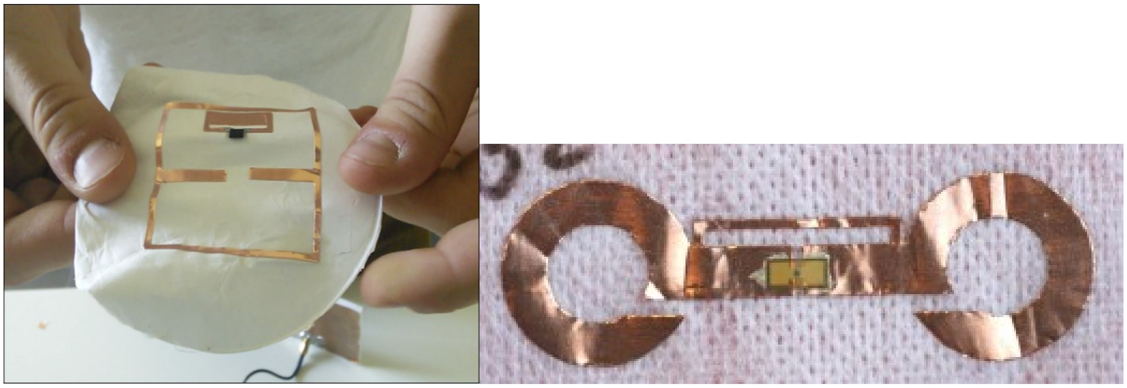

(b) (b)

Figure 15. (a) RFID single-layer loop tag [65], (b) RFID single-layer dipole tag [13].

Both of [65] and [27] are based on the one wavelength loop antenna presented in [66]. This paper presents a one-wavelength loop antenna fed by an inductively coupled loop for on-body applications. The performance of the antenna pasted on the chest of a reference model was simulated by HFSS and then verified by FEKO, which is based on The Method of Moment (MoM). Moreover, the author didn't specify which CEM method was used, keeping in mind that FEKO includes hybrid solvers such as MoM/FEM.

The forthcoming of printed electronics and special inks is always seeing interest in body-worn applications. In [55] a single-layer coplanar monopole was fabricated by depositing conductive silver-nanoparticles ink by an inkjet printer. However, the author intended to focus on the different fabrication techniques, design criteria, flexibility characterization, and the testing of flexible and wearable antennas.

Several wearable GPS multi-layer and single-layer antennas were fabricated and tested in [67], some of those where previously presented in [68] and [69]. The tests point out that when attached to a human body, most antennas exhibit a radiation pattern similar to that of a patch antenna. This is something that was also observed during the course of testing the antennas of this thesis at frequencies in the region of 1 GHz and above. The authors point out that a small separation (1-3 mm) between body and antenna is sufficient to keep the user's body from the reactive near-field of the antenna. This is important to note as the reactive near-field determines the input impedance of a closely spaced wearable antenna, hence, affecting its bandwidth, gain and efficiency.

As previously mentioned, embroidery is a common technique to fabricate wearable antennas. Several single-layer RFID tag dipoles were embroidered on cotton with using a zigzag sewing pattern in [70]. In [13], a dipole tag antenna for the European RFID band (866 MHz) was tested on a real human subject, see Figure 15(b). It was shown that a maximum read range up to 7 meters can be achieved given a 10 mm separation from the body. It was also noted that the actual range is also dependent on tag location on the body. Another embroidered RFID tag antenna [71] is optimized to achieve up to 2.5 m read range. This was achieved when the tag had a 1 mm thick of cotton-fabric separation from the body. Though not explicitly stated, the simulator used is HFSS as can be inferred from the outlook of the model and the default colors of rectangular objects.

2.5.3 Implanted antennas

The authors of [32] discuss RFID-inspired wireless brain-machine interface systems. It was demonstrated how millimeter-sized loop implanted antennas are capable of efficient coupling to an external transmitting loop antenna through an inductive link. The authors also discuss the use of conductive textiles and threads to fabricate wearable antennas. The paper presents, planar centimeter-sized loop antenna configurations as external antennas, and millimeter-sized three-dimensional loop antennas as the neural-sensor antennas.

In [15], an implanted RFID tag antenna for biomedical applications was fabricated and tested with a liquid phantom. The antenna is electrically small, and exhibits a directional radiation pattern. Hence, operation in passive-mode does not allow for appreciable communication range. If the tag was actively powered up to 20 dBm, a maximum communication range of 10 m could be achieved inside a closed room.

2.5.4 Stretchable and flexible materials

As evident from the literature examples presented so far, textiles are not the only materials that can be used for designing and building body-worn antennas. Different types of flexible and stretchable materials can be used to realize the making of these antennas. The use of such materials would be of critical value for epidermal antennas applications where the antenna structure is desired to be conformable to skin surface.

A prime example would be polymer-based materials, such as Dupont's Kapton polyimide, the silicon-based elastomer poly-dimethyl-syloxane (PDMS), and the FDA-approved skin adhesive Tegaderm. A polymer is a very large molecule comprised of smaller structural units called monomers. In other words, when a chain of atoms forms a backbone for other atoms to join in, a polymer is created through polymerization. Examples of common polymers include cotton, nylon and rubber.

The major advantage of using polymers lies in their high thermal resistivity, hardness and flexibility which all arise from the strong intermolecular forces present in their structures. These are all very desirable traits that find good use in the making of epidermal antennas. Now, Polymers come in different chemical configurations and categories. Three such categories of interest to epidermal antennas are:

1. Polyamides: which are formed when a repeating pattern of amide, -CO-NH-, links are present in a polymer structure. Proteins are examples of naturally occurring polyamides [72].

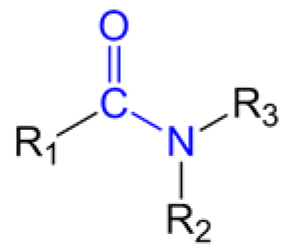

Figure 16. Structural formula of an amide [72].

2. Polyimides: are polymers formed from the presence of a repeating pattern of two acyl groups known as imides (C=O) bonded to nitrogen (N) [73].

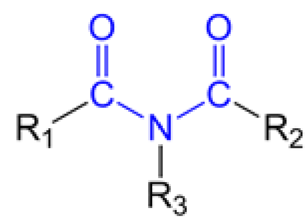

Figure 17. Structural formula of an imide [73].

3. Polymers which include a urethane linkage (Figure 32) in their backbones are called Polyurethanes. these polymers can take up the form of adhesives, paints, foams and fibers. This adaptability makes them very resourceful. Unlike other polymers which are produced and sold as powder or films, polyurethanes are made directly into the final product such as liquid spray or foam.

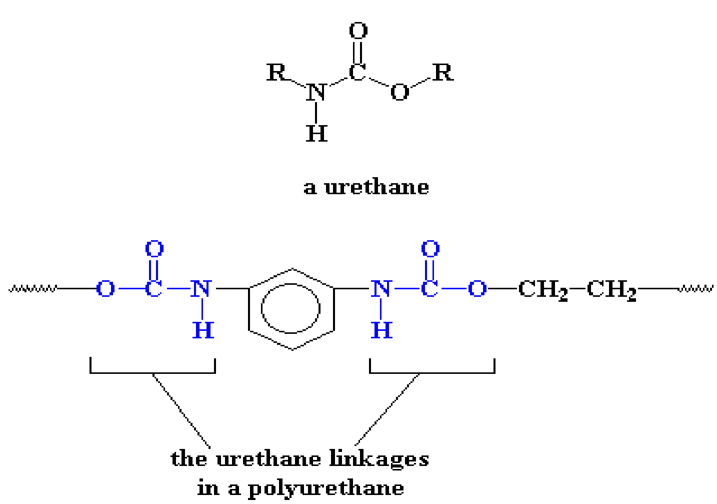

Figure 18. Structural formula of urethane [74].

4. Hybrid polymers: consist of organic and inorganic components (the latter contains no carbon atoms).

A well-known example of hybrid polymers would be PDMS. It is an elastic polymer, hence the name (elastomer). A comprehensive discussion about PDMS and its potential for use in antenna fabrication for WBAN is discussed in [75]. Also, PDMS finds implementation in rugged and high temperature settings; such is the case with outdoors and industrial sensing applications [76].

Another popular polymer based material is Tegaderm. This medical-grade adhesive consists of a thin polyurethane membrane coated with a layer of an acrylic adhesive. It is very elastic and can be stretched to over 300%. Besides the RFID sensing tag in [27], an epidermal inverted-F antenna also used Tegaderm as a stretchable substrate [77]. The antenna was reported to be tunable and could maintain robust operation 2.4 GHz. The flexibility and stretchability of Tegaderm enable the radiating element to withstand body moisture and skin deformation.

In [78], silicone and thermoplastic polyurethane (TPU) were used to test the performance of a 2.45 GHz wearable dipole antenna. HFSS simulations and physical phantom measurements have been carried out, where stretching the antenna caused a decrease in radiation efficiency. The phantom consisted of a plastic container filled with the SPEAG MSL2450 liquid.

Table III. Literature examples of multi-layer and single-layer antennas.

Paper	Antenna Topology	Materials/Fabrication	Application type/ Frequency band
[27]	• Single-layer RFID loop	• Adhesive copper • Adhesive film (Tegaderm)	RFID
[33]	• Single-layer Spiral monopole	• Copper and silver paste • textiles	MICS
[62]	• Single- layer Inverted-F antenna	• Tegaderm	ISM (2.45 GHz)
[76]	• Single-layer dipole	• PDMS	Industrial temperature sensing
[34]	• Non-planar 3D-Monopole	• IZTO as electrodes/conductors • physical vapor deposition process	Wearable glasses/ ISM(2.4-2.5) GHz
[40]	• Patch Antennas • Monopoles • Dipoles	• Not listed	FM/ Unspecified others
[41]	• Patch antennas	• Taconic (TLY-3/RF-60A) • PTFE woven glass	ISM 2.45GHz
[2]	• Broad-band textile Spiral antenna	• Silver-coated conducting thread Liberator™ • Entrepreneur Pro PR1000e digital embroidery machine	UHF broad-band
[31]	• Multi-layer Monopole (EBG)	• Semi-flexible RT/duroid 5880 substrate	ISM (2.4-2.5) GHz
[48]	• Multi-layer monopole (EBG)	• Inkjet-printing technology on commercially available photo paper • Cabot conductive ink CCI-300	WBAN/PAN
[32]	• Textile Patch antenna • Dipole • Loop	• Unspecified	RFID
[42]	• Multi-layer filtering antenna	• Ordinary	Biotelemetry

Conclusion

We have seen how the human body poses exceptional challenges to the performance of body-worn antennas. One could use software simulators and physical phantoms to study electromagnetic wave interaction between antennas and tissues. These software and physical solutions cannot hope to replicate the full complex makeup of an actual human body. Hence, it would be useful to use a combination of different modeling schemes and approaches to cover as much of the unique performance aspects of body-worn antennas as possible. This chapter also sought to bring insight into the various topologies and applications of body-worn antennas. The literature review presented various examples of such used topologies and associated fabrication methods. The next chapter shall address all of these topics in light of the goals and requirements of the project.

Chapter Three: The Epidermal QL Antennas

The previous chapter introduced the theory and techniques used in the design of body-worn antennas. In this chapter, we will further build upon these principles and relate them to the design of the quadruple loop (QL) antennas. The topology of the antennas and their electromagnetic features will first be addressed. Then, we will look at different simulation setups used in the simulations of the epidermal QL antennas. This is accompanied by a discussion of the simulated radiation patterns at three popular frequency bands. Finally, we will look at the various fabrication methods and tools used in their making.

3.1 Antennas of the Project

The project was aimed at coming up with a biotelemetry device capable of sensing body signs, and of reliable wireless communications. The primary sensing components included body-hydration, glucose, and blood pressure sensors. Such body-parameters can be reliably sensed only if the sensors are placed extremely close to skin surface. Hence, an epidermal antenna concept with a very thin substrate and no ground plane was the natural solution to proceed with.

The primary frequency bandwidth of interest was the ISM region of 2.4-2.5 GHz. Hence, a robust ultra-thin mono-layer square loop antenna was sought to work for a Bluetooth Smart/Bluetooth Low Energy (BLE) node. This node is intended for bio-sign sensing and telemetry communications between a human subject and a nearby access point, hence forming a WSN which would in turn relay data to medical staff located in another location. Several restrictions on the profile and geometry of the antenna were imposed as well. Substrate thickness had to be equal to or less than 1 mm in order to allow adjacent hydration sensors to work properly without the hindrance of a ground plane. As mentioned in Chapter 1, one of the objectives of the research project was to find an optimal frequency band for epidermal antenna applications. This meant that other loop antennas operating at different frequency bands (GSM-900 and GSM-1800) were also designed and fabricated besides the BLE antenna.

3.1.1 Topology

Since the project is concerned mainly with integrating close-proximity biometric sensors, a thin groundless antenna structure was needed. Usually single-layer antennas are disregarded for reliable off-body communications. This is due to the significant amount of absorption incurred due to the lack of a reflecting ground layer as well as the minimal spacing between the radiating element and the body. On the other hand, multi-layer antennas are usually non-conformable and rigid. Hence, the effort of the antenna design team was aimed at accomplishing two goals: designing an antenna structure that can reliably communicate without a ground plane and thus considerable EM wave absorption and loss would take place, second, find the optimal frequency band, at which the antenna would perform best.

It was decided that a large loop around one wavelength long would be a more practical option compared to a small (magnetic) loop antenna. This decision was reached to address the following: maximum power can be delivered to the antenna if it is in the order of one wavelength. This conclusion was reached after observing reflection coefficient values which reflect how much power was accepted by the antenna. This is in par with the intrinsically higher complex input impedance and low radiation efficiency of small loop antennas. As previously mentioned, the one-wavelength long loop emulates an array consisting of two quarter-wave dipoles. During the course of the research, all designed antennas were approximately one wavelength long for each antenna's respective frequency band of operation.

In the initial stage of research, two different square loop antennas were designed. The quadruple loop (QL) antenna operating at 2.45 GHz (Figure 19) showed better performance in comparison to the standard square loop [78]. Adding the four circular patches to the main radiating sides of the one-wavelength loop antenna improved both of the radiation efficiency and gain of the loop. Moreover, this modification made the loop antenna withstand frequency detuning. These improvements were observed in measurements and simulations as shall be seen in Chapter 4.

After accomplishing the first objective of designing a robust single-layer antenna to operate at BLE frequencies, the research later focused on studying overall QL antenna performance as an epidermal antenna in three major frequency bands: around GSM-900 (800 MHz-1000 MHz), around GSM-1800 (1.6-1.9 GHz), and ISM (2.4-2.5) GHz. It was necessary to consider the significant effects on antenna detuning as a function of antenna position on the forearm. Also, previous tests indicated the favorability of positioning the antenna on the ventral side of the forearm. In addition, modifications to simulation modeling had to be applied after observing the wider bandwidth phenomena seen in measurement results compared to those of previous simulations.

The largest antenna intended for GSM-900 implementations (Figure 21) is based on the QL antenna with the addition of matching circuitry. Different square-loop antenna shapes were also simulated and fabricated for 1.8 GHz tests but it was decided to stay with the simple QL antenna shape (Figure 20). Current distributions for each antenna can be seen in Figures 19-21.

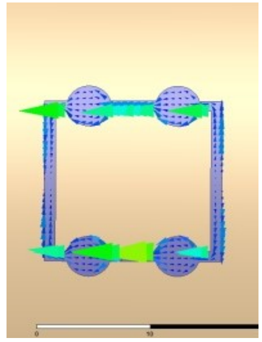

Figure 19. QL BLE antenna: (15*15) mm^2.

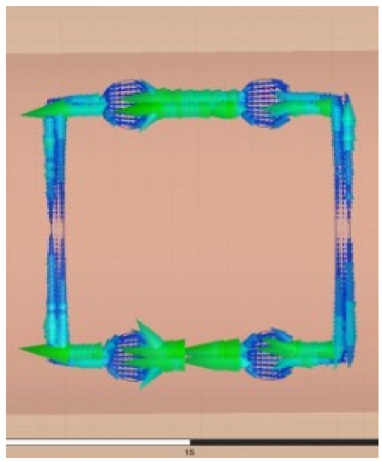

Figure 20. QL GSM-1800 antenna: (20*20) mm^2.

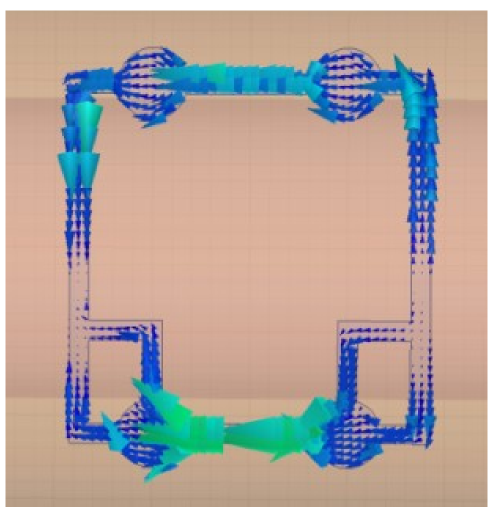

Figure 21. QL GSM-900 antenna: (37*37) mm^2.

Current distributions seen in the figures above indicate that the electrical lengths of all antennas are equivalent to one wavelength at their respective operating frequencies. It should be noted that at all frequencies where the antenna has better than a -10 dB of reflection coefficient, the current distribution on the antenna indicates a one-wavelength pattern of current maxima and minima. The addition of the circular patches forces the current to flow at different angles to cover the surface of the patches. This mechanism was intended to emulate that of current flow in spiral antennas which are characterized by their wide bandwidth due to quasi-circular current flow. The introduction of the circular patches also allows current to cover more conductor area freely which results in increasing the gain. The matching circuit in the GSM-900 antenna was necessary to miniaturize the antenna such that a further increase in its perimeter does not increase the capacitance incurred by further bending or wrapping around the arm.

3.2 Project modeling

The modeling approaches used in this research endeavor included the use of two transmission line models for theoretical predictions, and a multi-layer cylindrical HFSS model for simulations and analyses. Since the intended placement of the epidermal antenna is to be on the forearm of a human client, we were mainly interested in a simple multi-layered model which encompasses at least 3 or 4 layers of bio-tissues.

3.2.1 The software model

In effort to realize an optimal arm model to best predict and study epidermal antenna performance, several design geometries were utilized. Each of these models was used at different stages of the research project, with the rectangular model first, the elliptical cylindrical model second and then the same cylindrical model but with an added hand extension. HFSS was the primary simulation tool used due to its efficiency at solving problems which include multi-layers of dielectrics. Added to this are its immediate availability and ease of use. XFdtd and CST where also used at the intermediate stages of the research, but their respective results are not presented in this thesis.

- **Simulation set-up and models description**

We will look at the features of each HFSS model used and its respective reflection coefficient results. The simulation parametric set-up was common to all models. The electrical parameters of each bio layer were set to be frequency-dependent from 0.5 GHz to 4 GHz, with parametric definitions set in steps of 100 MHz.

First, a rectangular model that is uniformly flat on each of its sides was used, Figure 22. This model has shown an appreciable degree of predicting reflection coefficient measurements in real life.

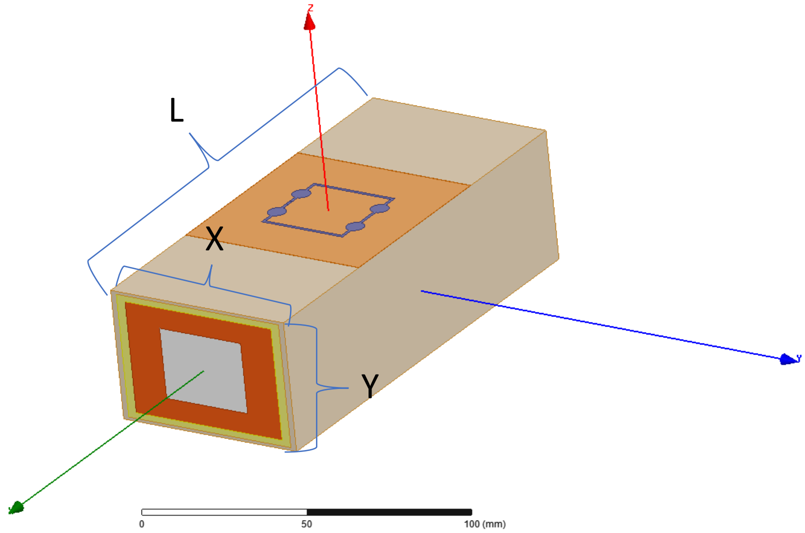

Figure 22. The rectangular HFSS arm model

Table IV. Dimensions of the rectangular and cylindrical arm models.

Tissue	Rectangular model X*Y (mm^2)	Cylindrical model X*Y (mm^2)
Skin	64x45	64x45
Fat	60x42	60x42
Muscle	54x38	54x38
Bone	30x24	30x24

Later, an elliptical cylindrical model was used to better realize an actual human arm, Figure 23. All biological tissues were shaped in an elliptically cylindrical fashion. each layer had a different major-to-minor axis ratio to add a sense of realism. Major and minor axes lengths are labeled as X and Y, respectively. All cylinders of the second model had length L = 150 mm.

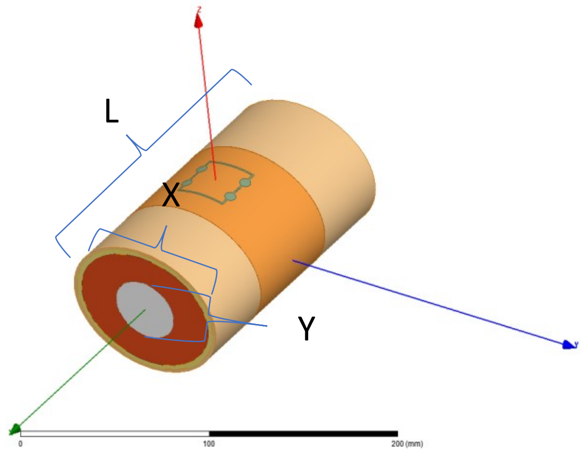

Figure 23. The cylindrical arm model.

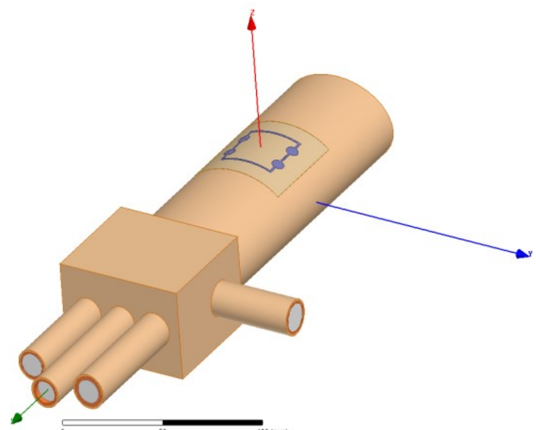

Figure 24. The same cylindrical model with a hand extension added.

Then the elliptical model mas modified to include a hand extension, Figure 24. The lengths of the added cylindrical fingers were variable, but all had the same cross section dimensions. The antenna was kept in the same position as it was in the previous two models. Adding the hand extension had no effect whatsoever on reflection coefficient values, but it did affect the shape of the 3D radiation patterns. Since the enhanced cylindrical model has a more realistic aspect to it, its associated 3D radiation patterns and current distributions will be used to study and analyze the performance of the modeled epidermal antennas. Figures 25-27 compare reflection coefficient results of the three antennas when placed on the rectangular and cylindrical arm models.

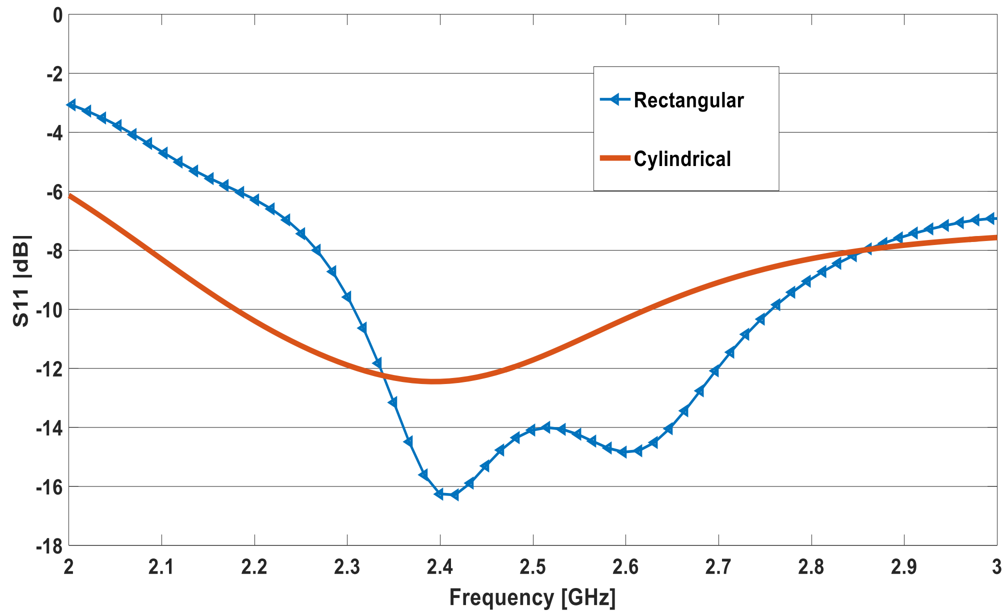

Figure 25. Reflection coefficient plots for the BLE antenna using the rectangular and cylindrical arm models.

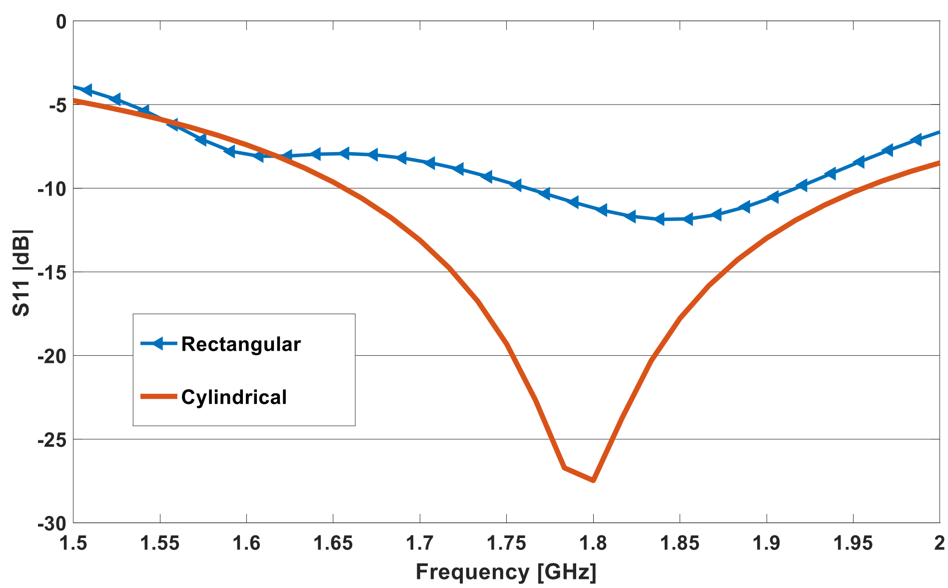

Figure 26. Reflection coefficient plots for the GSM-1800 antenna using the rectangular and cylindrical arm models.

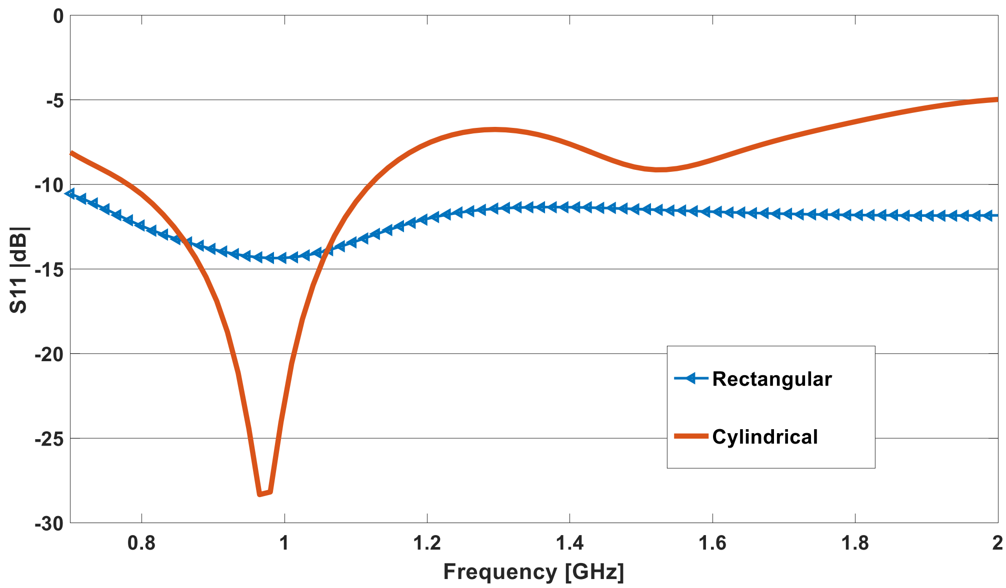

Figure 27. Reflection coefficient plots for the GSM-900 antenna using the rectangular and cylindrical arm models.

3.2.2 Understanding current distribution and radiation patterns

In this section, we will be looking at the current distributions within the cylindrical arm model as well as the 3D radiation patterns at each frequency of interest. penetration depths as well as the electrical lengths of the arm layers will all be used to find an explanation for the shape of the radiation pattern at the three different frequencies.

- **GSM-900 antenna at 900 MHz**

As mentioned previously, the antennas were designed to be one wavelength long at their respective operational frequencies. The wavelengths at 900 MHz and 1.8 GHz could be observed across the L dimension in Figures 28 and 31.

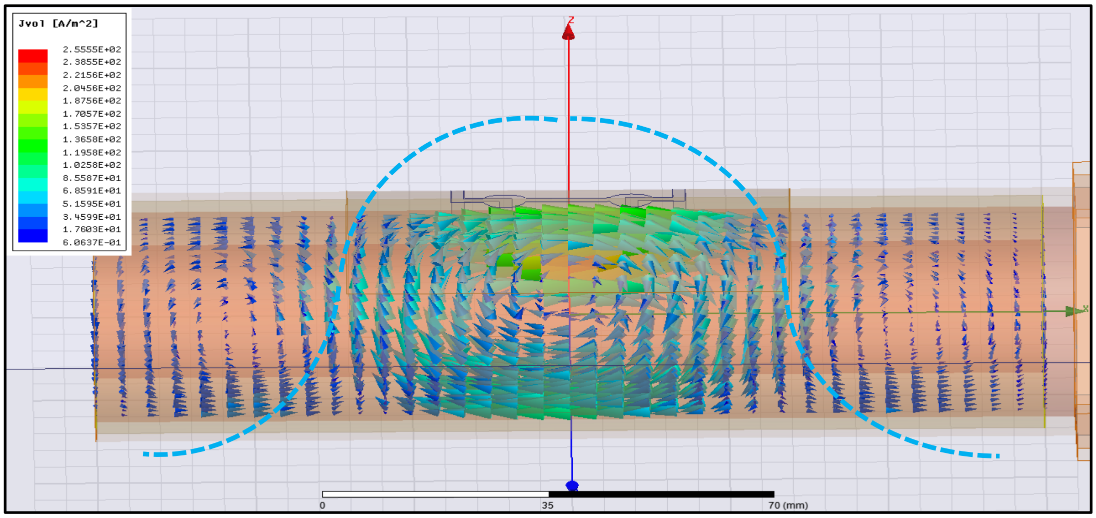

Figure 28. The simulated current distribution within and along the length of the arm model at 900 MHz.

A stack of tissue layers depicting the broadside view of the arm model can be seen in Figure 29. The current distribution within the tissue is approximated and portrayed in the stacked model. The B dimension corresponds to the start and end points of half-wavelength current distributions across the Y dimension. As can be seen in Figure 29, the length of B corresponds to approximately that of Y. Table V lists the penetration depths of all tissue at the three frequencies of interest. Given these values at 900 MHz and the actual thicknesses of the layers, it would be intuitive to say that a normally incident EM wave at 900 MHz on the top layer of the model, will make it through the whole stack and exit retaining more than 37% of its power. Hence, significant through-radiation can be observed in the 3D radiation pattern.

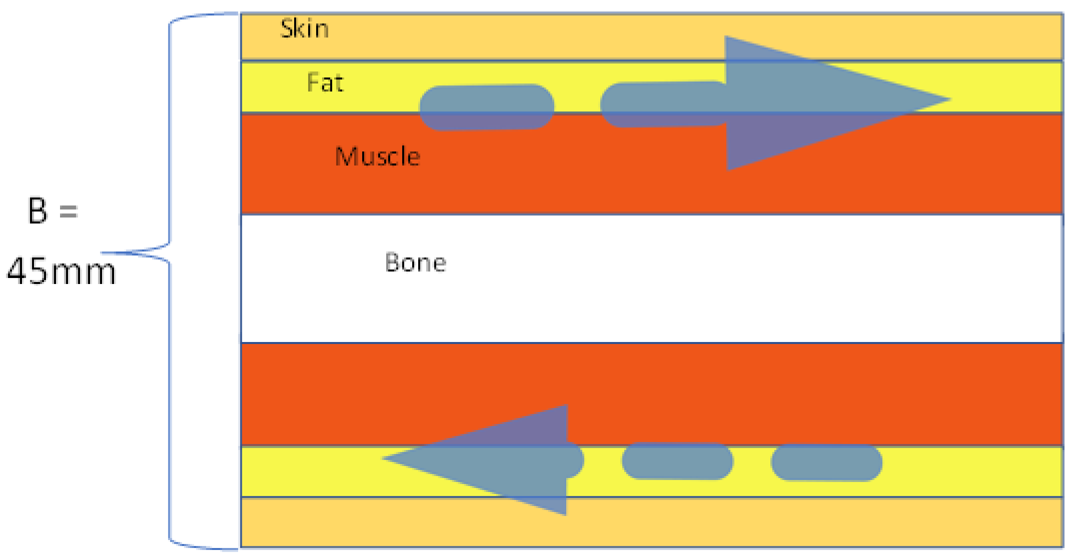

Figure 29. Approximate current distribution within arm tissues at 900 MHz.

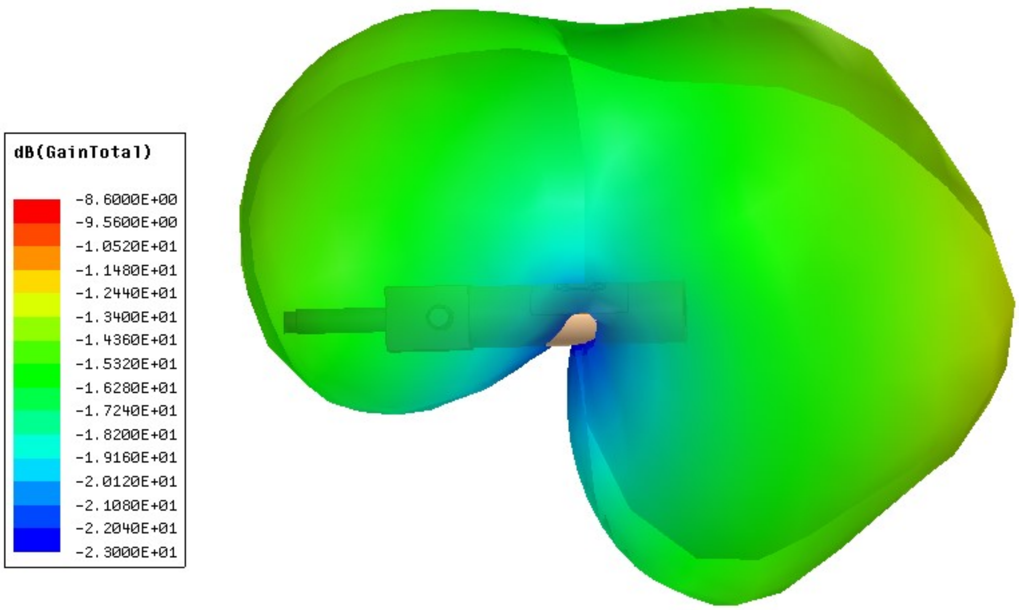

Figure 30. 3D radiation pattern at 900 MHz.

- **GSM-1800 antenna at 1.8 GHz**

Around 1.8 GHz the total length "L" of the arm is slightly greater than 1.5 times the electrical length of the antenna, Figure 31. Across the Y dimension, current which reaches the ventral side of the arm, still makes it possible for some through-radiation since the penetration depths are still large enough to let EM waves pass through with a little more than 37% of their original power. It can also be observed that B is approximately half the length of Y at this frequency. Compared to the pattern at 900 MHz, at 1.8 GHz the pattern is more directive as can be noticed from the red colored peak gain lobes, Figure 33.

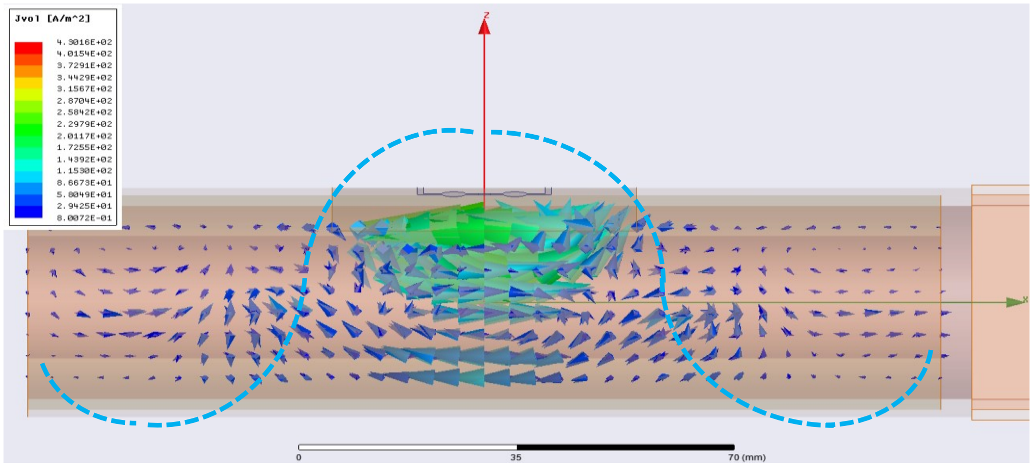

Figure 31. The simulated current distribution within and along the length of the arm model at 1.8 GHz.

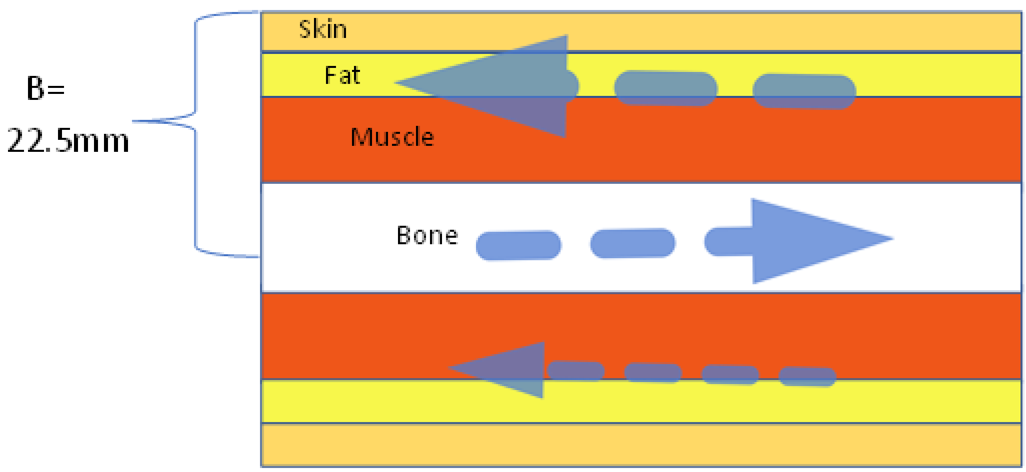

Figure 32. Approximate current distribution within arm tissues at 1.8 GHz.

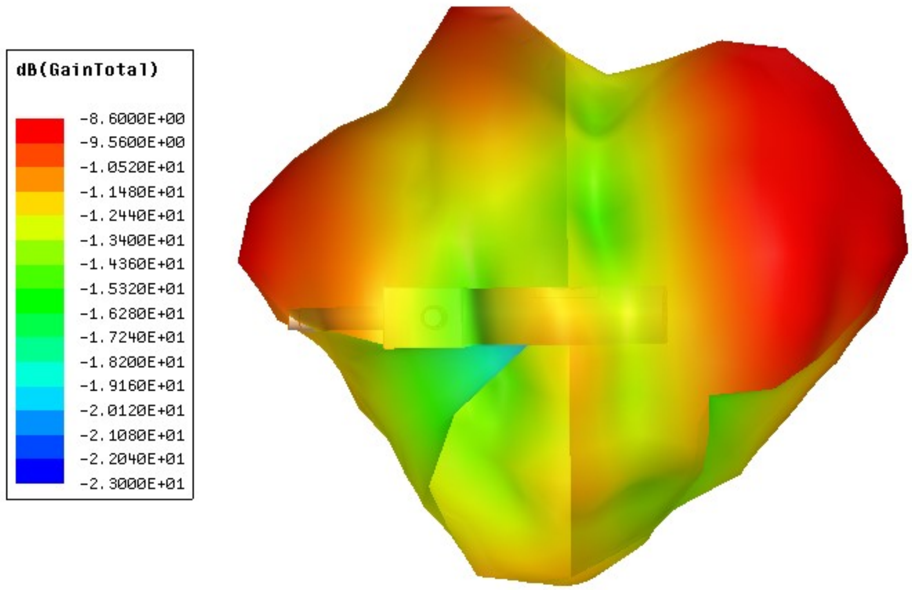

Figure 33. 3D radiation pattern at 1.8 GHz.

- **BLE antenna at 2.45 GHz**

Recall that the physical length of each side of the BLE antenna corresponds to one-quarter the wavelength of operation at 2.45 GHz. As a result of these shorter wavelengths and penetration depths, waves going through tissues attenuate much faster than at 900 MHz or 1800 MHz. Hence, through radiation is very minimal and is only visible right below the antenna location, Figure 36. Compared to the patterns at 1.8 GHZ and 900 MHz, the 2.45 GHz pattern is the most directive. This is a natural indication of the operation at higher frequencies. In essence, the higher the frequency of operation of a body-worn antenna, the more its radiation pattern resembles that of a patch antenna.

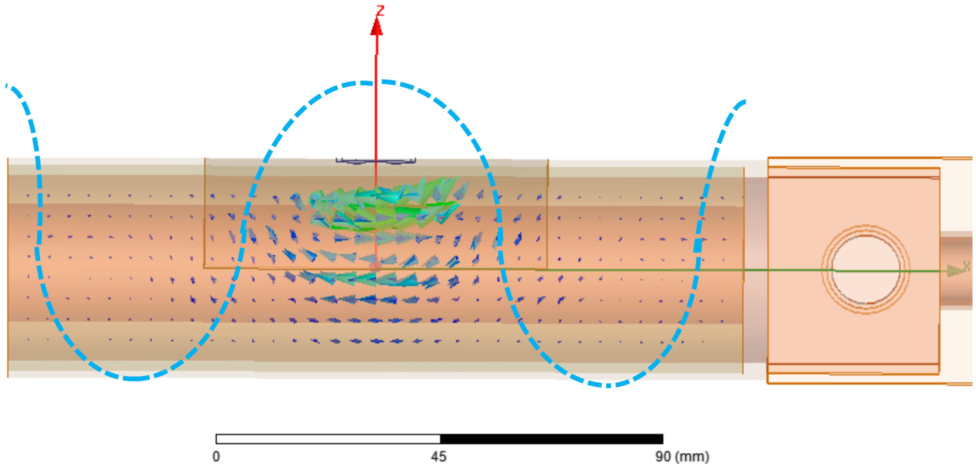

Figure 34. The simulated current distribution within and along the length of the arm model at 2.45 GHz

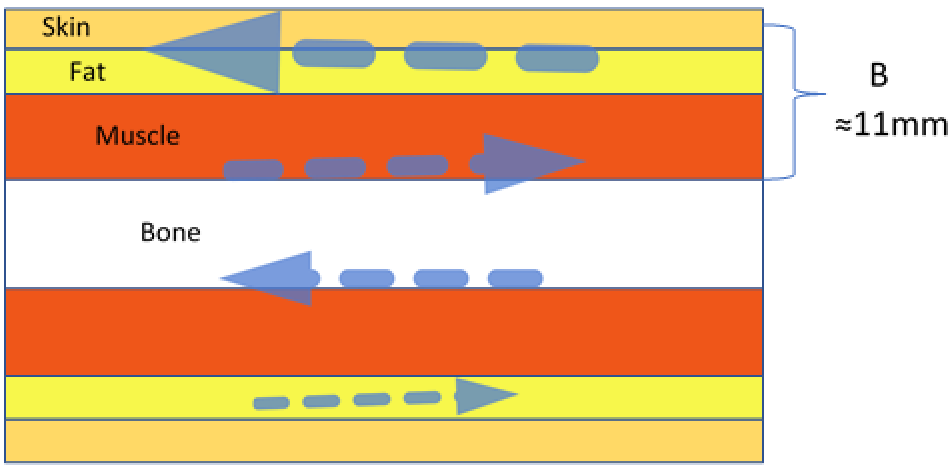

Figure 35. Approximate current distribution within arm tissues at 2.45 MHz.

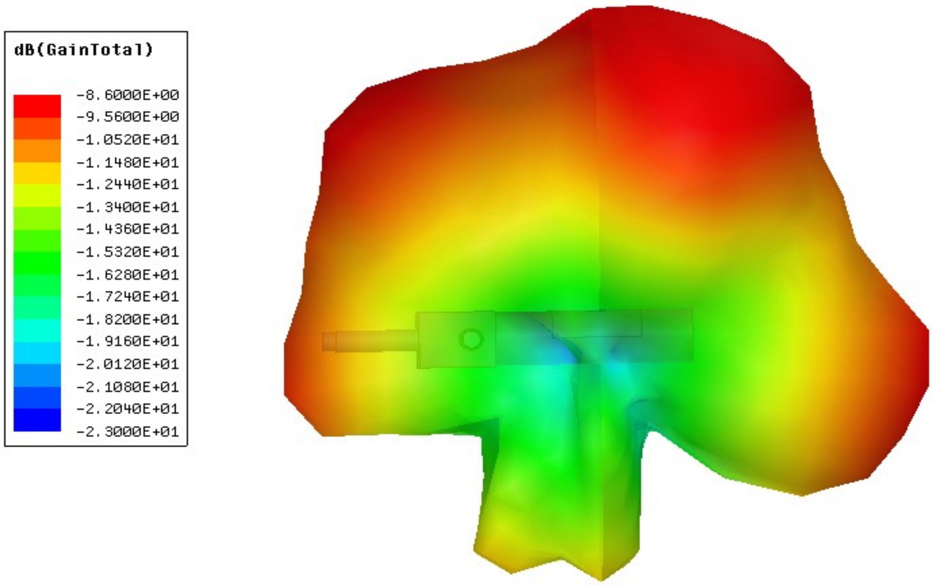

Figure 36. 3D radiation pattern at 2.45 GHz.

Table V. Wavelengths and penetration depths for tissues at different frequencies [24].

Frequency	Material or tissue	Wavelength [mm]	Penetration depth [mm]
900 MHz	Skin	50.71	40.23
	Fat	141.92	244.12
	Muscle	44.28	42.36
	Bone	93.78	131.57
	Air	333.10	---
1.8 GHz	Skin	26.42	28.25
	Fat	71.82	157.05
	Muscle	22.59	29.19
	Bone	48.20	66.65
	Air	166.55	---
2.45 GHz	Skin	19.66	22.57
	Fat	53.11	117.02
	Muscle	16.73	22.33
	Bone	35.99	45.78
	Air	122.36	---

3.2 Explaining Negative Gain

In this section, we will use wave propagation formulas to model plane wave interaction with arm tissues. For all practical purposes, this type of modeling acts as a simple way to approximate electromagnetic interaction between waves and bio-tissue. The main goal is to provide an explanation for the negative values of epidermal antenna gain. The model treats each bio-layer, as a lossy dielectric slab with its own primary and secondary coefficients, Figure 37. Each slab is cascaded with the others to form a cascaded arm model. Below the bottom slab of skin, free space is considered to be infinite and thus acts as a terminating load. The cascading order corresponds to the presumed approach of EM waves from free space to be incident on skin first, fat second, muscle third and fourthly on bone. From bone, the wave resumes its propagation downwards in the opposite order. As shall be pointed out, instead of taking into account the complete path the wave travels reaching all the way down to free space, the center slab of bone could be considered as the last layer or the terminating load the wave faces.

This of course, doesn't take into account that the actual geometries of tissues in the arm are more or less cylindrical; which would cause some parts of any tissue to be missed by any incident wave. The incident waves upon tissue are assumed to be normally-incident TEM plane waves; far-field conditions are assumed in this scenario.

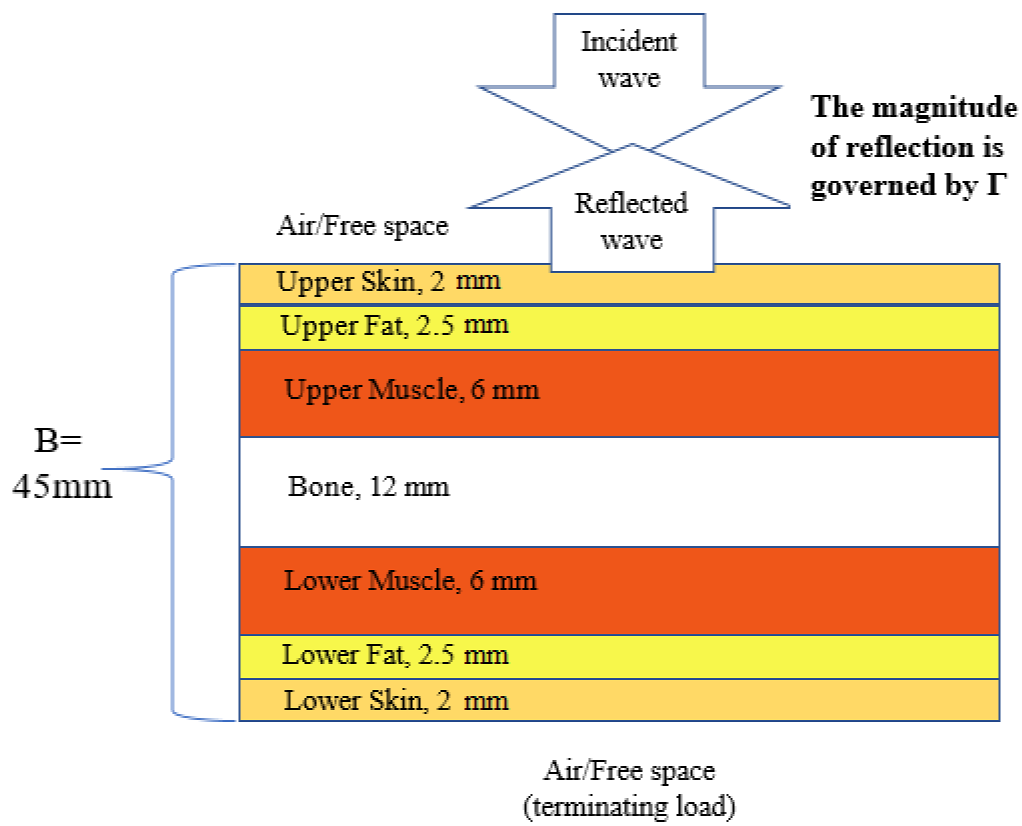

Figure 37. Multi-layer arm model

Our task now is to find the value of the reflection coefficient (Γ) an incoming incident wave sees upon contacting the upper skin tissue. The following calculations will be made for a 900 MHz wave; however, the same procedure can be followed for any frequency of interest.

First, penetration depths, δ_{tissue}, of tissues could be obtained by any of two ways:

1- Either directly by the penetration depth equation
2- Or by first finding out the expression of the propagation constant (γ) and then finding the inverse of its real part (all equations in this section are based on those from [79]) .

We will choose the second approach, hence:

$$\gamma = \sqrt{(j\omega\mu) * (\sigma + j\omega\varepsilon)} \tag{5}$$

where ε is the absolute permittivity:

$$\varepsilon = \varepsilon_r * \varepsilon_0 \tag{6}$$

For instance, by (5) the value of γ for skin is = 24.86 + 123.89j

The real part of γ is the attenuation constant (α) = Re(γ) = 24.86. And, taking the inverse of this number gives us the value of the penetration depth of skin tissue δ_{skin} = 40 mm. The phase constant (β) would be the imaginary part of (γ), thus (β) = Im(γ) = 123.89.

To find the reflection coefficient looking from air onto upper skin, we need to first find the input impedance of air looking downwards into upper skin. This entails finding the input impedance of each interface, starting from the lower skin-air interface all the way up to the upper air-skin interface. In addition, the characteristic impedance value of each layer needs to be computed to be used in the formula of its respective input impedance. These values will be complex (include a reactive part) due to the loss-incurring parameters of biological tissue. The characteristic impedance of any tissue can be found by:

$$\eta_{\text{tissue}} = \sqrt{\frac{j\omega\mu}{\sigma + j\omega\varepsilon}} \tag{7}$$

Table VI. Calculated characteristic impedance of each tissue η_{tissue}.

Tissue	η_{tissue} (Ω)
Bone	104.72 + 11.93j
Muscle	48.71 + 8.10j
Fat	159.14 + 14.72 j
Skin	55.12 + 11.09j
Air	377

The input impedance looking downwards from the top of tissue_1 into tissue_2 is:

$$\eta_{\text{input\_tissue\_1}} = \eta_{\text{tissue\_1}} \left(\frac{\eta_{\text{tissue\_2}} + \eta_{\text{tissue\_1}} * (\tanh(\gamma t))}{\eta_{\text{tissue\_1}} + \eta_{tissue\_2} * (\tanh(\gamma t))} \right) \tag{8}$$

Where "t" is the thickness of tissue_1

We also need the wave impedance of free space to calculate the reflection coefficient between the air-skin interface:

$\eta_{air} \approx 377\ \Omega$

The input impedance at the upper air-skin interface was found to be:

$\eta_{\text{input\_skin}} = 28.20 - 4.99j$

Now, we can calculate the reflection coefficient seen by a normally incident wave on the dorsal (upper) side of the arm.

$$\Gamma = \frac{\eta_{\text{input\_skin}} - \eta_{\text{free\_space}}}{\eta_{\text{input\_skin}} + \eta_{\text{free\_space}}} \tag{9}$$

Hence, $\Gamma = -0.86 - 0.02j$

Consequently, the phase angle of the reflection coefficient is almost 180 degrees or π radians. This value corresponds to an almost complete out-of-phase reflection of waves. Therefore, we should expect significant amounts of destructive interference between incident and reflected waves. By looking at the different characteristic impedance values for different tissues, we could also infer that multiple out-of-phase reflections occur between the tissues themselves. All of these phenomena contribute to the degradation of gain down to negative values. As a side note, if we were to consider bone to be the last layer an incident wave sees, Γ would be equal to = -0.86 + 0.04j. This value is almost equivalent to the value of Γ calculated when all the layers where taken into account. This only means that the higher values of relative permittivity for any tissue result in reflecting waves with phase shifts almost completely out of phase; hence, destructively interfering with incident wave and resulting in degraded outwards radiation.

3.3 Finding an Equivalent Single-Dielectric Model

As each of the four tissues comprising the HFSS arm model has its own frequency dependent values of relative permittivity and loss tangent, it would be useful to find an equivalent model comprised of just a single lossy dielectric with its own frequency-dependent parameters. In this section, we will look at how we could obtain a single-layer arm model by translating the original four-layer model into a system of 4 parallel-plate capacitors connected in parallel to each other. This would enable us to find the frequency dependent values of relative permittivity which are equivalent or representative for the four layers of skin fat muscle and bone. Consequently, we would assign the computed relative permittivity values into an HFSS unipolar Debye model to come up with an equivalent single-layer arm model as seen in Figure 40.

3.3.1 Parallel plate capacitor modeling

Since the currents induced by the antenna travel back and forth along the “L” dimension of the arm, we could consider L to be the separation gap “d” for each of the four parallel plate capacitors. The plates are hollow ellipses and their respective bio-dielectrics are hollow elliptical cylinders, Figure 38. The plates and the dielectrics can also be considered circular instead of elliptical as long as the circular radii could produce the same values of area cross section. This is necessary since the area cross section of the plates as well as the separation gap “L”, and the frequency-dependent relative permittivity of each tissue will be used to compute their capacitances.

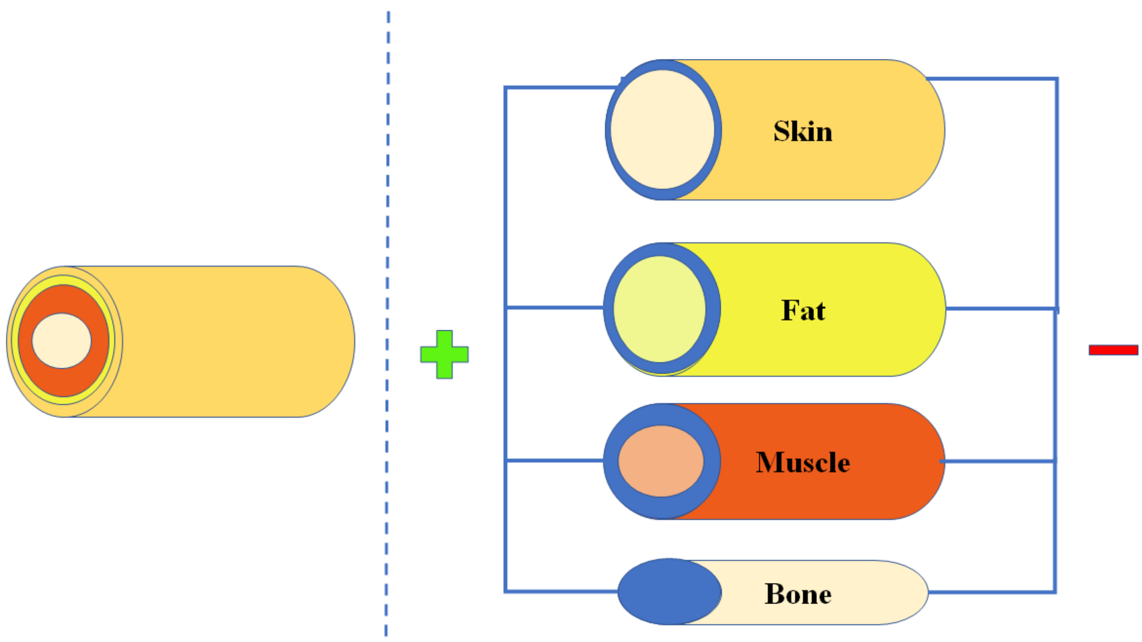

Figure 38. The parallel plate capacitor configuration of arm tissues.

The capacitance at any frequency for any tissue is computed by:

$$C_{tissue} = \frac{\varepsilon_r(f)\varepsilon_o A}{d} \tag{10}$$

Where $\varepsilon_r(f)$ is the frequency-dependent relative permittivity for a given tissue; this could be obtained from [24]. Given the parallel capacitance configuration of the fours tissues, the total equivalent capacitance is:

$$C_{eq} = C_{skin} + C_{fat} + C_{muscle} + C_{bone} \tag{11}$$

The equivalent relative permittivity is then:

$$\varepsilon_{eq}(f) = \frac{C_{eq}}{C_o} \tag{12}$$

These equations were used in MATLAB to find $\varepsilon_{eq}(f)$ from 0.5 GHz to 3 GHz. The resulting curve is labeled as PPC in Figure 39.

3.3.2 Equivalent single-layer modeling.

The prior approach of PPC modeling is the first step in realizing an equivalent single-layer arm model. Substituting the four-layer arm model with that of only a single layer would result in faster simulation time and a more efficient use of processor resources. HFSS provides a range of assigning dielectric parameters into materials, of which we used the unipolar Debye model. The model calculates the frequency-dependent parameters of relative permittivity and loss tangent based on two inputs for a lower frequency limit and two other inputs for an upper frequency limit.

Based on the relative permittivity values obtained using the PPC computations for the upper and lower frequencies of 0.5 GHz and 3 GHz, relative permittivity values were slightly adjusted (30.26 → 30 at 0.5 GHz and 27.04 → 27 at 3 GHz) and then assigned to the unipolar Debye model tool found in HFSS. Loss tangents were specified to be 0.4 at 0.5GHz and 0.25 at 3 GHz.

The resulting Debye model used in HFSS was:

$$\varepsilon_{eq}(f) = 24.63 + \frac{5.37}{1 + 1.41 * 10^{-19} * f^2} \tag{13}$$

Figure 39 demonstrates the relative permittivities of muscle, skin, bone, and fat versus frequency. In addition, the two modeling methods used, namely, the Debye model equivalent and the parallel plate capacitor (PPC) equivalent.

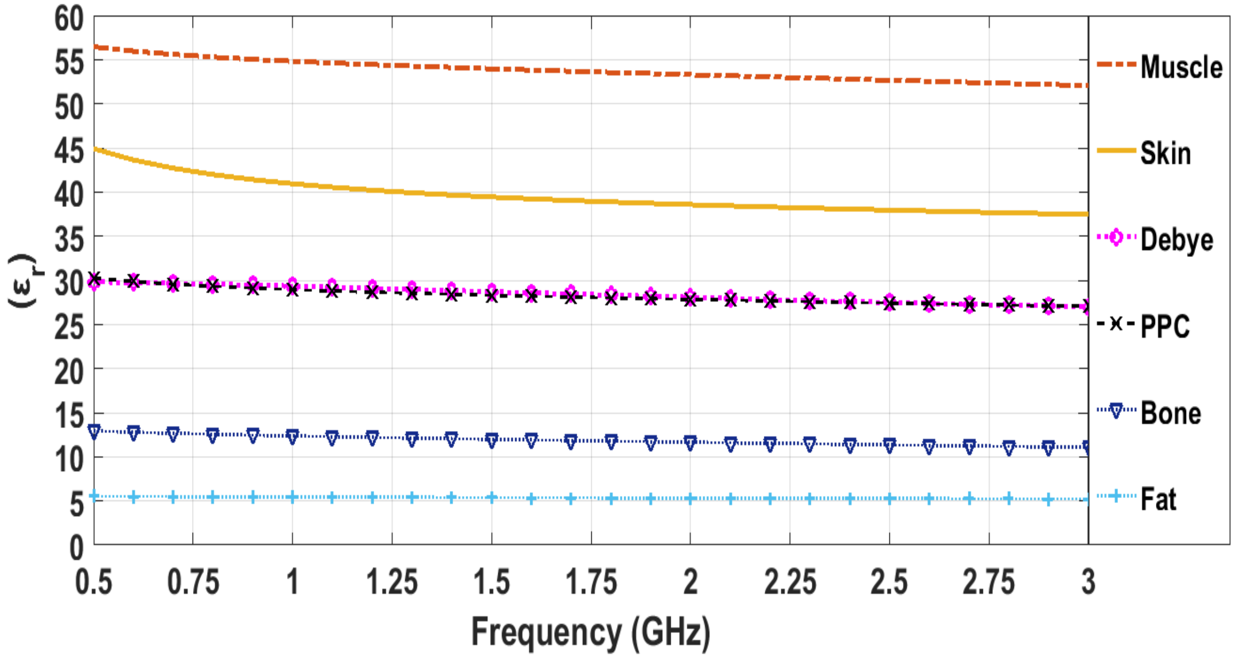

Figure 39. Relative permittivity vs. frequency for different tissues and models.

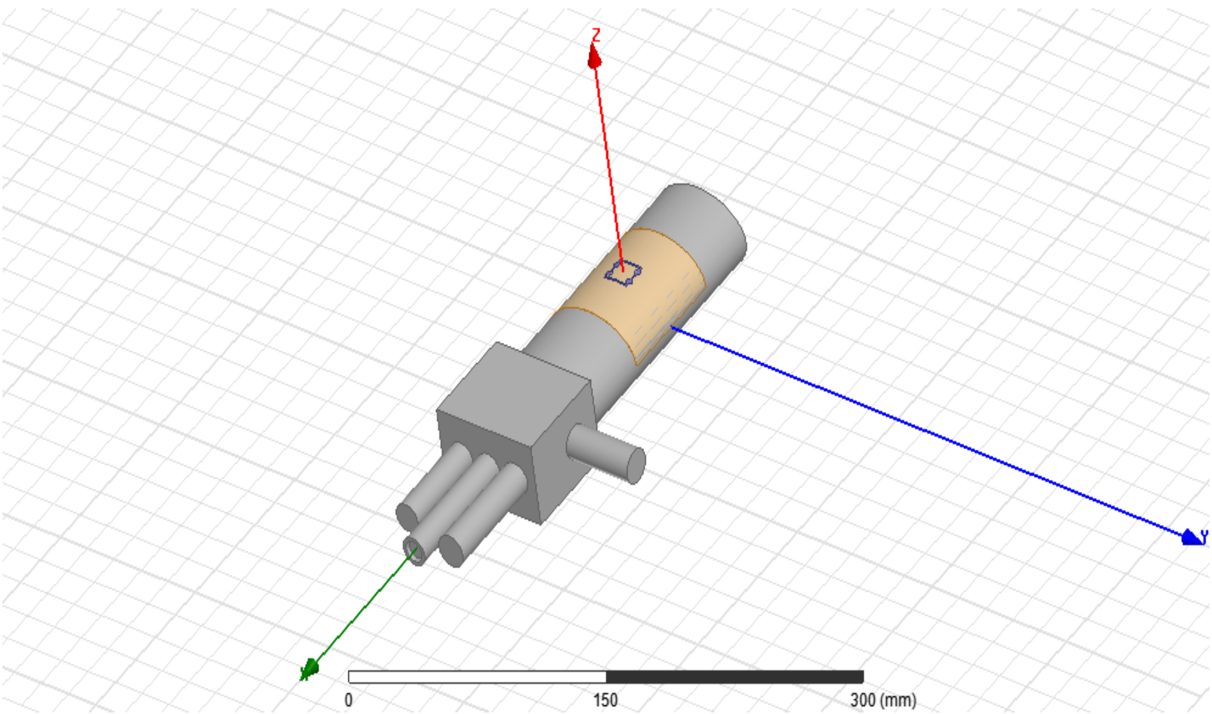

Figure 40. The single layer HFSS model.

Figure 41 below shows the reflection coefficient values obtained from the cylindrical 4-layer model introduced in section 3.2.1 versus those obtained from the Debye equivalent single-layer model.

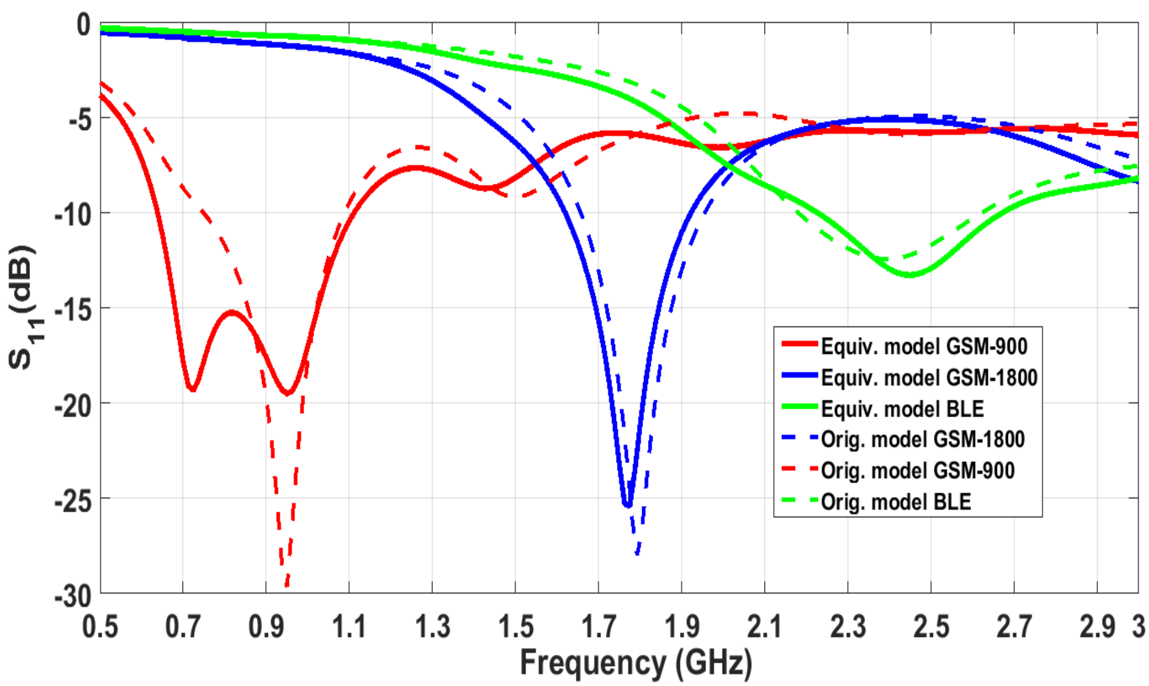

Figure 41. Comparison of reflection coefficient values for the original and equivalent HFSS models.

The significance of the equivalent arm model, does not only lie in its ability to greatly reduce simulation time and enhance processing economy, but also in its potential to be realized as a physical phantom with the specified dielectric parameters calculated and presented above.

3.3.3 Effective relative permittivity

The equivalent single-layer arm model and its accompanying values of relative permittivity are not directly related to the actual wavelengths previously presented in table. Rather, these wavelengths are related to an effective permittivity which takes into account not just the equivalent relative permittivity of the single-layer arm model (or the original 4-layer model), but also that of the free space surrounding it. This frequency-dependent effective permittivity could be simply found by:

$$\lambda_L = \frac{\lambda_o}{\sqrt{\varepsilon_{eff}}} \tag{14}$$

Table VII. Calculated effective relative permittivity at different frequencies.

Frequency (GHz)	λ_o (mm)	λ_L (mm)	ε_{eff}
0.9	333	148	5.06
1.8	167	80	4.36
2.45	122	60	4.13

An interesting observation of the dielectric parameters of fat indicated their proximity to the effective values presented in Table VIII. This observation could be used as a reference-line in the design of single-layer epidermal and wearable antennas with extremely thin substrates or with body-antenna separation gaps that do not exceed 0.1mm from the body. Such a miniscule separation gap is characterized by very strong coupling between body tissues and the radiating element. This characteristic is the basis for this observation and the modeling concept presented in this section.

Table VIII. Physical lengths of QL antennas vs. wavelength in fat.

Frequency (GHz)	λ_{fat} (mm) [24]	ε_{fat}	λ_{eff}(mm)
0.9	142	5.462	148
1.8	72	5.35	80
2.45	53	5.28	64

3.4 Fabrication of the epidermal antennas

The epidermal antennas were fabricated using different materials and techniques throughout project evolution. Except for the later fabricated stretchable antennas, all antenna structures were less than 0.1mm thick to emphasize the epidermal nature of the antennas. Below are the details of fabrication and materials specifications used to fabricate all of the GSM-900, GSM-1800, and BLE antennas.

- In the first stage of research, fabrication of the antennas was done to test the performance of the design concept. Hence, simple materials and tools were used to this end. The radiating elements were cut from copper-coated Kapton sheets via a cutting printer. The dielectric substrates were cut from 75um Kapton polyimide sheets. Results of tests of these antennas were published in [80] and are presented in Chapter 4. The procedure of making these antennas is summarized in Figure 42 below:

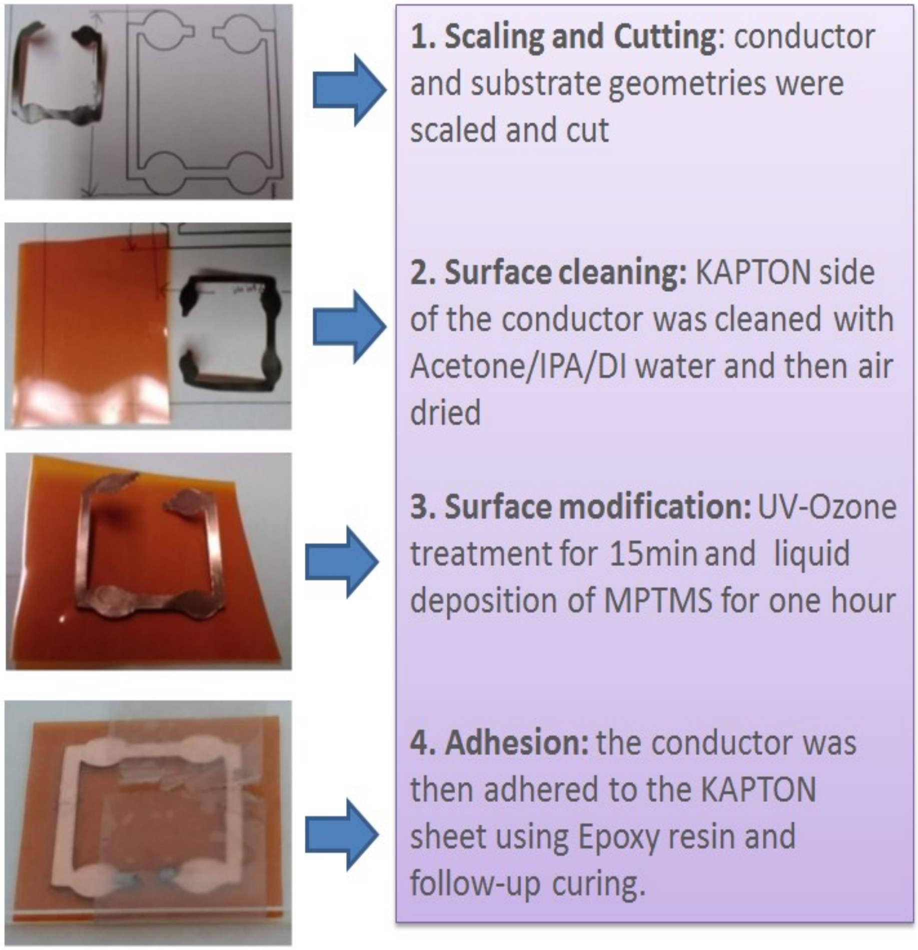

Figure 42. Fabrication of copper-coated Kapton antennas.

- The second type of copper antennas (Figure 43) had the same Kapton substrate, but the radiating element was made from adhesive copper sheets. Cutting the antennas into shape was primarily done with an LPKF machine. Some manual handcraft was involved to trim the LPKF-cut adhesive copper antennas into shape. This is due to the minute but effective drag effect caused by the LPKF needle as it drills and cuts through the flexible adhesive sheet. These antennas were made at the intermediate stage of the project. At that stage, measuring the radiation pattern of antennas was of primary focus. The reflection coefficient and the radiation pattern results of these antennas are presented in Chapter 4.

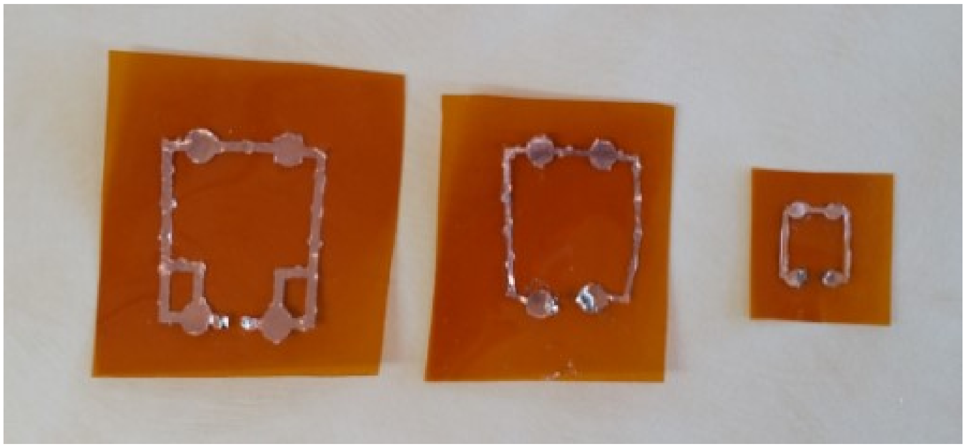

Figure 43. Adhesive copper antennas, from left to right: GSM-900 antenna, GSM-1800 antenna, and the BLE antenna.

- After the design concept was thoroughly tested by measurements, silver ink was used to fabricate more of the epidermal antennas. The novel (at the time) silver ink was supposed to adhere very well to the surfaces of different kinds of polymers. Hence, we used two different substrates to exploit the potential of the novel ink:

a) Silver ink on Kapton (Figure 44): The first antennas to be made with this novel ink used Kapton substrates for ink to be deposited upon. Although the antenna structures were well made, they were not measured or tested due to the inability of the ink to withstand soldering heat.

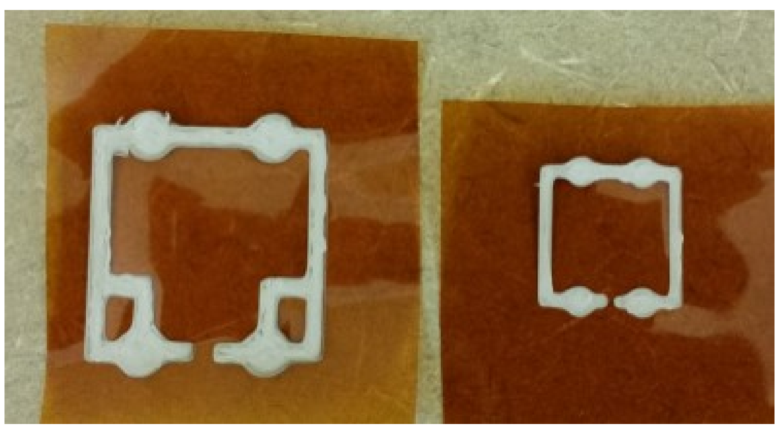

Figure 44. Silver ink on Kapton antennas.

b) The fourth type was made by depositing silver ink on a transparent 1mm thick VHB stretchable substrate. For Kapton and VHB silver ink antennas, the ink printing procedure was done using an N-Scyrpt 3Dn Printing machine. Measurement tests for the stretchable VHB antennas were possible after improvising the antenna feeding mechanism. Performance results for these antennas are presented in chapter 4. The stretchable antennas could be seen in

Figure 45. The visible red background cover (seen with the 37mm*37mm antenna) is just a protective cover for the stretchable VHB substrate. The ink deposition process is illustrated in Figure 46.

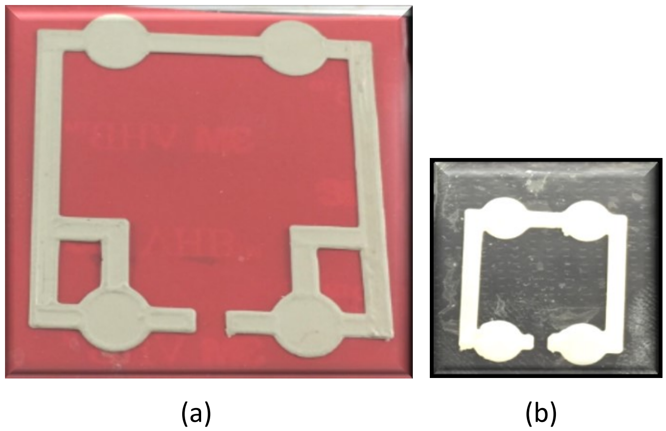

Figure 45. Stretchable (a) 37mm*37mm, and (b) 16mm*16mm antenna.

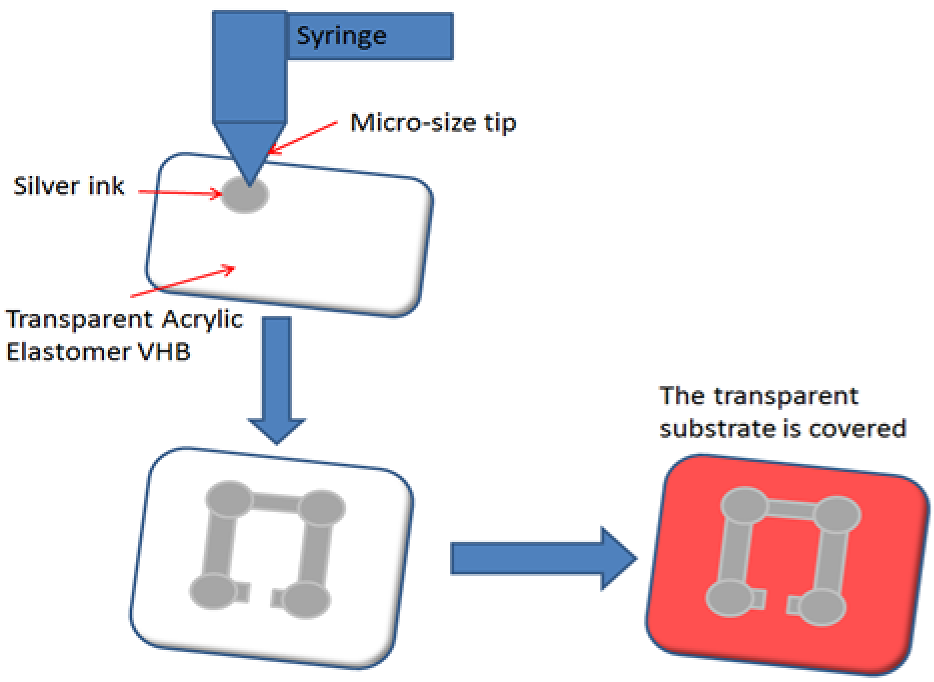

Figure 46. Silver ink printing process on polymer substrates.

❖ Remarks

The copper-coated Kapton antennas were in good shape regardless of dimensional imperfections in the radii of the circular patches. Before cutting them into shape, DXF files imported from HFSS were used as the reference for antenna geometry and layout. For the second research stage, the LPKF system also had DXF files uploaded to it in order to cut the adhesive copper sheets. Unfortunately, the LPKF drilling needle was not able to operate smoothly as it was cutting through the adhesive material. Hence, manual cutting was needed to trim some of the unfinished edges of the antennas.

Conclusion

Since the project was aimed at delivering an epidermal antenna with sensing components, it was important to consider a very thin antenna structure. Such an antenna should minimize conductor area, and avoid the use of any ground structure. Hence, this was the approach taken in the design of the QL epidermal antennas. HFSS simulations of a 4-layer arm model gave interesting insight into wave penetration and current distributions within body matter. Analyses of them helped explain the shape of the radiation pattern at each of the three frequencies of interest. In addition, mathematical analysis was used to explain the reason behind the negative values of gain body-worn antennas usually have. it was desired to find an equivalent arm model consisting of only one lossy dielectric instead of the four tissue-representing layers. This serves as a more efficient means for resource allocation and simulation runtime. In addition, this equivalent model can be realized into a physical phantom whose dielectric parameters could be recreated by chemical recipes. Different fabrication tools and materials were used at different times as the research progressed and project objectives were achieved. The next chapter presents measurement test results of these fabricated antennas. The next chapter presents measurement test results of these fabricated antennas.

Chapter Four: Results of Measurements and Simulations

As we saw in chapter two, there are different tools used to simulate and measure the performance of body-worn antennas. We also saw how physical phantoms could come in different forms. For a number of reasons, it can be quite inconvenient to perform antenna tests on actual humans. In this manner, obtaining consistent measurement results is particularly difficult. Nonetheless, such an approach would reflect the most realistic measurements for body-worn antennas. In this chapter, we will be looking at the measurements of the fabricated epidermal antennas presented in chapter three. Moreover, data communication tests and results for the GSM standard are also presented.

4.1 Comparison of Measurement Approaches

Body-worn antennas, like conventional antennas, have fundamental parameters that must be measured to validate their corresponding simulation results. These parameters include reflection coefficients, radiation patterns, efficiency, and gain. Reflection coefficient measurements are simple to conduct with the help of a VNA. However, measuring the other said parameters for body-worn antennas can be more challenging than measuring those of conventional antennas. There is a range of techniques and tools used to measure the different parameters mentioned above, all of which can be performed on:

1- A human volunteer
2- Physical body phantoms and dielectric slabs
3- A dead or a living animal

Ideally, measurements are to be done with the antenna worn by a human volunteer. This allows for the most realistic results that could be obtained out of the previously mentioned methods. Usually, body phantoms that mimic certain human body electrical properties are used instead. Such phantoms could come in various shapes and forms. They are generally made by stacking synthesized jelly-like or liquid-based layers together. The overall shape of the phantom might replicate that of a human body, and in some cases only rectangular slabs of 1 to 3 layers are used. Moreover, some research made use of animals as test subjects instead of phantoms and human volunteers. This is due to their similar electric and dielectric parameters to those of human beings. Pigs are among the most used mammals for body-worn antenna measurements, and implanted antennas in particular [60] [32] [5].

The first option is the least commonly used for radiation pattern measurements. Not all anechoic chambers make this a feasible option. Hence, measurements with an actual human volunteer would be done in an adequately large room with the help of a testing probe, a VNA, fixtures, and other tools as necessary. For reliable measurements with this approach, special care should be given to the surrounding environment. If a regular room is used, sources of EM interference and reflection should be identified and neutralized. Wi-Fi access points installed in the ceiling, metallic drawers, and cupboards are a few such examples. To block reflections from larger immovable objects, microwave absorbers could be used.

Repeatability of results should be sought, still however, without an anechoic chamber this objective could be quite challenging. Important considerations for all kinds of measurements should take into account any amount of air-gap separations between the worn antenna and the test subject. Added to this would also be the amount of pressure applied on the subject by the antenna. Stronger antenna pressure on the body results in stronger bio-tissue and EM-wave coupling. Hence, measured reflection coefficients and radiation efficiencies would therefore be affected.

Perhaps, using physical phantoms inside an anechoic chamber would yield more consistent and repeatable test results. These phantoms would have known frequency-dependent relative permittivity and loss tangent parameters which mirror those of the human body. Thus, this approach is more common and convenient to implement than the one discussed above.

Now, we will be looking at the simulation test results and those of actual measurements done with the aid of human volunteers for all three epidermal antennas. Measurement and simulation test results are presented first for all the fabricated GSM-900, GSM-1800, and BLE copper antennas. Then, results for the silver ink stretchable BLE antenna are presented.

4.2 Research Stage One: Copper-coated Kapton BLE Antennas

In an earlier publication [80], two different single-layer loop antennas were fabricated and compared. The quadruple loop (QL) antenna showed better performance in comparison to the standard square loop. This was achieved after adding the four circular patches discussed in Chapter 3. Figure 47 shows the measured results versus those of simulations for the two antennas.

❖ Reflection coefficient of the BLE antenna

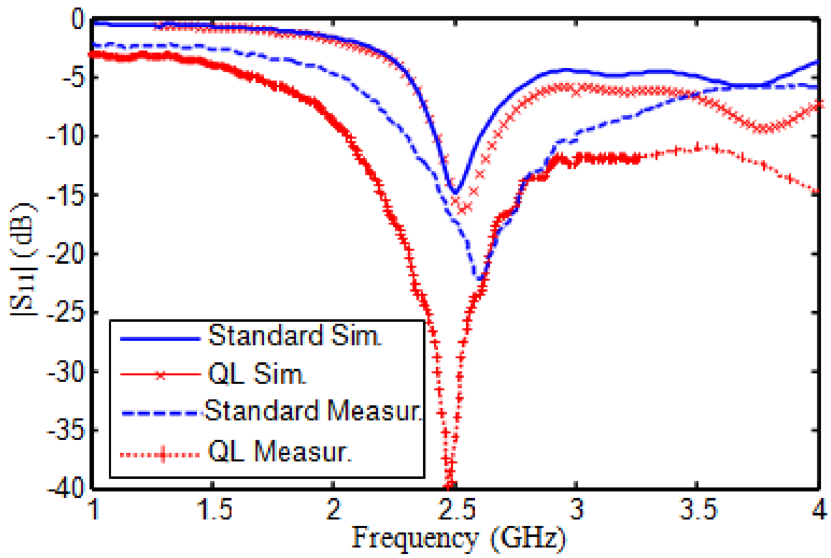

Figure 47. Measured vs. simulated reflection coefficients of both antennas [80].

It has to be noted that for initial simulations, electrical parameters for the different body layers were manually set for only the center frequency (2.45 GHz) with the other frequencies being left to be automatically adjusted. The results of simulations thus have been not very accurate to reflect the losses incurred by the body. With the aid of an EMscan platform, measured radiation efficiency and maximum gain were 5% and –10 dBi, respectively, for the QL antenna. On the other hand, maxima of 2% for radiation efficiency and –12 dBi in gain were obtained for the standard square loop.

It was necessary to consider the significant effects on antenna detuning as a function of antenna position on the forearm. Figure 48 shows the different reflection coefficient curves for three different antenna placements on the forearm. Despite differences in location, the reflection coefficient was always better than -10 dB within the 2.4-2.5 GHz band of interest.

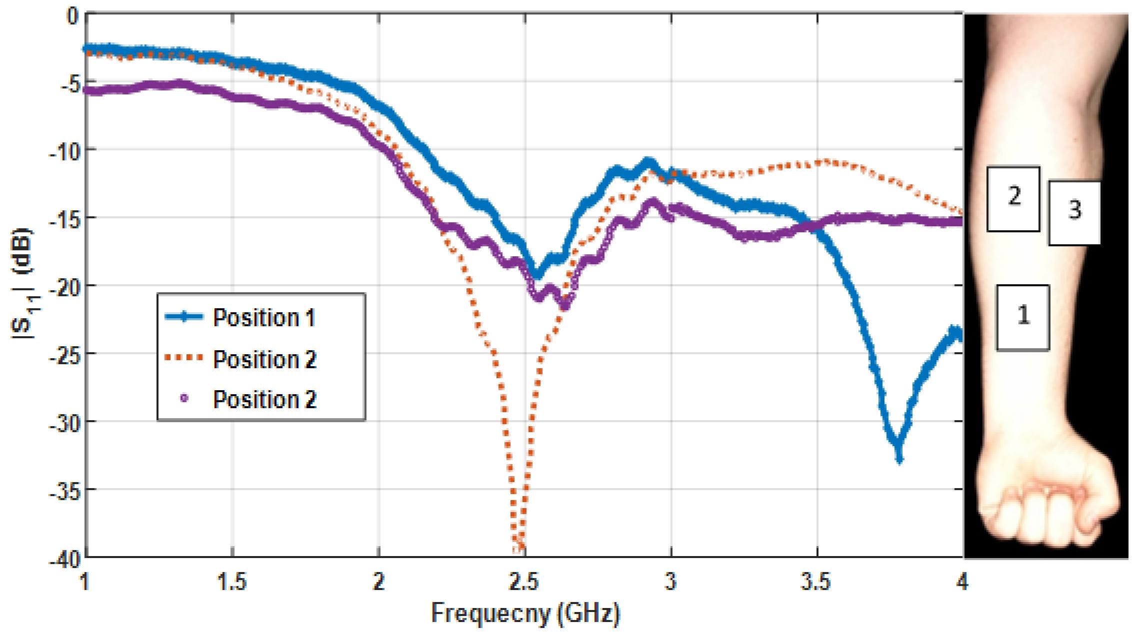

Figure 48. Reflection coefficient measurements taken for different placements on the forearm.

The simulation set-up was later modified after observing the wider impedance bandwidth phenomena seen in measurement results compared to those of simulations. The electrical parameters for frequencies from 0.5 GHz to 4 GHz were added in steps of 100 MHz. Figure 49 shows the new simulated and measured reflection coefficient results for the BLE antenna. The center resonant frequency observed from simulations is higher due to the simplified nature of the HFSS model in comparison to the measured center frequency of an actual human arm.

The non-inclusion of bodily fluids and blood in the simulation models is reflected in the lower reflection coefficient values obtained. The presence of blood and body fluids, both of which have high relative permittivities, results in higher absorption and loss of EM waves. Hence, measurements on an actual arm yield greater measured reflection coefficient results.

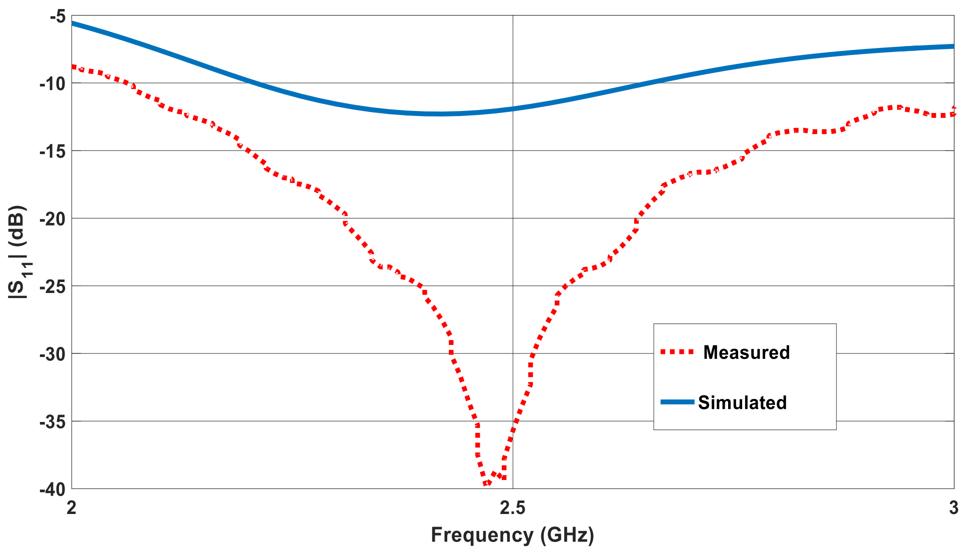

Figure 49. Measured and simulated reflection coefficient for the QL BLE antenna.

4.3 Research Stage Two: Radiation Patterns and Data communications

4.3.1 Radiation Patterns at 2.4 GHz

It was necessary to evaluate the radiation patterns of the QL antennas at all frequencies of interest. The sought measurement procedure had to be repeatable and extensive. In addition, the tests involved actual human volunteers in order to compare real-life measurement results to those of simulations.

The measurement set-up could be seen in Figure 50, and it included:

1. A wide-band ridged horn antenna, NSI-RF-RGP-10, to act as a probe
2. R&S®ZVL13 Vector Network Analyzer
3. Microwave absorbers (Eccosorb AN-77)
4. 1-meter diameter paper protractor
5. MCDAVID® Compression band to keep the epidermal antenna fixed in place
6. (20x12) m room.

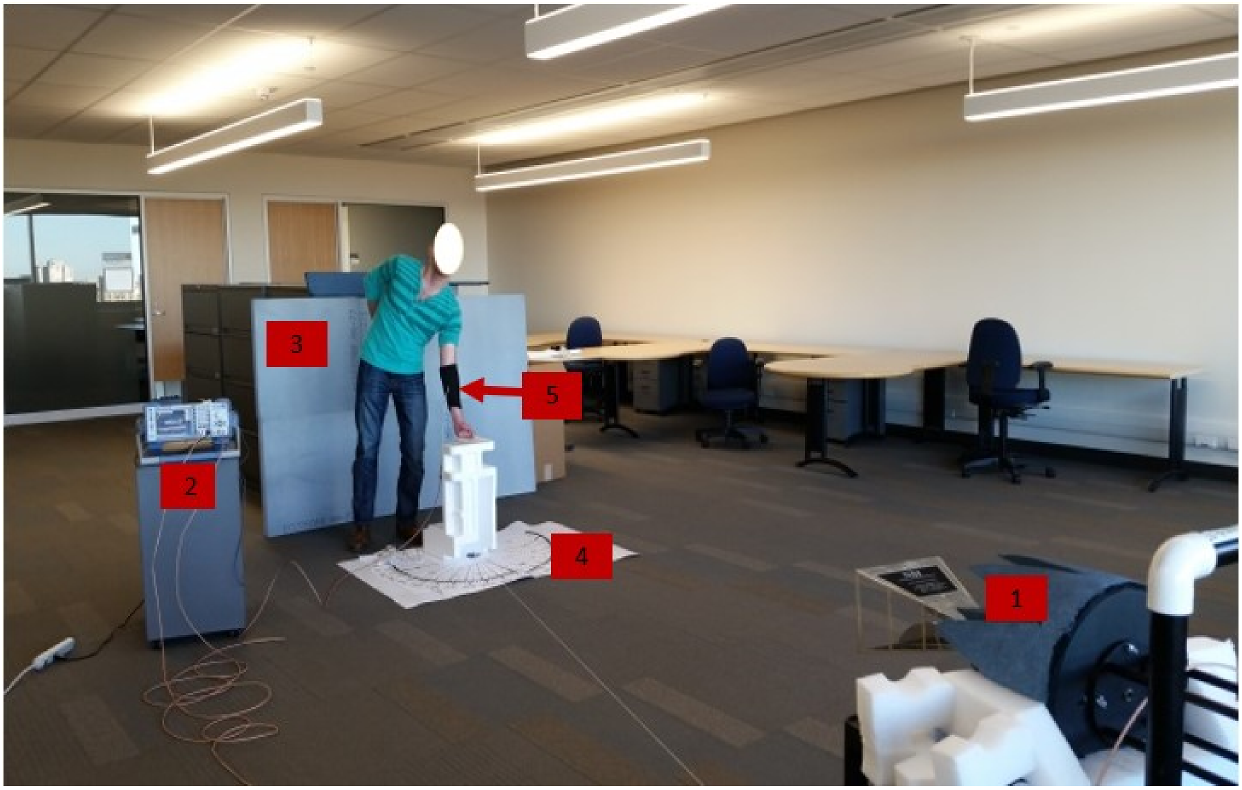

Figure 50. Set-up for radiation pattern measurements.

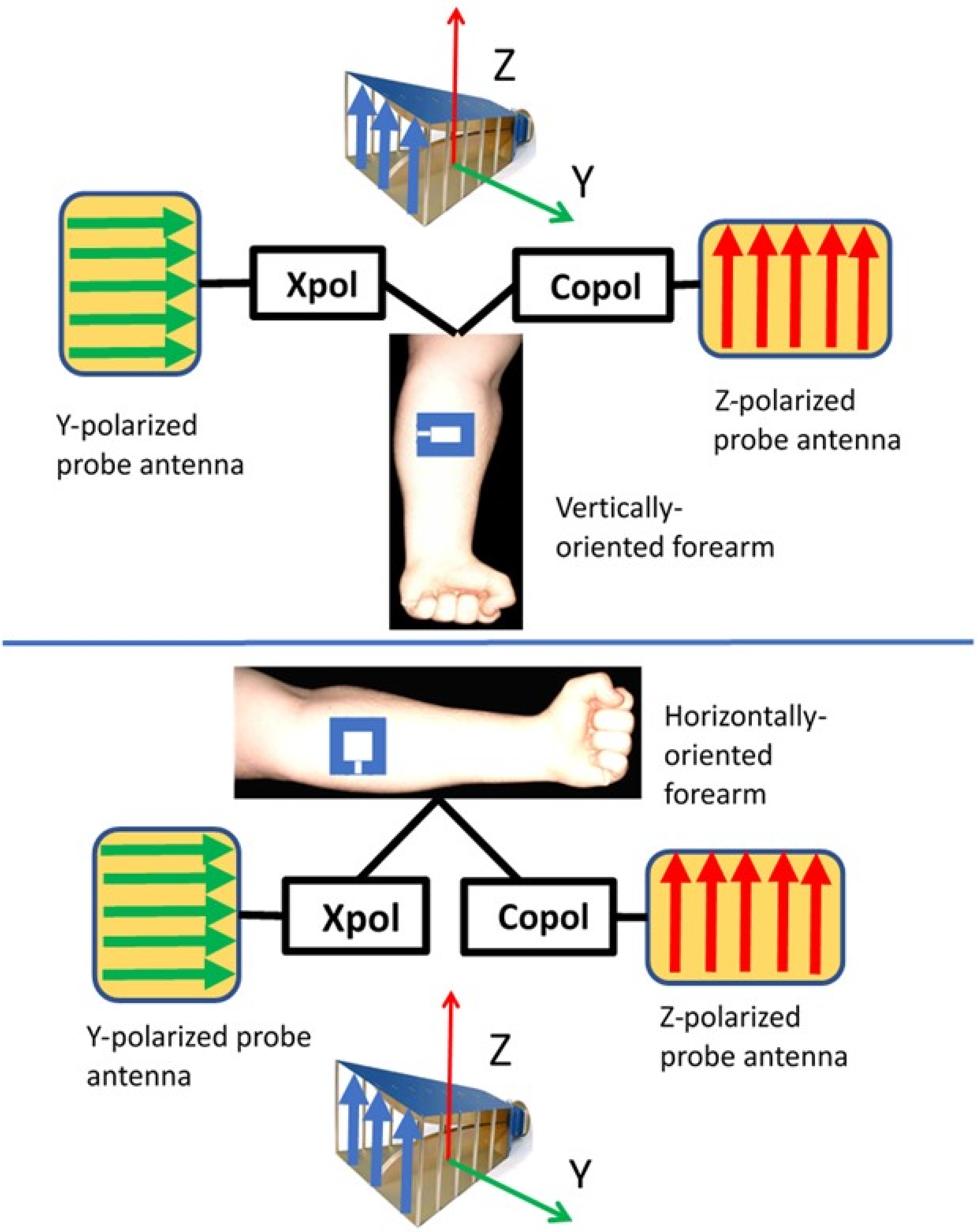

Figure 51.Configurations of radiation pattern measurements.

A volunteer had to wear the Kapton-printed antennas with a compression band to keep the antenna in place. The antenna was positioned in a manner which oriented the feed port of the antenna in the same manner as that of computer simulations. The epidermal antenna under test was connected to one of the VNA ports while the horn antenna was connected to another port. The volunteer would then have to position his arm in the center of the protractor.

The measurements had to cover 4 different arm and probe antenna orientations or combinations as seen in Figure 51. Each arm orientation (vertical and horizontal) had to have the cross-polarization (Xpol) and co-polarization (Copol) pattern measured. To achieve this, the probe antenna was oriented in two different orientations as seen in Figure 51. The arm would be oriented either perpendicular (vertical arm) or parallel (horizontal arm) to the floor. In turn, the probe antenna would measure and cover 120 degrees of the radiation pattern. This was done twice to cover the Z(Copol) and Y(Xpol) probe-antenna orientations. Each pattern took 20 minutes on average to capture. That is 20 x 4 = 80 minutes of almost un-interrupted stillness. The volunteer had to stay still for each single hand orientation (20+20 = 40 minutes). The overall tests were repeated several times for all three QL antennas (GSM-900, GSM-1800, and BLE).

The plots of the measured and simulated radiation patterns are presented in the following pages. Except for Figure 52, all radiation pattern plots in this chapter were curve fit using MATLAB. Figure 52 shows raw measurement curves for both of the cross-polarization and co-polarization at 2.4 GHz when the arm is in the vertical position. No curve fitting was done to this figure in order to illustrate the measure of agreement already present with raw measurement points.

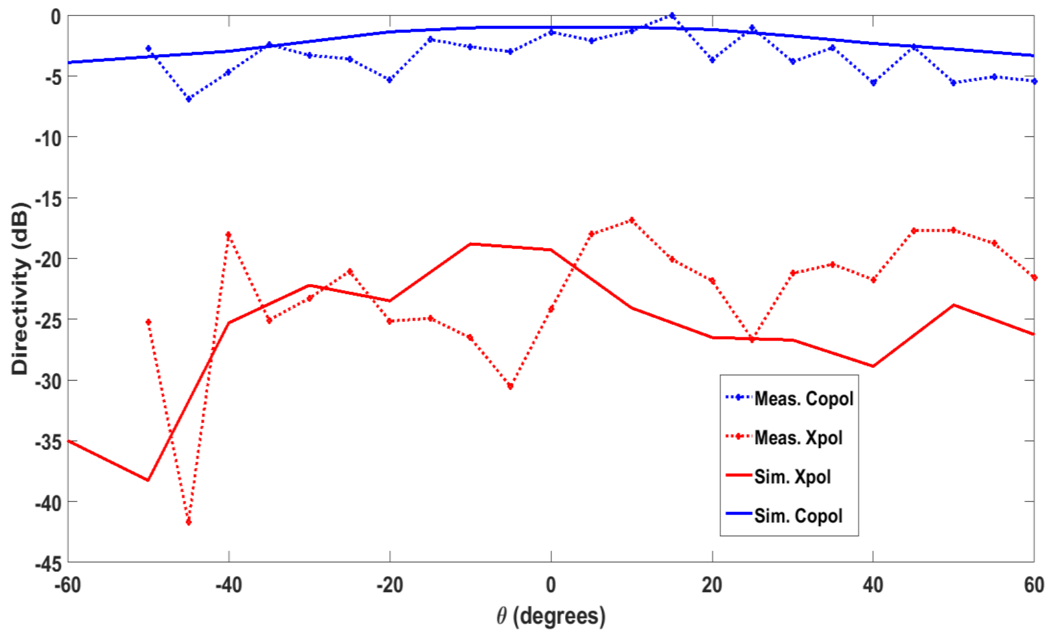

Figure 52. Radiation patterns for the vertical arm at 2.4 GHz.

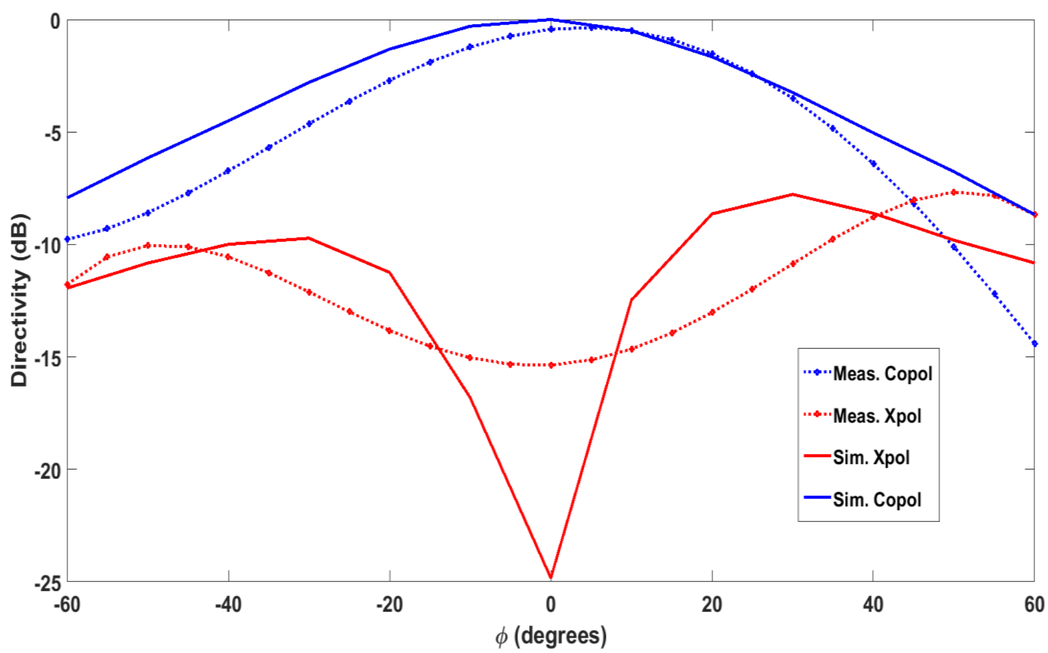

Figure 53. Radiation patterns for the horizontal arm at 2.4 GHz.

As can be inferred from figure 52 there is a difference of more than 15 dB between the peaks of the co- and cross-polarizations for the vertical orientation of the arm. Copol looks almost completely uniform when compared to the bumpy pattern of its Xpol counterpart. For simulation patterns of the horizontal arm, Figure 53, a difference of 25 dB between the relatively symmetric maximum of the Copol and minima of the Xpol can be seen. The measurements of this arm orientation do match simulations in their angular pattern but do not match exactly in amplitude.

4.3.2 GSM-1800 and GSM-900 results

To the best of our knowledge at the time, the QL antennas intended for cellular operation at 900/1800 MHz are unique as no published work ever reported any epidermal single-layer antenna intended for such an application. Figure 54 presents the simulated and measured reflection coefficient for the GSM-1800 antenna. The measured reflection coefficient exhibited a larger bandwidth than that of its simulated counterpart, however, this is due to extra losses incurred from the presence of other biological matter (e.g. blood) instead of actual radiation. In Figure 55. the same phenomenon is also observed with the QL GSM-900 antenna.

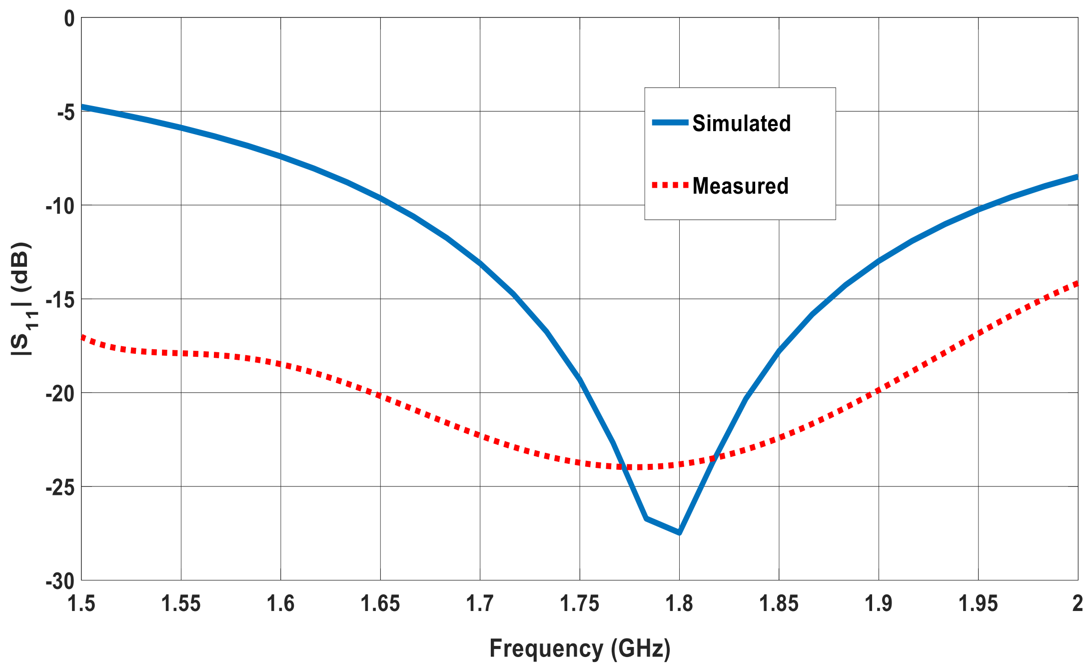

Figure 54. Measured and simulated reflection coefficient for the GSM-1800 QL antenna.

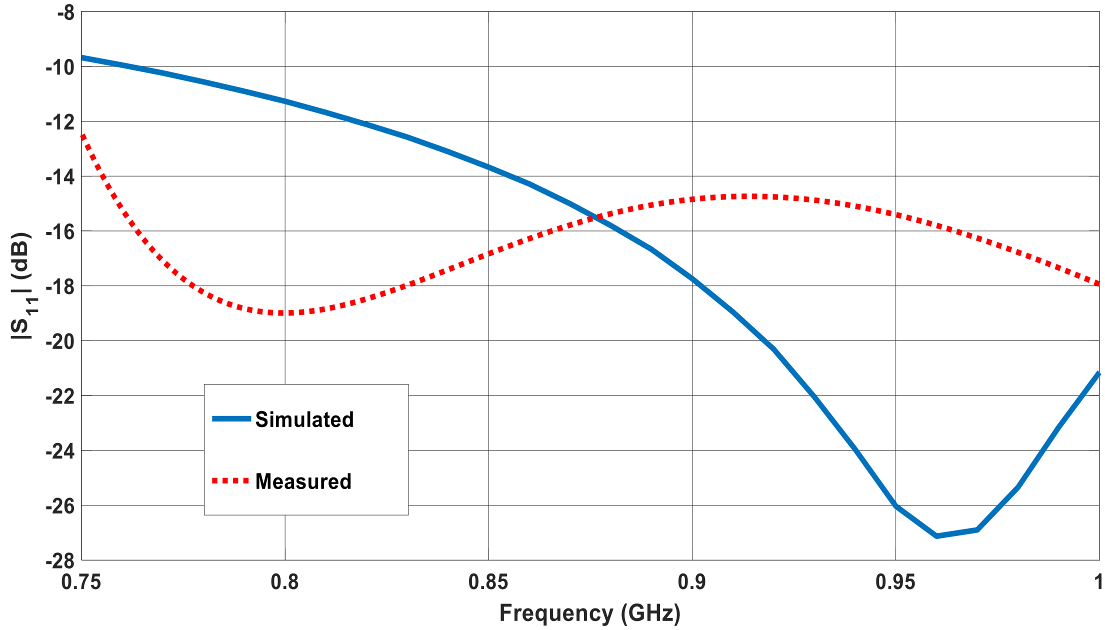

Figure 55. Measured and simulated reflection coefficient for the GSM-1800 QL antenna.

❖ The Patterns at 1.8 GHz

Radiation pattern measurements are scarcely reported for body-worn applications, especially for those done with human volunteers. The closest frequency to 1.8 GHz whose measured radiation pattern was reported for body-worn applications is the 1.5 GHz GPS antenna in [67]. Compared to 2.4 GHz, EM waves at 1.8 GHz would be less affected by the geometry of the arm due to diffraction properties of the longer wave. Since GSM-1800 antennas are intended for cellular applications, transmission and reception are desired to be omnidirectional. These features were realized to a certain degree in the radiation patterns seen in Figures 56-57. At this lower frequency, we could still see that the Copol and Xpol of the vertical arm still share a resemblance to those of 2.4 GHz. The main difference lies in the 10 degrees shift in location and magnitude of the null present in the Xpol. For the horizontal arm, Figure 57, maxima and minima for simulation patterns for both Copol and Xpol are mirrored in their measured counterparts. The differences between the simulated and measured maxima and minima, lie mainly in their respective breadth and scale.

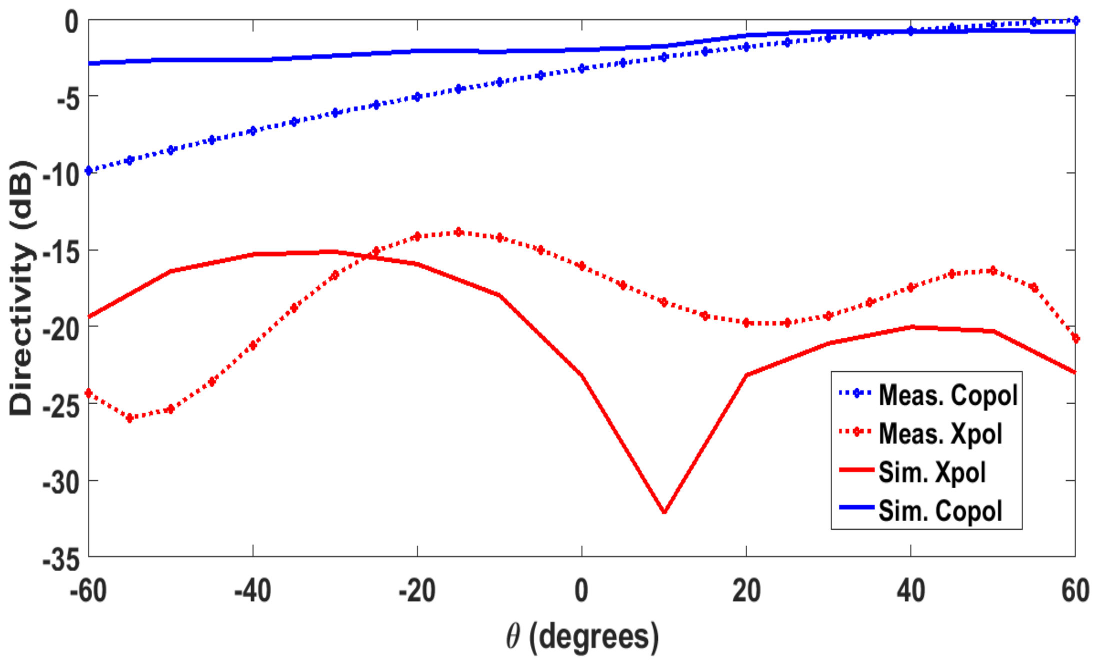

Figure 56.Radiation patterns for the vertical arm at 1.8 GHz.

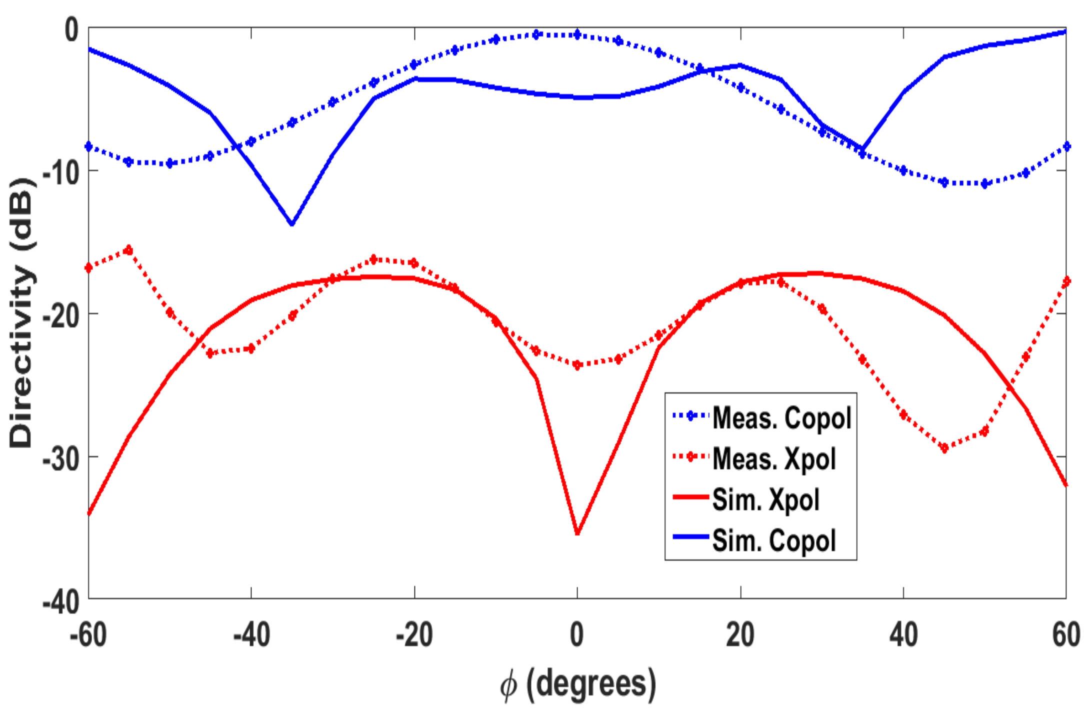

Figure 57. Radiation patterns for the horizontal arm at 1.8 GHz.

❖ The Patterns at 900 MHz

The patterns obtained at 900 MHz reveal yet again a good match between simulations and measurements. Just as with the GSM-1800 antenna, it is much easier for longer waves to find their way in, out, and around the arm at 900 MHz than at higher frequencies. In effect, the arm becomes less of a “visible” obstacle for wave propagation.

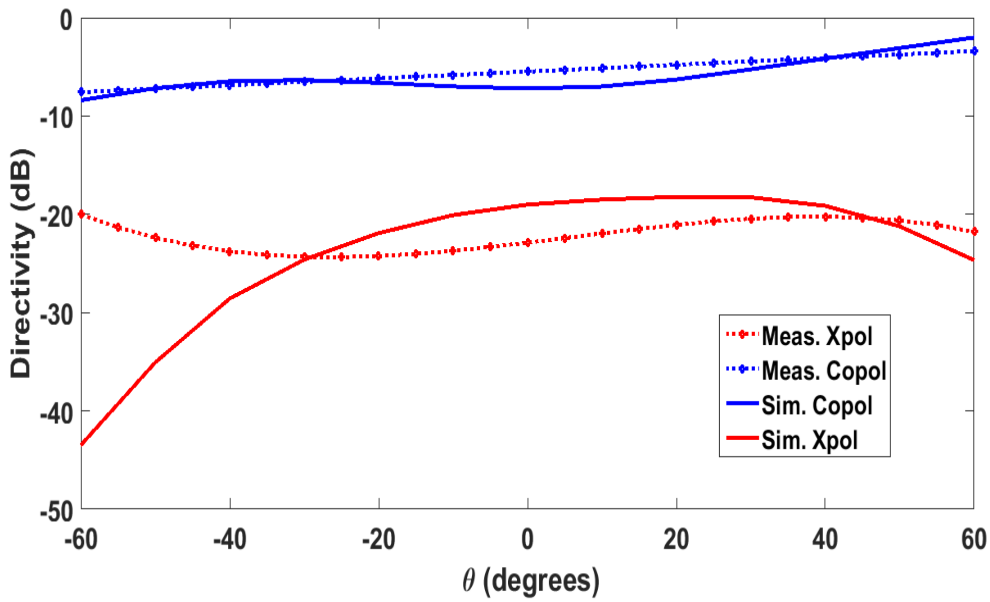

Figure 58. Radiation patterns for the vertical arm at 900 MHz.

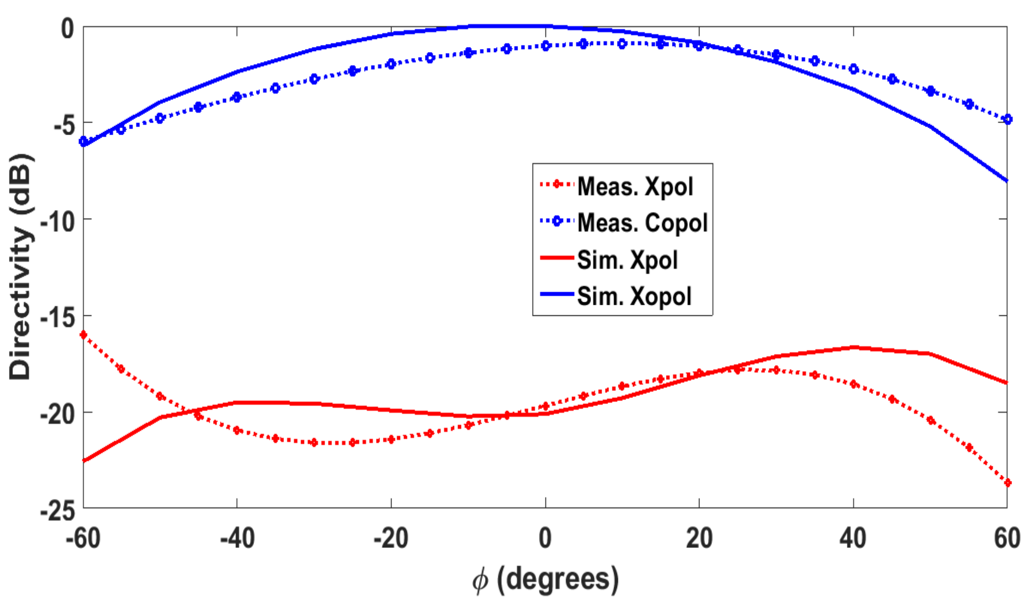

Figure 59. Radiation patterns for the horizontal arm at 900 MHz.

Remarks on Radiation Pattern Results

It should be noted that the fabricated copper antennas, especially those which were made with the LPKF machine, were not an exact replica of the original software designs. This is due to fabrication inaccuracies incurred through the use of drilling needles and cutting through adhesive flexible copper sheets. As mentioned before, these minute differences have a more pronounced effect on measurement results at higher frequencies. Nonetheless, the level of similarity between simulated and measured results were unexpected given the priori of the unpredictability of single-layer body-worn antennas. The matching level between the majority of the simulated and measured radiation patterns was unexpectedly good. As previously noted, the differences lie mostly in the relative locations of the troughs and crests of the patterns.

4.3.3 Radiation pattern link budget

Besides capturing the directivity of the epidermal antennas, it would also be appropriate to find out the amount of power they received from the probing ridged horn. The received power at the epidermal antenna side could be calculated from the Friis transmission equation [81]:

$$P_r = P_t + G_t + G_r + 20\log_{10}\left(\frac{\lambda}{4\pi R}\right) \tag{15}$$

- Where P_r is the received power in dBm.
- P_t is the transmitted power in dBm.
- G_t is the gain in dB of the transmitting (probe) antenna.
- G_r is the gain in dB of the receiving (epidermal) antenna.
- R is the distance between the transmitting and receiving antennas.

For this formula to be used validly, the waves reaching the receiving epidermal antenna should be plane waves and in the far-field of the transmitting antenna. To realize these requirements, the following conditions [58] need to be satisfied:

$$R \gg D \tag{16-a}$$
$$R \gg \lambda \tag{16-b}$$
$$R > d_f \tag{16-c}$$
$$\text{Where } d_f = 2\frac{D^2}{\lambda} \tag{16-d}$$

In words, "R" is the distance between the transmitting and receiving antennas. It has to be much larger than both: 1- the largest dimension, D = 204 mm, of the transmitting antenna, and 2- The free space wavelength, λ. Free space wavelength is chosen since it is the primary medium of wave propagation from transmitter to the receiver. For radiation pattern measurements, R was 5 meters (5000 mm). The Fraunhofer distance, d_f, sets the limit between the near-field and far-filed regions. R is larger than d_f for all test frequencies; it also satisfies all of the above-mentioned conditions. Thus, the Friis transmission equation can be used to find the received power at the epidermal antenna side.

Transmission power, P_t, was set to be 0 dBm for all frequencies. The measured gain of the BLE, GSM-900, and GSM-1800 antennas are -10 [80], -11, and -8, respectively. On another note, radiation efficiencies (e_{rad}) were 5%, 8%, and 12%, again respectively. These parameters are related to the directivity (D) of the antenna by:

$$\mathbf{G} = \mathbf{e_{rad}} * \mathbf{D} \tag{17}$$

This relationship helps realize why the GSM-900 antenna has the lowest gain among all of the three epidermal antennas. Basically, although the radiation efficiency of the GSM-900 antenna is the highest, its directivity is much lower than any of the other antennas.

Table IX. Link budget calculations of radiation pattern measurements

Frequency (GHz)	d_f (mm)	λ(mm)	G_t(dBi)	G_r(dBi)	P_r(dBm)
0.9	250	333	4	-11	-52.51
1.8	500	167	10	-8	-49.53
2.4	666	125	11	-10	-53.03

4.3.4 Data communications

A true measure of antenna efficiency would be to test its performance in a real wireless communications link. Hence, the GSM-900 and the BLE/ISM (2.4-2.5) GHz antennas were each tested for their error vector magnitudes (EVM).

EVM is a measure of how accurately a radio is transmitting or receiving symbols within a constellation. suppose a radio is receiving symbols or data packets through a 4-QAM constellation. In reality, the signals received would be deviated from the four ideal constellation points. The difference between the point on the constellation representing the received symbol and an ideal reference point is the error vector. The root-mean-square of the EVM for all received symbols is [82]:

$$\mathbf{EVM_{RMS}}(\%) = \sqrt{\frac{\mathbf{P_{error}}}{\mathbf{P_{reference}}}} \text{ x } 100\% \tag{18}$$

Where P_{error} is the power (magnitude) of the error vector, and $P_{reference}$ is the power of the reference ideal point.

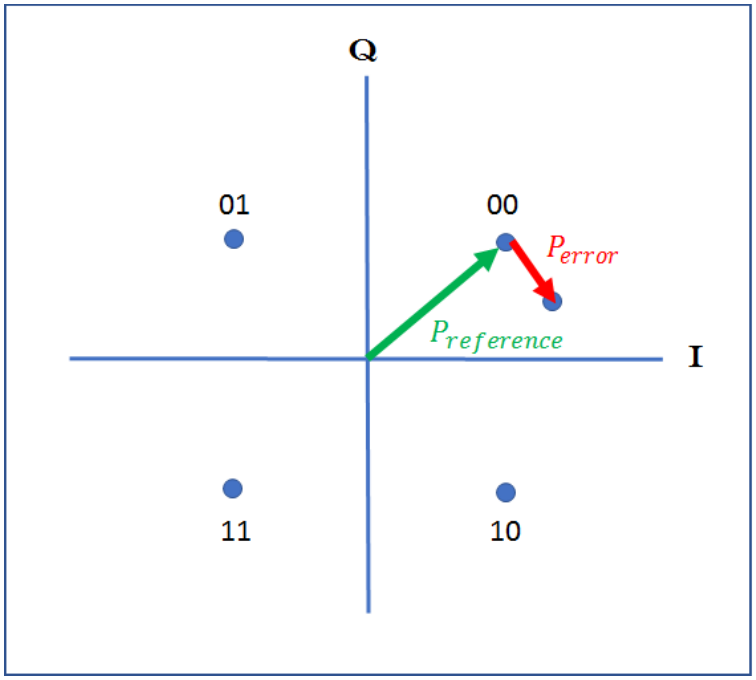

Figure 60. Error vector magnitude (EVM).

The VSG was set-up to generate 4-QAM packets at a frequency of 915 MHz for the epidermal GSM-900 antenna and then at 2.45 GHz for the epidermal BLE antenna. The Epidermal antennas were worn as receiving antennas and were connected to an R&S FSV. Figure 61 shows the test link set-up:

Figure 61. Data communication tests set-up.

1- R&S®SMBV100A Vector Signal Generator: this device acted as the transmit system where the frequency, communications protocol, and transmitted power levels were set.
2- Transmit antennas:
    - RP circular 915 MHz antenna (ALR-9611-CR).
    - Omnidirectional 2.45 GHz antenna (CAF94150 030421).
3- R&S®FSV Signal and Spectrum Analyzer: this device provided real time measurements of EVM as well as real time display of constellation diagrams.
4- Receive epidermal antennas:
    - Kapton-based adhesive copper GSM-900 and BLE antennas.

Tests for communication at each frequency (915 MHz, 2.45 GHz) involved different arm-body orientations and positions, and different transmit power levels: -10 dBm, 0 dBm, and 10 dBm. A power level of 10 dBm is relatively high for body-worn applications, and it was used only for research and experimentation purposes. Results for these tests are seen in Tables X-XII:

Figure 62. Top side of the antenna facing the transmitter, "Position A".

Table X. "Position A" EVM results.

Frequency	Transmitter Power level (dBm)	EVM_{RMS} (%)
915 MHz	-10	17.55
	0	9.23
	10	2.10
2.45 GHz	-10	8.10
	0	2.29
	10	0.75

Figure 63. Lateral side of the antenna facing the transmitter, “Position B”.

Table XI. Position “B” EVM results.

Frequency	Transmitter Power level (dBm)	EVM_{RMS} (%)
915 MHz	-10	18.04
	0	13.70
	10	5.31
2.45 GHz	-10	6.10
	0	3.52
	10	1.33

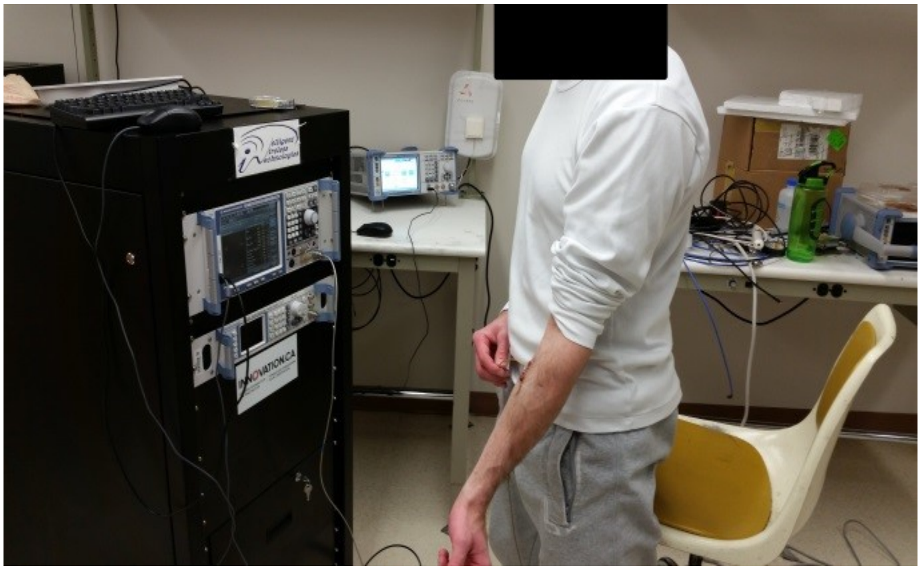

Figure 64. Feed terminals of the antenna facing the transmitter "Position C".

Table XII. Position "C" results.

Frequency	Transmitter Power level (dBm)	EVM_{RMS} (%)
915 MHz	-10	16.20
	0	14.00
	10	7.45
2.45 GHz	-10	16.05
	0	12.88
	10	3.75

Although EVM_{RMS} results provide adequate information about the performance of the receive system, bit-error-rate (BER) is a more popular means to gauge the performance of a communications system, and this is particularly true with GSM standards. Hence, it was necessary to find a means to convert EVM_{RMS} values into corresponding BER ones and then compare them with a 4-QAM standard.

$$\mathrm{BER} = \mathrm{Q}\left(\frac{1}{\mathrm{EVM_{RMS}}}\right) \quad \text{(19) from [83]}$$

Where Q(.) is the Gaussian co-error function:

$$\mathbf{Q(x)} = \int_{\mathbf{x}}^{\infty} \frac{\mathbf{1}}{\sqrt{\mathbf{2\pi}}} \left(\mathbf{e}^{-\frac{y^2}{2}} \right) \mathbf{dy} \tag{20}$$

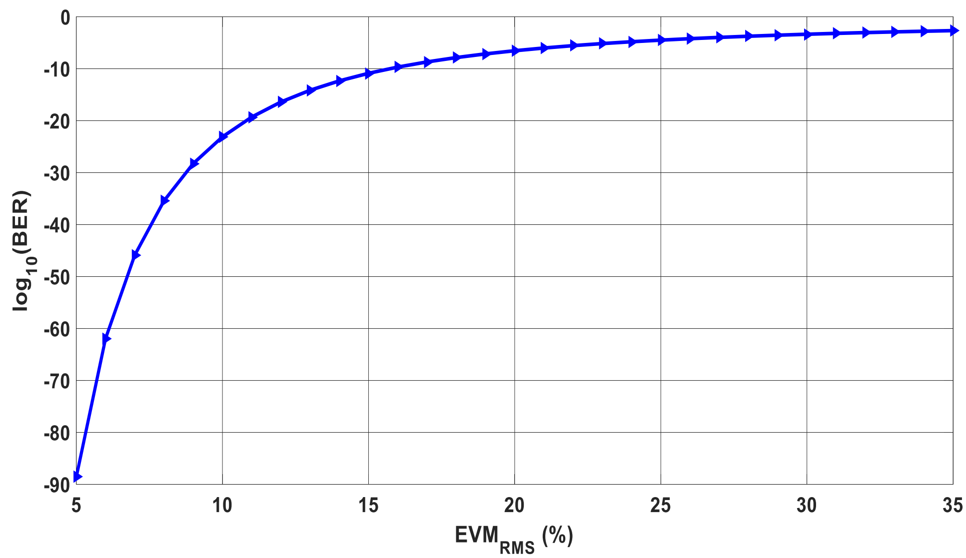

Figure 65. Relationship between BER and EVM for 4-QAM.

Since all measured EVM values were better than 19%, their translation into corresponding BER values yield less than 0.1% (1 erroneous bit in a 1000 bits). For Bluetooth communications, a minimum receiver sensitivity of -70 dBm with a BER of 0.1% or better is required. According to the plot, 0.1% percent corresponds to an EVM value of about 30%. Although the calculated received powers shown below are not less than -52.7 dBm, it is expected that even at -70 dB the BER would not exceed 0.1%. This can be inferred from when the transmitted power was decreased from 0 to -10 dB, the EVM values for both of the BLE and GSM-900 antennas increased to no more than 4-5%. Hence, it is expected that if the received power was at -70 dBm we should expect EVM values of no more than 25% which correspond to BER values of better than 0.1%.

4.3.5 Data communications link budget

Besides capturing EVM readings for the epidermal antennas, it was also necessary to find out the amount of received power reaching then from their respective transmitting antennas. Hence, The Friis transmission equation (14) was used again. Here, R has to be much larger than both: 1- the largest dimension, D, of the transmitting antenna, and 2- The free space wavelength λ. Instead of the wavelength found within biological tissue, that of free space should be used since it is the primary medium of communications between transmitters and receivers. For communication link tests, R was 2 meters (2000 mm). R was larger than d_f for both transmit antennas (915 MHz and 2.45 GHz) and it also satisfied all of the above-mentioned conditions.

Table XIII. Link budget calculations for data communications set-up.

Frequency (GHz)	λ(mm)	G_t(dBi)	G_r(dBi)	P_t(dBm)	P_r(dBm)
0.915	327	6	-11	0	-42.70
2.45	125	3	-10		-53.25
0.915	327	6	-11	-10	-52.70
2.45	125	3	-10		-63.25

4.4 Research Stage 3: Silver Ink Stretchable Antennas

The other set of antennas tested were those presented in Chapter 3 as silver ink antennas printed on VHB stretchable substrates. These antennas are the embodiment of combining the different fields of chemical, materials, and electrical engineering to exploit the potential of body-worn antennas. The idea was to design an antenna which when stretched to double its size (100% stretch), resonates at 1.8 GHz, hence working as a GSM-1800 antenna.

4.4.1 Performance of the stretchable antenna

As the antenna-body separation gap increases, electromagnetic coupling with bio-matter decreases and the electrical lengths of the antennas decrease. The thickness of the stretchable VHB substrate is 1mm. Hence, compared to the Kapton and copper antennas, we should expect a shift in the operational center frequencies to the right. Measured and simulated reflection coefficient results for the (16*16)mm^2 antenna could be seen in Figure 67. Radiation pattern measurements for the antenna unstretched could be seen in Figure 70.

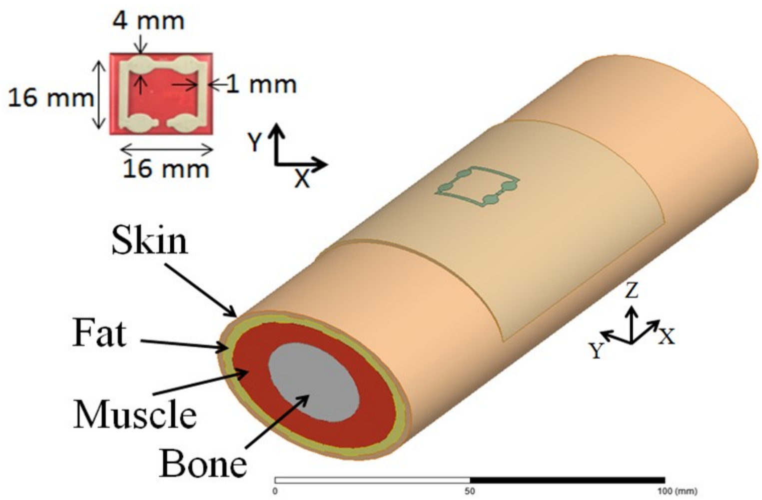

Figure 66. The fabricated and simulated stretchable VHB QL antenna.

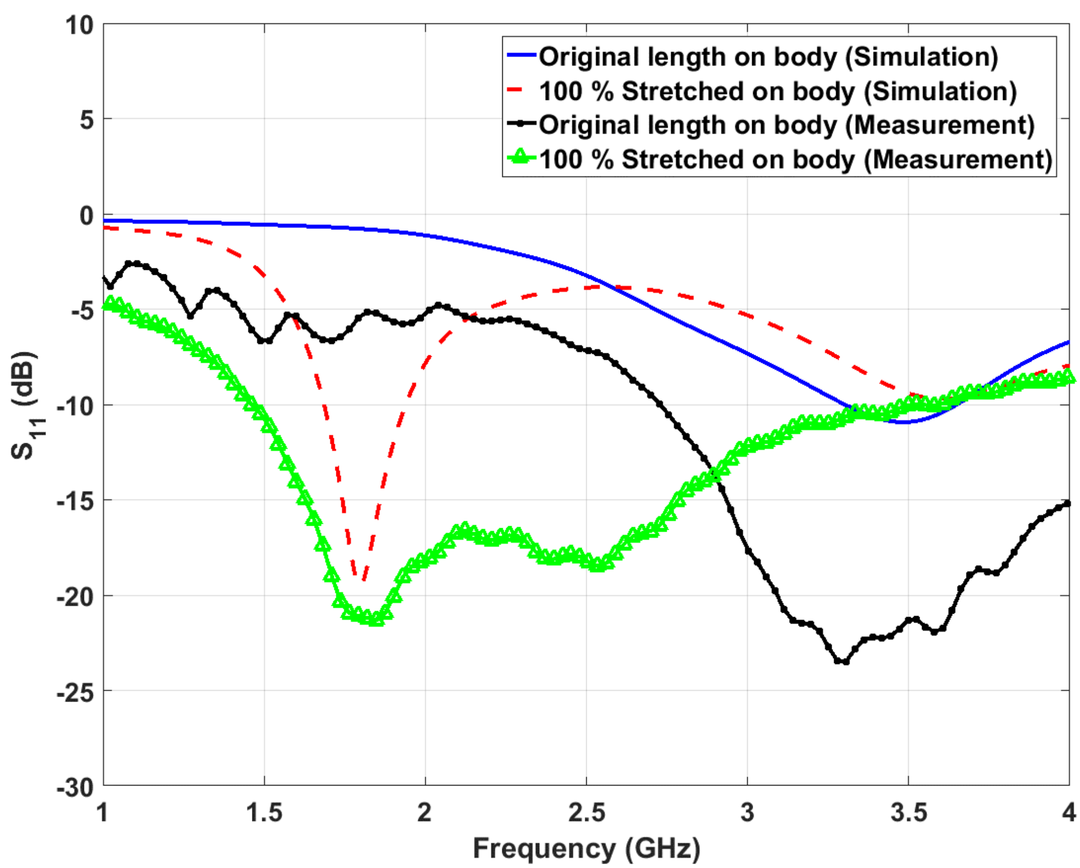

Figure 67. Simulated and measured reflection coefficients for the stretched and unstretched stretchable antenna.

As can be seen in the above plots, simulations and measurements show considerable degrees of agreement. This is especially true when the stretching-to-frequency-shift ratio is compared. The wider impedance bandwidth seen in measurements is mainly due to energy loss and coupling to body tissues. These differences are typical for body-worn antennas as simulation models do not account for all bio-matter present in an actual arm.

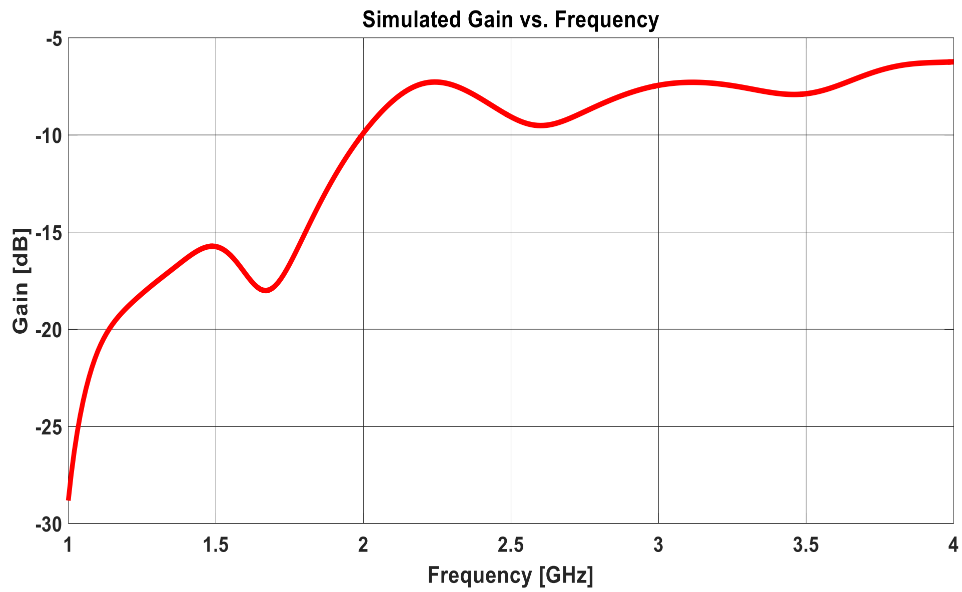

Figure 68. Gain of the (16*16)mm^2 QL antenna.

❖ Radiation patterns of the unstretched antenna

Radiation pattern measurements were taken with the aid of RFexpert EMscan platform, Figure 69. The antenna was fed with 1 dBm of power from a signal generator, and platform boundaries were necessary to define for EMscan to properly scale its radiation pattern measurement algorithm. The obtained patterns covered the entire 180 degrees span of the top side of the antenna. As seen in Figure 66, very good agreement between measured and simulated radiation patterns for the unstretched antenna was obtained.

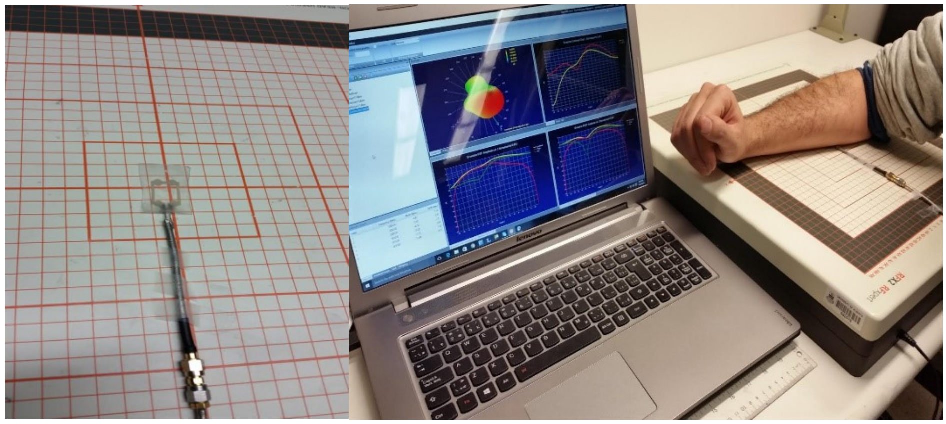

Figure 69. The EMscan platform used to measure radiation patterns.

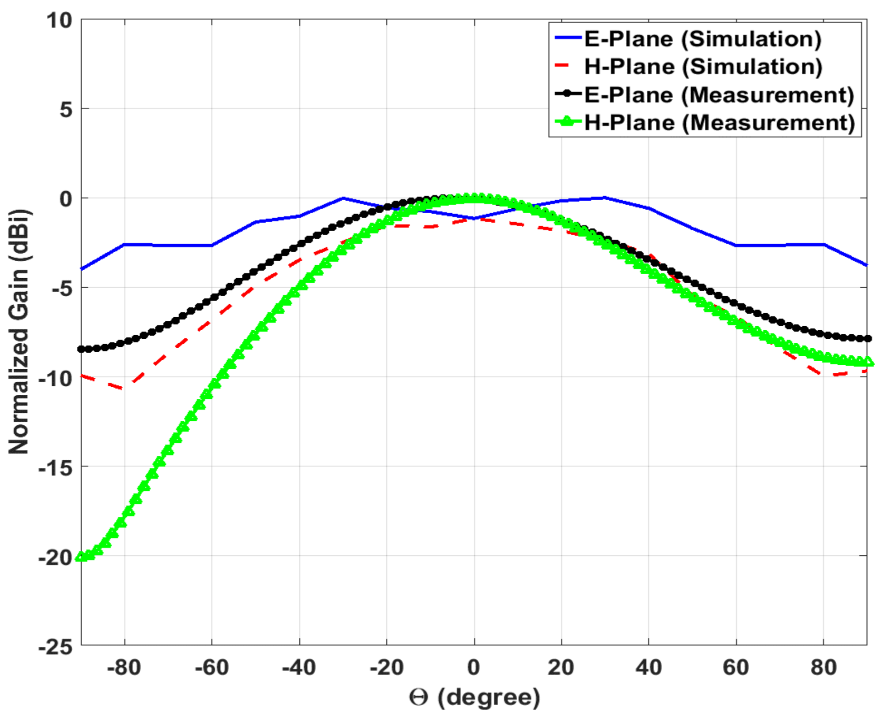

Figure 70. Simulated and measured radiation patterns.

Conclusion

In this chapter, we saw the performance of various QL antennas as they were put to the test. The initial research stage was completed after test results confirmed the superior performance of the QL antenna to the standard square loop. This was evident in gain, reflection coefficient, and radiation efficiency improvements. In the second research stage, the primary measurements taken focused on capturing the radiation pattern of the GSM-900, GSM-1800, and BLE Kapton-fabircated antennas. the measured patterns were compared to their simulation counterparts and yielded excellent overall matching. Moreover, data communication tests showed that the acquired BER readings could qualify the BLE and GSM-900 Kapton antennas to work as part of 4-QAM wireless links. Lastly, a stretchable QL epidermal antenna had its measured results agree with simulations. This stretchable antenna is intended to work in the GSM-1800 band when stretched to double its length.

Chapter Five: Summary and Future Work

5.1 Summary

The QL epidermal antennas were designed to cover three major frequency bands: ISM (2.4-2.5) GHz, GSM-1800, and GSM-900. They were made to be very thin single-layer groundless structures to allow for the accommodation of neighboring electronics and sensors. To exploit their potential, different fabrication tools and materials were used to make the antennas. From there, comprehensive measurements and tests were conducted. The types of measurements taken were in step with research progression and objective completion. The first research stage was completed after measurement results confirmed the superiority of the QL antenna to the standard loop antenna. This was evident in gain and impedance bandwidth enhancement after the inclusion of circular patches to the standard loop. In the second stage, radiation pattern measurements were made to compare with simulated radiation patterns. The results showed satisfying levels of agreement with simulation patterns. Later, data communication tests showed that the acquired BER readings could qualify the BLE and GSM-900 antennas to work in 4-QAM wireless links. In the third stage, a stretchable epidermal antenna was tested for stretchability and reflection coefficient performance. The radiation patterns where captured by RFexpert technology, and they were in agreement with simulation results.

The human body surely poses special challenges when used as an antenna platform. As analysis tools, different HFSS arm models composed of skin, fat, muscle and bone layers were used throughout the project. The four-layer cylindrical model was later adopted as the standard model to help explain the shape of the radiation pattern for the designed epidermal antennas. From then, it was desired to find an equivalent arm model consisting of only one lossy dielectric instead of the four tissue-representing layers. This serves as a more efficient means for resource allocation and simulation runtime. In addition, this equivalent model can be realized into a physical phantom whose dielectric parameters could be recreated by chemical recipes.

5.2 Future Work

An epidermal sensing antenna was designed and simulated in the first stage of research. This metamaterial-inspired loop antenna is quasi-composed of two complementary split ring resonators (CSRR), hence the name Quasi-Metamaterial Loop (QML) antenna, Figure 71. The feeding terminals are present in the outer ring, and the radiation mechanism is based on Babinet's principle. The differences between the dimensions of the concentric loops allows for two non-harmonic resonances. The two frequencies could be tuned by changing each loop's length. Due to fabrication difficulties associated with the fine dimensions and minute gaps within its concentric loops, it was not possible to test the potential of this novel antenna.

The main goal of any future work aimed at bringing this antenna into life should seek to fabricate the antenna accurately. Several attempts were made to fabricate the antenna in the same manner the QL antennas were fabricated, but none of could came out as desired. Further research should be done to find a better way or a new fabrication technique to accurately realize the QML antenna.

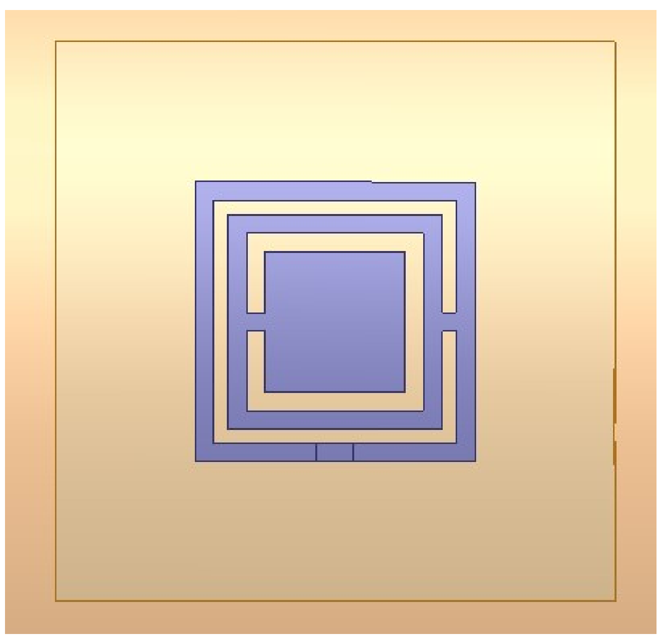

Figure 71. The QML sensing antenna: (15*15)mm^2.

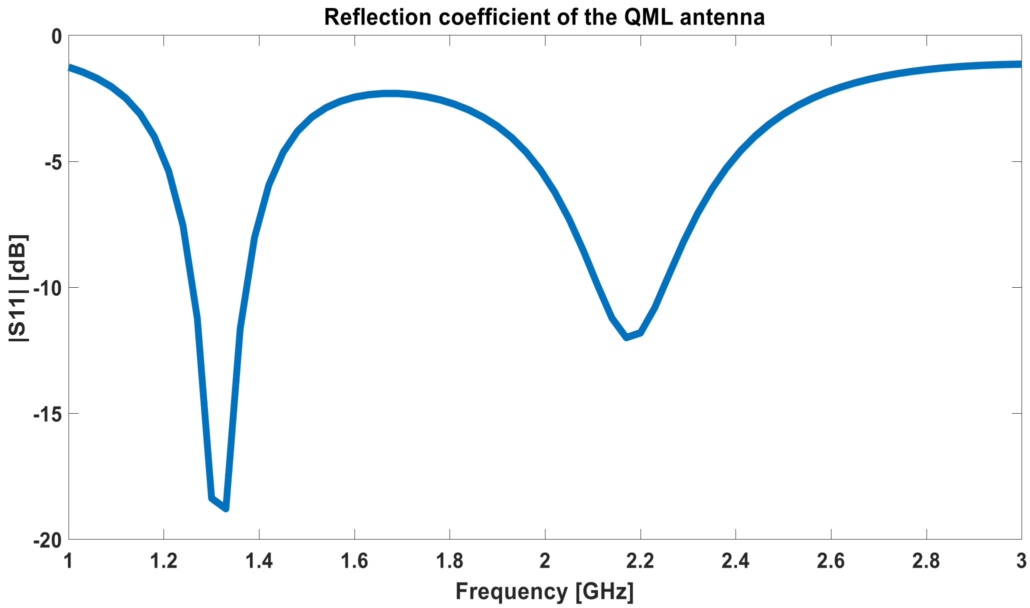

Figure 72. Simulated reflection coefficient of the QML sensing antenna.

On another note, the GSM-900 (with its original dimensions of (37*37)$\mathrm{mm}^2$was also fabricated with silver ink deposited on VHB stretchable substrate. However, except for reflection coefficient measurements, full performance tests were yet to be completed. If work is to be resumed with these stretchable antennas, full tests including radiation pattern measurements and data communications will be conducted to invest in their potential for epidermal and non-epidermal applications.

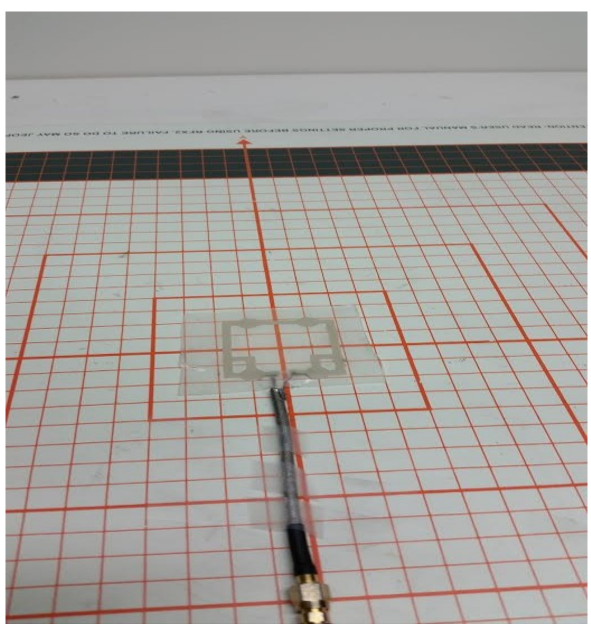

Figure 73. The stretchable (37*37)mm^2 epidermal antenna.

Bibliography

[1] H. Khaleel, *Innovation in wearable and flexible antennas*. Wit Press, 2014.

[2] S. Zhang, A. Paraskevopoulos, C. Luxey, J. Pinto, and W. Whittow, “Broad-band embroidered spiral antenna for off-body communications,” *IET Microw. Antennas Propag.*, vol. 10, no. 13, pp. 1395–1401, 2016.

[3] X. Huang *et al.*, “Epidermal impedance sensing sheets for precision hydration assessment and spatial mapping,” *IEEE Trans. Biomed. Eng.*, vol. 60, no. 10, pp. 2848–2857, 2013.

[4] J.-W. Jeong *et al.*, “Epidermal Electronics: Capacitive Epidermal Electronics for Electrically Safe, Long-Term Electrophysiological Measurements (Adv. Healthcare Mater. 5/2014),” *Adv. Healthc. Mater.*, vol. 3, no. 5, pp. 621–621, 2014.

[5] E. Y. Chow, M. M. Morris, and P. P. Irazoqui, “Implantable RF medical devices: The benefits of high-speed communication and much greater communication distances in biomedical applications,” *IEEE Microw. Mag.*, vol. 14, no. 4, pp. 64–73, 2013.

[6] “3 types of wearable/M2M technology to make Rugby World Cups safer,” *Gemalto blog*, 17-Sep-2015. .

[7] M. Combe, “ZigBee Vs. Bluetooth: A Use Case With Range Calculations.” [Online]. Available: http://www.link-labs.com/blog/zigbee-vs-bluetooth. [Accessed: 31-Jan-2017].

[8] “How can police use drones?,” *HowStuffWorks*, 14-Jul-2015. [Online]. Available: http://people.howstuffworks.com/can-police-use-drones.htm. [Accessed: 31-Jan-2017].

[9] F. C. Commission and others, “WT Docket No. 99-66, RM-9157,” *Amend. Parts 2 95 Comm. Rules Establ. Med. Implant Commun. Serv. 402–405 MHz Band*, pp. 99–66.

[10] “47 CFR I - Medical Implant Communications (MICS).” [Online]. Available: https://www.gpo.gov/fdsys/search/pagedetails.action?collectionCode=CFR&searchPath=Title+47%2FChapter+I%2FSubchapter+D%2FPart+95&granuleId=CFR-2004-title47-vol5-part95-subpartI&packageId=CFR-2004-title47-vol5&oldPath=Title+47%2FChapter+I%2FSubchapter+D%2FPart+94&fromPageDetails=true&collapse=true&browsePath=Title+47%2FChapter+I%2FSubchapter+D%2FPart+95%2FSubpart+I&fromBrowse=true. [Accessed: 31-Jan-2017].

[11] “FCC Adopted Rules for New Advanced Medical Technologies, ET Docket No. 06-135,” *Federal Communications Commission*, 17-Dec-2015. [Online]. Available: https://www.fcc.gov/document/fcc-adopted-rules-new-advanced-medical-technologies-et-docket-no-06. [Accessed: 31-Jan-2017].

[12] D. H. Werner and Z. H. Jiang, *Electromagnetics of Body Area Networks: Antennas, Propagation, and RF Systems*. John Wiley & Sons, 2016.

[13] T. Kellomäki, T. Björninen, L. Ukkonen, and L. Sydänheimo, “Shirt collar tag for wearable UHF RFID systems,” in *Proceedings of the Fourth European Conference on Antennas and Propagation*, 2010, pp. 1–5.

[14] G. Marrocco, “RFID antennas for the UHF remote monitoring of human subjects,” *IEEE Trans. Antennas Propag.*, vol. 55, no. 6, pp. 1862–1870, 2007.

[15] A. Sani, M. Rajab, R. Foster, and Y. Hao, “Antennas and propagation of implanted RFIDs for pervasive healthcare applications,” *Proc. IEEE*, vol. 98, no. 9, pp. 1648–1655, 2010.

[16] A. Ghildiyal, K. Amara, R. Dal Molin, B. Godara, A. Amara, and R. K. Shevgaonkar, “UWB for in-body medical implants: A viable option,” in *Ultra-Wideband (ICUWB), 2010 IEEE International Conference on*, 2010, vol. 2, pp. 1–4.

[17] J. Y. Khan and M. R. Yuce, “Wireless body area network (WBAN) for medical applications,” *New Dev. Biomed. Eng. INTECH*, 2010.

[18] “Fitbit Surge™ Fitness Super Watch.” [Online]. Available: https://www.fitbit.com/en-ca/surge. [Accessed: 31-Jan-2017].

[19] "TomTom Adventurer | Explore with your heart." [Online]. Available: https://www.tomtom.com/en_ca/sports/outdoor-watches/. [Accessed: 31-Jan-2017].
[20] "TomTom Spark 3 Cardio + Music GPS Fitness Watch." [Online]. Available: https://www.tomtom.com/en_ca/sports/fitness-trackers/gps-fitness-watch-cardio-music-spark3/black-large/. [Accessed: 31-Jan-2017].
[21] S. Knapton, "Google Glass may revolutionise medical treatment," 09-Apr-2014.
[22] "Project Jacquard." [Online]. Available: https://atap.google.com/jacquard. [Accessed: 31-Jan-2017].
[23] W. M. Haynes, *CRC Handbook of Chemistry and Physics, 95th Edition*. CRC Press, 2014.
[24] "Dielectric Properties of Body Tissues: Home page." [Online]. Available: http://niremf.ifac.cnr.it/tissprop/. [Accessed: 31-Jan-2017].
[25] "Water in the body," *H4H Initiative*. [Online]. Available: http://www.h4hinitiative.com/h4h-academy/hydration-lab/water-and-hydration-physiological-basis-adults/water-body. [Accessed: 31-Jan-2017].
[26] K. Tiiti, *Effects of The Human Body on Single Layer Wearable Antenna*. Tampere University Of Technology, 2012.
[27] S. Amendola, S. Milici, and G. Marrocco, "Performance of epidermal RFID dual-loop tag and on-skin retuning," *IEEE Trans. Antennas Propag.*, vol. 63, no. 8, pp. 3672–3680, 2015.
[28] B. Hu, G.-P. Gao, L.-L. He, X.-D. Cong, and J.-N. Zhao, "Bending and on-arm effects on a wearable antenna for 2.45 GHz body area network," *IEEE Antennas Wirel. Propag. Lett.*, vol. 15, pp. 378–381, 2016.
[29] S. Amendola, G. Bovesecchi, A. Palombi, P. Coppa, and G. Marrocco, "Design, Calibration and Experimentation of an Epidermal RFID Sensor for Remote Temperature Monitoring," *IEEE Sens. J.*, vol. 16, no. 19, pp. 7250–7257, 2016.
[30] "neva," *neva*. [Online]. Available: http://www.nevaelectromagnetics.com. [Accessed: 31-Jan-2017].
[31] M. A. B. Abbasi, S. Nikolaou, M. Antoniades, M. N. Stevanovic, and P. Vryonides, "Compact EBG-Backed Planar Monopole for BAN Wearable Applications," *IEEE Trans. Antennas Propag.*, 2016.
[32] S. Rao *et al.*, "Miniature implantable and wearable on-body antennas: towards the new era of wireless body-centric systems [antenna applications corner]," *IEEE Antennas Propag. Mag.*, vol. 56, no. 1, pp. 271–291, 2014.
[33] S. Kang and C. W. Jung, "Wearable fabric antenna on upper arm for MedRadio band applications with reconfigurable beam capability," *Electron. Lett.*, vol. 51, no. 17, pp. 1314–1316, 2015.
[34] S. Hong, S. H. Kang, Y. Kim, and C. W. Jung, "Transparent and Flexible Antenna for Wearable Glasses Applications," *IEEE Trans. Antennas Propag.*, vol. 64, no. 7, pp. 2797–2804, 2016.
[35] "Hand / Arm Transplant | Johns Hopkins Comprehensive Transplant Center." [Online]. Available: http://www.hopkinsmedicine.org/transplant/programs/reconstructive_transplant/hand_transplant.html. [Accessed: 31-Jan-2017].
[36] "FDTD Simulation Software and the FDTD Method - Remcom." [Online]. Available: http://www.remcom.com/xf7-fdtd-method. [Accessed: 31-Jan-2017].
[37] "http://www.ansys.com/de-DE/products/electronics/ansys-hfss/hfss-features." [Online]. Available: http://www.ansys.com/de-DE/products/electronics/ansys-hfss/hfss-features. [Accessed: 31-Jan-2017].
[38] Z. Rahimi, "The Finite Integration Technique (FIT) and the Application in Lithography Simulations," 2011.
[39] D. Morris, "Which Electromagnetic Simulator Should I Use?" Keysight Technologies, 2011.
[40] Z. H. Hu, M. Gallo, Q. Bai, Y. I. Nechayev, P. S. Hall, and M. Bozzetti, "Measurements and simulations for on-body antenna design and propagation studies," in *Antennas and Propagation, 2007. EuCAP 2007. The Second European Conference on*, 2007, pp. 1–7.
[41] G. A. Conway and W. G. Scanlon, "Antennas for over-body-surface communication at 2.45 GHz," *IEEE Trans. Antennas Propag.*, vol. 57, no. 4, pp. 844–855, 2009.
[42] Z. H. Jiang, M. D. Gregory, and D. H. Werner, "Design and experimental investigation of a compact circularly polarized integrated filtering antenna for wearable biotelemetric devices," *IEEE Trans. Biomed. Circuits Syst.*, vol. 10, no. 2, pp. 328–338, 2016.

[43] "HUGO Human Body Model." [Online]. Available: https://www.cst.com/Applications/Article/HUGO+Human+Body+Model. [Accessed: 31-Jan-2017].
[44] G. Hartsgrove, A. Kraszewski, and A. Surowiec, "Simulated biological materials for electromagnetic radiation absorption studies," *Bioelectromagnetics*, vol. 8, no. 1, pp. 29–36, 1987.
[45] T. Karacolak, A. Z. Hood, and E. Topsakal, "Design of a dual-band implantable antenna and development of skin mimicking gels for continuous glucose monitoring," *IEEE Trans. Microw. Theory Tech.*, vol. 56, no. 4, pp. 1001–1008, 2008.
[46] C.-K. Chou, G.-W. Chen, A. W. Guy, and K. H. Luk, "Formulas for preparing phantom muscle tissue at various radiofrequencies," *Bioelectromagnetics*, vol. 5, no. 4, pp. 435–441, 1984.
[47] "Liquids | SAR & HAC Test Benches," 07-Oct-2010. [Online]. Available: http://www.satimo.com/zh-hans/zh-hans/content/products/liquids, http://www.satimo.com/zh-hans/content/products/liquids. [Accessed: 31-Jan-2017].
[48] S. Kim, Y.-J. Ren, H. Lee, A. Rida, S. Nikolaou, and M. M. Tentzeris, "Monopole antenna with inkjet-printed EBG array on paper substrate for wearable applications," *IEEE Antennas Wirel. Propag. Lett.*, vol. 11, pp. 663–666, 2012.
[49] M. A. B. Abbasi, D. Philippou, and S. Nikolaou, "Comparison Study of Layered Homogeneous Models with Detailed Human Tissue Models for Through-body Communications," *Liver*, vol. 51, pp. 0–65.
[50] L. M. Surhone, M. T. Tennoe, and S. F. Henssonow, *Specific Absorption Rate*. Betascript Publishing, 2011.
[51] "INTERNATIONAL CO ., LTD." [Online]. Available: http://www.amphenol-atc.com/en/page/custom24. [Accessed: 31-Jan-2017].
[52] P. J. Soh, G. Vandenbosch, F. H. Wee, A. van den Bosch, M. Martinez-Vazquez, and D. Schreurs, "Specific absorption rate (SAR) evaluation of textile antennas," *IEEE Antennas Propag. Mag.*, vol. 57, no. 2, pp. 229–240, 2015.
[53] "Dosimetric Assessment of the Mobile Nokia 5110 with and without the PAM System devices According to the European CENELEC Requirements." Kamp-Lintfort. Kamp-Lintfort, Germany: IMST GmbH, Jul-2000.
[54] J. Trajkovikj and A. K. Skrivervik, "Diminishing SAR for wearable UHF antennas," *IEEE Antennas Wirel. Propag. Lett.*, vol. 14, pp. 1530–1533, 2015.
[55] H. R. Khaleel, "Design and fabrication of compact inkjet printed antennas for integration within flexible and wearable electronics," *IEEE Trans. Compon. Packag. Manuf. Technol.*, vol. 4, no. 10, pp. 1722–1728, 2014.
[56] T. Kellomäki and L. Ukkonen, "Design approaches for bodyworn RFID tags," in *2010 3rd International Symposium on Applied Sciences in Biomedical and Communication Technologies (ISABEL 2010)*, 2010, pp. 1–5.
[57] C. A. Balanis, *Antenna theory: analysis and design*. John Wiley & Sons, 2016.
[58] W. L. Stutzman and G. A. Thiele, *Antenna theory and design*. John Wiley & Sons, 2012.
[59] S.-J. Ha and C. W. Jung, "Reconfigurable beam steering using a microstrip patch antenna with a U-slot for wearable fabric applications," *IEEE Antennas Wirel. Propag. Lett.*, vol. 10, pp. 1228–1231, 2011.
[60] Q.-N. Zhang, J. Zhang, D.-Y. Zhang, W.-J. Lu, K. F. Tong, and H.-B. Zhu, "A wearable loop-dipole combined antenna," in *Electromagnetics: Applications and Student Innovation Competition (iWEM), 2016 IEEE International Workshop on*, 2016, pp. 1–3.
[61] J. G. Santas, A. Alomainy, and Y. Hao, "Textile antennas for on-body communications: Techniques and properties," in *Antennas and Propagation, 2007. EuCAP 2007. The Second European Conference on*, 2007, pp. 1–4.
[62] S. Bashir, M. Hosseini, R. M. Edwards, M. I. Khattak, and L. Ma, "Bicep mounted low profile wearable antenna based on a non-uniform EBG ground plane-flexible EBG inverted-l (FEBGIL) antenna," in *Antennas and Propagation Conference, 2008. LAPC 2008. Loughborough*, 2008, pp. 333–336.

[63] Z. Duan, D. Linton, W. Scanlon, and G. Conway, “Improving wearable slot antenna performance with EBG structures,” in *Antennas and Propagation Conference, 2008. LAPC 2008. Loughborough*, 2008, pp. 173–176.
[64] S. Zhu and R. Langley, “Dual-band wearable textile antenna on an EBG substrate,” *IEEE Trans. Antennas Propag.*, vol. 57, no. 4, pp. 926–935, 2009.
[65] S. Milici, S. Amendola, A. Bianco, and G. Marrocco, “Epidermal RFID passive sensor for body temperature measurements,” in *2014 IEEE RFID Technology and Applications Conference (RFID-TA)*, 2014, pp. 140–144.
[66] M.-C. Tsai, C.-W. Chiu, H.-C. Wang, and T.-F. Wu, “Inductively coupled loop antenna design for UHF RFID on-body applications,” *Prog. Electromagn. Res.*, vol. 143, pp. 315–330, 2013.
[67] T. Kellomaki, J. Heikkinen, and M. Kivikoski, “One-layer GPS antennas perform well near a human body,” in *Antennas and Propagation, 2007. EuCAP 2007. The Second European Conference on*, 2007, pp. 1–6.
[68] J. Heikkinen, T. Laine-Ma, A. Ruhanen, and M. Kivikoski, “Flexible antennas for GPS reception,” in *Antennas and Propagation, 2006. EuCAP 2006. First European Conference on*, 2006, pp. 1–4.
[69] M. A. Habib, T. A. Denidni, and G. Y. Delisle, “Design of a new wide-band CPW-fed circular slot antenna,” in *Antennas and Propagation Society International Symposium, 2005 IEEE*, 2005, vol. 1, pp. 565–568.
[70] E. Moradi, T. Björninen, L. Ukkonen, and Y. Rahmat-Samii, “Characterization of embroidered dipole-type RFID tag antennas,” in *2012 IEEE International Conference on RFID-Technologies and Applications (RFID-TA)*, 2012, pp. 248–253.
[71] E. Moradi, K. Koski, L. Ukkonen, Y. Rahmat-Samii, T. Björninen, and L. Sydänheimo, “Embroidered RFID tags in body-centric communication,” in *Antenna Technology (iWAT), 2013 International Workshop on*, 2013, pp. 367–370.
[72] “polyamides - nylon and Kevlar.” [Online]. Available: http://www.chemguide.co.uk/organicprops/amides/polyamides.html. [Accessed: 31-Jan-2017].
[73] “Polyimides.” [Online]. Available: http://pslc.ws/macrog/imide.htm. [Accessed: 31-Jan-2017].
[74] “Polyurethanes.” [Online]. Available: http://www.pslc.ws/macrog/kidsmac/polyure.htm. [Accessed: 31-Jan-2017].
[75] J. Trajkovikj, J.-F. Zürcher, and A. K. Skrivervik, “PDMS, a robust casing for flexible W-BAN antennas [EurAAP corner],” *IEEE Antennas Propag. Mag.*, vol. 55, no. 5, pp. 287–297, 2013.
[76] A. Kiourti and J. L. Volakis, “Stretchable and flexible E-fiber wire antennas embedded in polymer,” *IEEE Antennas Wirel. Propag. Lett.*, vol. 13, pp. 1381–1384, 2014.
[77] A. Haj-Omar, W. L. Thompson, Y.-S. Kim, P. Glick, M. Tolley, and T. P. Coleman, “Stretchable and flexible adhesive-integrated antenna for biomedical applications,” in *Antennas and Propagation (APSURSI), 2016 IEEE International Symposium on*, 2016, pp. 459–460.
[78] A. Arriola, J. I. Sancho, S. Brebels, M. Gonzalez, and W. De Raedt, “Stretchable dipole antenna for body area networks at 2.45 GHz,” *IET Microw. Antennas Propag.*, vol. 5, no. 7, pp. 852–859, 2011.
[79] D. M. Pozar, *Microwave Engineering, 4th Edition*. Wiley Global Education, 2011.
[80] H. A. Damis, R. Mirzavand, H. J. Chung, and P. Mousavi, “Flexible printed square loop antennas for wearable applications,” in *2016 17th International Symposium on Antenna Technology and Applied Electromagnetics (ANTEM)*, 2016, pp. 1–2.
[81] “Radio Links Part II.” [Online]. Available: http://www.enigmatic-consulting.com/Communications_articles/Radio_links_part2/Radios2_antennas.html. [Accessed: 01-Feb-2017].
[82] R. A. Shafik, M. S. Rahman, and A. R. Islam, “On the Extended Relationships Among EVM, BER and SNR as Performance Metrics,” in *2006 International Conference on Electrical and Computer Engineering*, 2006, pp. 408–411.
[83] R. Zhang, J. Ma, and X. Xin, “Full-duplex fiber-wireless link for alternative wired and 40-GHz band wireless access based on differential quaternary phase-shift optical single sideband millimeter-wave signal,” *Opt. Eng.*, vol. 54, no. 2, pp. 026101–026101, 2015.